Heinrich Heine
Universität Düsseldorf

Untersuchung zum Einfluss von Ameisensäure, Essigsäure, Oxalsäure und Salzsäure als Modulatoren in der Synthese auf das Metall-organische Netzwerk MIL-160

Dissertation

zur Erlangung des Doktorgrades
der Mathematisch-Naturwissenschaftlichen Fakultät
der Heinrich-Heine-Universität Düsseldorf

vorgelegt von

Dominik Moritz Steinert
aus Meerbusch

Düsseldorf, Februar 2022

aus dem Institut für Anorganische Chemie und Strukturchemie I
der Heinrich-Heine-Universität Düsseldorf

Gedruckt mit der Genehmigung der
Mathematisch-Naturwissenschaftlichen Fakultät der
Heinrich-Heine-Universität Düsseldorf

1. Berichterstatter: Univ.-Prof. Dr. Christoph Janiak
2. Berichterstatter: Univ.-Prof. Dr. Christian Ganter

Tag der Disputation: 28.03.2022

Eidesstattliche Erklärung

Ich, Dominik Moritz Steinert, versichere an Eides statt, dass die vorliegende Dissertation von mir selbstständig und ohne unzulässige fremde Hilfe unter Beachtung der „Grundsätze zur Sicherung guter wissenschaftlicher Praxis“ an der Heinrich-Heine-Universität Düsseldorf erstellt worden ist. Die aus fremden Quellen direkt oder indirekt übernommenen Gedanken sind als solche kenntlich gemacht. Die Arbeit wurde bisher weder im Inland noch im Ausland in gleicher oder ähnlicher Form einer anderen Prüfungsbehörde vorgelegt. Es wurden keine früheren erfolglosen Promotionsversuche unternommen.

…….....

Ort, Datum

…….....

Unterschrift

Danksagung

An dieser Stelle möchte ich mich bei all denjenigen bedanken, die mich während der Anfertigung dieser Dissertation unterstützt und motiviert haben.

Zunächst danke ich Herrn Prof. Dr. Christoph Janiak für die Möglichkeit diese Dissertation in seinem Arbeitskreis anzufertigen und die Betreuung während dieser Zeit. Weiter bedanke ich mich für den gewährten wissenschaftlichen Freiraum sowie die Unterstützung bei der Erstellung der Publikationen.

Herrn Prof. Dr. Christian Ganter danke ich für die freundliche Übernahme des Koreferates.

Dem gesamten Arbeitskreis gilt mein Dank für die Zusammenarbeit und die Unterstützung in jeder Form in den letzten Jahren.

Besonderer Dank gilt dabei folgenden Personen:

Alexa Schmitz für die inhaltliche und persönliche Unterstützung während der Promotion. Daniel Komisarek, Stefanie Bügel, Simon Millan, Bastian Moll, Dietrich Püschel, Christian Jansen, Alex Spieß, Tobias Heinen und Marcus Fetzer danke ich für die anregenden Gespräche, den wissenschaftlichen Austausch, sowie für die gemeinsam verbrachte Zeit.

Den von mir betreuten (Abschluss-) Studenten Waldemar Schuh, Philipp Seifert und Dietrich Püschel danke ich für ihr Interesse und ihre engagierte Arbeit.

Mein größter Dank gilt meiner Familie und insbesondere meinem Vater Dr. Ali Ümit Ertürk, für den Rückhalt und die Unterstützung die ich während meines gesamten Studiums und meinem persönlichen Werdegang erfahren habe. Danke, dass ihr mich in all den Jahren fortwährend unterstützt und aufgemuntert habt und trotz aller Hürden an mich und meinen Erfolg geglaubt habt.

Inhaltsverzeichnis

Kurzfassung

Im ersten Teil dieser Dissertation wurde auf Basis vorhandener wissenschaftlicher Arbeiten der derzeitige Kenntnisstand zu MOFs (metal organic frameworks) im Hinblick auf ihre Anwendung für die Adsorptionswärmetransformation untersucht. Besonderes Augenmerk lag hierbei auf der Eignung von MOFs für den Einsatz in thermisch betriebenen Adsorptionskältemaschinen und Adsorptionswärmepumpen. Der aktuelle Stand der Wissenschaft wurde vor diesem Hintergrund eingehend betrachtet und evaluiert.

Die Adsorptionswärmetransformation (AHT) ist ein umweltfreundliches Energiesparverfahren, das zur Klimatisierung, d.h. entweder zur Kühlung (auch zur Eisbereitung und Kühlung) oder zum Heizen dient. Die AHT basiert auf der zyklischen Adsorption und Desorption eines Arbeitsmediums in einem porösen Material. Wenn das Arbeitsmedium durch das aktivierte leere Sorptionsmaterial zur Verdampfung gebracht wird, wird die benötigte Verdampfungswärme in nutzbare Kälte umgewandelt. Die Antriebswärme regeneriert das leere Sorptionsmittel durch Desorption des Arbeitsmediums. Die Adsorptionswärme im Sorptionsmaterial und die Kondensationswärme des Arbeitsmediums können im Adsorptionswärmepumpenbetrieb genutzt werden. Damit trägt die Adsorptionswärmeumwandlung zu energiesparenden Technologien bei. Die Adsorbentienentwicklung spielt eine entscheidende Rolle für die Verbesserung der AHT-Technologien. Neben Kieselgel und Zeolithen als Adsorptionsmittel, die bisher in den kommerziell erhältlichen AHT-Geräten eingesetzt werden; erhielten insbesondere metall-organische Gerüste (MOFs) mehr und mehr Aufmerksamkeit für diese Anwendung in den letzten Jahren. Kompositmaterialien aus Salzen mit Kieselgelen, Zeolithen und MOFs sowie Aktivkohlen wurden ebenfalls erforscht, um zu den AHT-Technologien beizutragen. Die Reduktion der Installations-/Produktionskosten und

Erhöhung der Effizienz von AHT-Geräten ist dabei eine notwendige Voraussetzung, um den breiten Einsatz von AHT zu ermöglichen.

Im zweiten Teil dieser Dissertation wurde der Einfluss verschiedener Modulatoren auf das Syntheseergebnis von MIL160, einem literaturbekannten MOF, untersucht.

Modulatoren werden häufig bei der Synthese von metallorganischen Gerüsten (MOFs) zur Verbesserung der Porosität und Morphologie eingesetzt. Für Aluminium-MOFs wurde bisher selten über Modulationen berichtet, und wie hier am Beispiel des Aluminium-Furandicarboxylat-MOFs MIL-160 gezeigt wird, sind die positiven Auswirkungen von Modulatoren gering und nachteilige Auswirkungen wahrscheinlicher. Ameisensäure als Modulator kann die BET-Oberfläche und das Porenvolumen von MIL-160 bis zu einem Modulator:Linker-Verhältnis von 1.25:1 leicht erhöhen. Essigsäure zeigt nur beim kleinsten getesteten Verhältnis von 0.125:1 eine geringe Zunahme der Oberfläche und des Porenvolumens. Die stärkeren Säuren Oxalsäure und Salzsäure mit den ebenfalls stärker aluminiumkoordinierenden Anionen haben keinen positiven Porositätseffekt und vermindern die BET-Oberfläche und das Porenvolumen schon bei kleinen Mengen. Bei einem Modulator:Linker-Verhältnis von 1:1 für Oxalsäure und 0.75:1 für Salzsäure bildet sich nach der Analyse durch Pulverröntgenbeugung und Stickstoffsorption kein poröses MOF mehr. Die thermogravimetrische Analyse und die Rasterelektronenmikroskopie legen nahe, dass keiner der getesteten Modulatoren einen merklichen positiven Einfluss auf die Entstehung von Linkerdefekten oder die Verbesserung der Kristallinität oder Kristallgröße hat.

Abstract

In the first part of this dissertation, the current state of knowledge on MOFs with regard to their application for adsorption heat transformation was investigated on the basis of existing scientific work. Particular attention was paid to the suitability of MOFs for use in thermally driven adsorption chillers and adsorption heat pumps. The current state of science was considered and evaluated in detail against this background.

Adsorption heat transformation (AHT) is an environmentally friendly energy-saving process used for air conditioning, i.e., either cooling (including ice making and refrigeration), or heating. AHT is based on the cyclic adsorption and desorption of a working fluid in a porous material. When the working fluid is caused to evaporate by the activated empty sorption material, the required heat of evaporation is converted to useful cold in thermally driven adsorption chillers. The driving heat regenerates the empty sorbent by desorption of the working medium. The adsorption heat in the sorbent and the condensation heat of the working medium can be used in adsorption heat pump operation. Thus, adsorption heat conversion contributes to energy-saving technologies. Adsorbent development plays a crucial role in improving AHT technologies. In addition to silica gel and zeolites as adsorbents, which have been used in the commercially available AHT devices so far; especially metal-organic frameworks (MOFs) received more and more attention in recent years for this application. Composites of salts with silica gels, zeolites and MOFs, and activated carbons have also been explored to contribute to AHT technologies. In this regard, reducing the installation/production cost and increasing the efficiency of AHT devices is a necessary condition to enable the widespread use of AHT. In the second part of this dissertation, the influence of different modulators on the synthesis result of MIL-160, a literature known MOF, was investigated.

Modulators are commonly used in the synthesis of metal-organic frameworks (MOFs) to improve porosity and morphology. Modulations have rarely been reported for aluminum MOFs. As shown in this work with the aluminum furandicarboxylate MOF MIL-160 as an example, the beneficial effects of modulators are small and adverse effects are more likely. Formic acid as a modulator can slightly increase the BET surface area and pore volume of MIL-160 up to a modulator:linker ratio of 1.25:1. Acetic acid shows some increase in surface area and pore volume only at the smallest ratio tested of 0.125:1. The stronger acids oxalic acid and hydrochloric acid, with the anions also more strongly coordinating with aluminum, have no positive porosity effect and decrease BET surface area and pore volume even at small amounts. At a modulator:linker ratio of 1:1 for oxalic acid and 0.75:1 for hydrochloric acid, porous MOF is no longer formed, according to analysis by powder X-ray diffraction and nitrogen sorption. Thermogravimetric analysis and scanning electron microscopy suggest that none of the modulators tested have a noticeable positive effect on introducing linker defects or improving crystallinity or crystal size.

Publikationsliste

Dominik Moritz Steinert, Sebastian-Johannes Ernst, Stefan K. Henninger, Christoph Janiak:

"*Metal-Organic Frameworks as Sorption Materials for Heat Transformation Processes"*

Eur. J. Inorg. Chem. **2020**, 4502-4515. DOI: 10.1002/ejic.202000834

Dominik Moritz Steinert, Alexa Schmitz, Marcus Fetzer, Philipp Seiffert, Christoph Janiak:

"A caveat on the effect of modulators in the synthesis of the aluminum furandicarboylate metal-organic framework MIL-160"

Z. Allg. Anorg. Chem. **2022**, e202100380 DOI: 10.1002/zaac.202100380

Abkürzungsverzeichnis

Å	Ångström (1 Å = 10^{-10} m)
Abb.	Abbildung
BDC	*1,4-benzenedicarboxylate* (Benzoldicarboxylat)
BET	Brunauer -Emmet-Teller
°C	Grad Celsius
d	day
DMF	N,N-Dimethylformamid
EDX	Energy dispersive X-Ray spectroscopy (Energiedisperse Röntgenspektroskopie)
eq	Äquivalent
Fa.	Firma
g	gramm
h	*Hour* (Stunde)
HHU	Heinrich-Heine Universität
HKUST	*Hong Kong University of Science and Technology*
HOMO	*highest occupied molecular orbital* (höchstes besetztes Molekülorbital)
HSAB	*hard and soft acid and bases* (Harte und weiche Säuren und Basen)
Hz	(SI-Einheit für Frequenz, 1 Hz = 1 s^{-1})
IUPAC	*International Unit of Pure and Applied Chemistry* (Internationale Union für reine und angewandte Chemie)
K	Kelvin
L	Liter

LUMO	*lowest unoccupied molecular orbital* (Niedrigstes unbesetztes Molekülorbital)
m	Meter
mg	milligram
MHz	Megahertz (1 MHz = 1 x 10^6 Hz)
min	Minute (60 s)
MIL	*Matériaux de l'Institut Lavoisier* (Materialinstitut Lavoisier)
min	Minute
MOF	*metal-organic framework* (Metall-organische Gerüstverbindung)
mL	Milliliter (10^{-3} L)
mmol	Millimol (10^{-3} mol)
mol	Mol (SI-Einheit der Stoffmenge (6.02 x 10^{23} Teilchen))
nm	Nanometer (1 nm = 1 x 10^{-9} m)
µm	Mikrometer (1 µm = 1 x 10^{-6} m)
ppm	parts per million (Millionstel)
W	Watt
∅	Durchschnitt
et al.	et alii/aliae/alia (und andere)
Gew.-%	Gewichtsprozent
Lit.	Literatur
max.	maximal
PXRD	*powder X-ray diffraction* (Pulverröntgendiffraktometrie)
REM	Rasterelektronenmikroskop
RPM	*Rounds per minute* (Umdrehungen pro minute)
SBU	*Secondary building unit* (sekundäre Baueinheit)
SEM	*Scanning elektron microscope* (Rasterlektronenmikroskop)

theo.	theoretisch
u. a.	unter anderem
UiO	Universitet i Oslo

Inhalt

1 Einleitung

1.1 MOFs

Metall-organische Gerüste (MOFs) sind potentiell poröse Koordinationsnetzwerke aus Metallknoten und organischen Linkern, die sich selbst zu einem ausgedehnten (kristallinen) zwei- oder dreidimensionalen Netzwerk zusammenlagern.[1,2,3] Ihre hohe innere Oberfläche und ein großes Porenvolumen, eine einstellbare dreidimensionale Struktur sowie ihre einstellbare innere und äußere Mikroumgebung lassen MOFs für eine Vielzahl von Anwendungen geeignet erscheinen.[4,5,6,7] Vor allem in der Gasspeicherung und -trennung,[8,9] als poröse Füllstoffe in Mixed-Matrix-Membranen,[10,11,12,13,14] für Katalyseanwendungen,[15] als Arzneimittelträgerstoff,[16,17] oder auch zur Enzymimmobilisierung.[18] Seit ihrer Entdeckung in den frühen 1990er Jahren haben MOFs sich mehr und mehr als geeignet für spezifische Adsorption von Gasen und Dämpfen gezeigt.[4,5,6,7] Im Vergleich zu klassischen Sorptionsmaterialien wie Aktivkohlen, Kieselgelen oder Zeolithen, lassen sich die Sorptionseigenschaften von MOFs besser über die Wahl der organischen Liganden steuern. Aufgrund der chemischen Robustheit von MOFs können die Liganden durch organisch-chemische Reaktionen (Substitutionen, Additionen) auch noch nach der Synthese modifiziert werden. Hierfür wurde für MOFs der Begriff "postsynthetische Modifikation" geprägt.[19] Vereinfacht dargestellt, bestehen klassische Sorptionsmaterialien wie Zeolithe und Kieselgele rein aus SiO_4 und AlO_4 Bausteinen, die über ihre Ecken zu Netzwerken verbunden sind[20]. Im Vergleich zu MOFs ist eine Modifikation des Aufbaus dieser Bausteine ist nur in relativ engen Grenzen möglich Für MOFs steht die im Wesentlichen unendliche Vielfalt der organischen Chemie zur Verfügung, um Modifikationen von MOF-Liganden vorzunehmen. MOFs sind Rekordhalter für die Größe der inneren Oberfläche.[21] Spezifische innere Oberflächen von MOFs liegen typischerweise in einem Bereich von 1000-4000 m^2/g, aber auch von Werten über

6000 m^2/g wurde berichtet (MIL-210 oder NU-100).[22] Im Gegensatz dazu liegen die spezifischen inneren Oberflächen von Zeolithen und Silica Gelen nur bei 1000 m^2/g und darunter[2324]. Die Porenöffnungen oder Kanaldurchmesser in MOFs reichen von 0,3 bis 3,4 nm, mit spezifischen Porenvolumina bis zu 1,5-2 cm^3/g.[25,26.]Ein Vorteil von MOFs gegenüber amorphen Sorptionsmaterialien wie z. B. Aktivkohle oder Kieselgel ist ihre identische Porengröße über die gesamte Netzwerkstruktur. Im Gegensatz dazu sind Aktivkohlen und Kieselgele amorphe Materialien, deren Mikrostruktur nicht genau bekannt ist.[27,28,29,30] In den letzten Jahren hat sich die Wassersorption zu einem immer wichtigeren Forschungsgebiet entwickelt.[31,32] Dazu gehört auch die mögliche Nutzung poröser Materialien zur Adsorption und Desorption von Wasserdampf unter atmosphärischen Bedingungen ohne externe Energiequellen als eine vielversprechende Methode für die Aufnahme und Abgabe von Wasser in ariden oder wüstenartigen Regionen der Welt. Das Potenzial von metallorganischen Gerüsten als Wassergewinnungsmaterialien für die Süßwassergewinnung in trockenen Regionen mit mittlerer oder hoher Luftfeuchtigkeit während der Nacht wurde zuerst von *Kim* et al. und *Trapani* et al. im Jahr 2016 entdeckt.[33,34] Die mögliche Erzeugung von Trinkwasser durch die Adsorption von Feuchtigkeit aus der Luft wurde dann von *Yaghi* et. al. im Jahr 2017 weiterverfolgt.[35] Die energieeffiziente Adsorption von atmosphärischem Wasser und dessen Abtrennung zur anschließenden Nutzung stellt allerdings noch immer eine technische und wirtschaftliche Herausforderung dar.,[36,37,38,39] Ein Hindernis auf dem Weg zu breiteren Anwendungen von MOFs war lange Zeit ihre unzureichende hydrothermale Stabilität.[40] Inzwischen sind jedoch MOFs bekannt, welche stabil gegenüber längerem Kontakt mit Wasser sind. Dies hat die potentielle Anwendung der zyklischen Wassersorption mit wasserstabilen MOFs in Adsorptionswärmepumpen (AHP), einschließlich Adsorptionskältemaschinen, ermöglicht.[41] Physikalische Adsorptions- und Desorptionsprozesse an inneren

Oberflächen hochporöser Materialien können zur Umwandlung von Wärme in Wärmetransformationsprozessen genutzt werden.[42] Adsorption ist ein Prozess der Anhaftung von Atomen, Molekülen oder Ionen eines Gases oder Flüssigkeit an der Oberfläche eines Festkörpers oder einer Flüssigkeit. Ein Großteil der Forschung konzentriert sich dabei auf die Adsorption an der Festkörperoberfläche und die Physisorption, d.h. der Prozess, bei dem die adsorbierten Spezies keine chemischen Bindungen mit der Oberfläche eingehen, sondern nur durch physikalische Kräfte (Dispersion, Elektrostatik, etc.) binden.

1.1.1 Aluminium MOFs

Zu den vielversprechendsten MOFs im Hinblick auf mögliche Anwendungen gehören aluminiumbasierte MOFs (Al-MOFS) wie MIL-53,[43] Al-Fumarat (Aluminiumfumarat, Basolite A520),[44,45] CAU-10-H,[46] und MIL-160[47]. Al-MOFs weisen typischerweise (helikale) Ketten mit entweder trans- (MIL-53 und Aluminiumfumarat) oder cis- (CAU-10-H und MIL-160) eckenteilenden AlO6-Oktaedern auf, bei denen die gemeinsamen Ecken OH-Anionen oder Sauerstoffatome aus den Carboxylatgruppen der organischen Linkermoleküle sind.[48] Eine räumliche Darstellung dieser Strukturen ist in Abbildung 1 gezeigt.

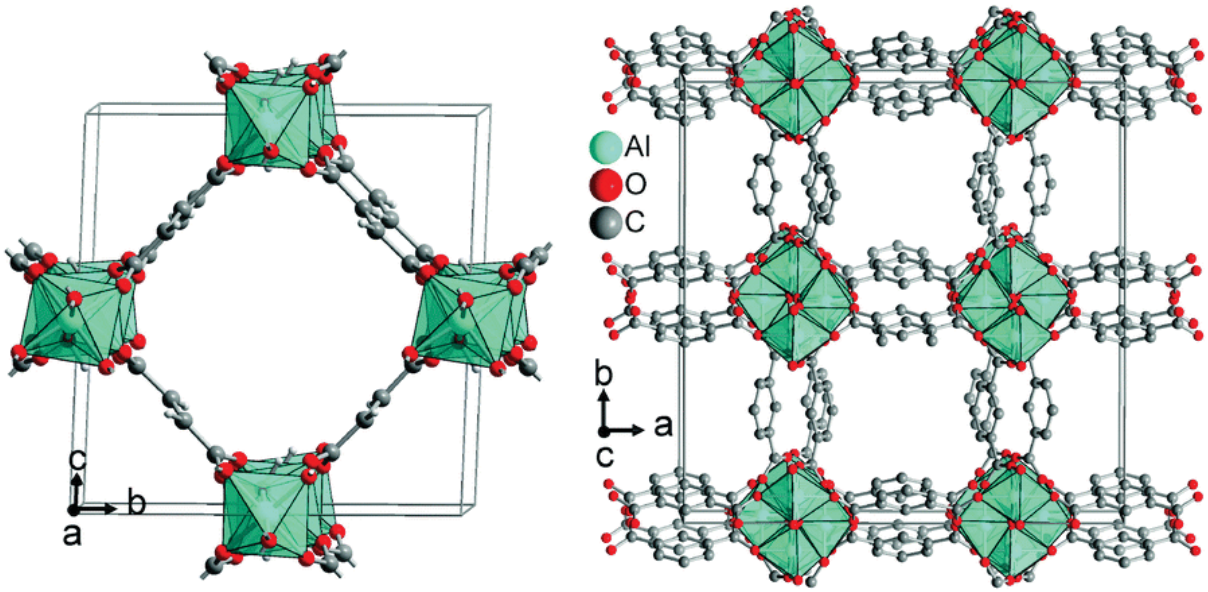

Abbildung 1: Struktur von Aluminumfumarat auf der linken Seite und CAU-10H auf der rechten Seite, welches in der Struktur MIL-160 entspricht. Die Aluminiumatome sind polyhedral dargestellt. Entnommen aus Referenz 48 mit Genehmigung der Royal Society of Chemistry.

Al-MOFs zeigen mikroporöse, enge Porengrößenverteilungen, die von parallelen eindimensionalen quadratischen bis rautenförmigen Kanälen ausgehen. Ein Merkmal von Al-MOFs ist ihre hohe chemische und hydrothermale Stabilität,[49,50,51,52] was sie für Anwendungen unter realen Bedingungen prädestiniert, bei denen Wassergehalt oder Feuchtigkeit nicht vermieden werden können. Aluminiumfumarat und CAU-10-H haben ihre Stabilität bereits über 4500 bzw. 10 000 Wasseradsorptions- und -Desorptionszyklen bewiesen.[49,52] Beide zeigen eine steile s-förmige Wassersorptionsisotherme mit Aufnahme in einem relativ niedrigen Partialdruckbereich.[50,52] Außerdem gilt Aluminium als ungiftig und ist eines der am häufigsten vorkommenden (8,3 Gew.-% in der Erdkruste) und preiswerten Metalle. Aluminium-MOFs haben besondere Aufmerksamkeit in den Bereichen hierarchische Porosität,[53,54] Gasspeicherung und Gastrennung,[55] Adsorption von organischen Stoffen,[56] Katalyse,[57,58] mechanische Energiespeicherung,[59] Wasser- und Luftreinigung/-sanierung,[60,61,62] Wassergewinnung,[63,64,65] Entsalzung,[38] Sensorik,[66] Protonenleitfähigkeit,[67] Mixed-Matrix-Membranen[68] und in Wärmetransformationsanwendungen erhalten.[50,52, 69,70,71,72,73,74] In den letzten Jahren

sind Aluminiumfumarat und CAU-10-H daher von Materialien für die Grundlagenforschung zu Adsorbentien in vorindustriellen Großgeräten geworden.[63,67,6869,73,74]

1.1.2 MOF-Modulation

Die Fähigkeiten von MOFs haben sich in ihren chemischen Eigenschaften in vielen verschiedenen Dimensionen als beeinflussbar erwiesen,[75] was zu einem immer noch steigenden wissenschaftlichen und kommerziellen Interesse an diesem Gebiet führt, was die verschiedenen potentiellen Anwendungen betrifft.[76,77,78,79,80,81,82,83,84,85] Um ihre Eigenschaften für spezielle Anwendungen gezielt einzustellen, wurde das Engineering von MOFs in den Fokus genommen, um beispielsweise Morphologie, Kristallitgröße oder Defekte in MOF-Netzwerken gezielt zu verändern.[86,87,88] Ein vielversprechender Ansatz, um die Eigenschaften von MOFs in günstige Richtungen zu beeinflussen, ist die Modulation der Synthese.[89,90] Dabei wird die Kinetik der Wechselwirkungen zwischen Metallionen und Liganden während des Kristallwachstums durch Modulatormoleküle innerhalb der Synthese beeinflusst. Die Modulatoren binden intermittierend an das Metallion, konkurrieren mit dem Linker und verlangsamen dadurch den Kristallwachstumsprozess. Die Modulatoren beeinflussen so das Koordinationsgleichgewicht des Metalls mit dem Linker während der Synthese des MOFs. Auch der teilweise dauerhafte Einbau des Modulators anstelle eines Linkers in das Netzwerk ist möglich[87,88,.91 ,92,93,94,95] Dies kann verschiedene, zum Teil positive Auswirkungen auf das MOF haben, wobei sich die verschiedenen Modulatoren sowohl in ihrer Wirksamkeit als auch in ihrer Wirkungsweise unterscheiden. So ist Ameisensäure als Modulator dafür bekannt, die Bildung von MOF-Kristallen zu beschleunigen und so im Fall von UiO-MOFs (MOFs die in der Universitet i Oslo publiziert wurden) Defekte zu induzieren[96], indem sie die Reaktion mit Formiat anreichert. Starke Säuren wie Salzsäure hingegen verlangsamen die

MOF-Entstehung, indem sie den Linker protoniert in der Lösung halten und können so unter Umständen die erhaltene BET-Oberfläche ebenso wie die Ausbeute der Reaktion erhöhen.[97] So konnten Zhao et al. für MIL- 101(Cr) zeigen, dass die Zugabe von Salpetersäure sowohl die Ausbeute als auch die Porosität des MOFs verbessert, während die stärkeren anorganischen und schwachen organischen Kohlenstoffsäuren zu abnehmender Ausbeute und Porosität führten.[98] Gleichzeitig fanden Zhao et al. heraus, dass das MOF-Wachstum unterdrückt wurde, wenn Essigsäure als Modulator für MIl-101(Cr) verwendet wurde, was zu einer kleineren Partikelgröße führt. Große Mengen Essigsäure veränderten sogar die Morphologie des MOFs.[99,100] Eine Veränderung der Morphologie wurde auch von Yang et al. beobachtet, die die Bildung von MIL-88B(Cr) anstelle von MIL101(Cr) in Gegenwart großer Mengen von Benzoesäure zeigten.[101] Ähnliche Effekte konnten für UiOs gezeigt werden. Gökpinar et al. beobachteten einen Anstieg der gemessenen BET-Oberflächen, sowie steigende Ausbeuten durch die Verwendung von HCl.[97] Morphologische Effekte durch den Einsatz von Modulatoren sind ebenfalls für UiOs bekannt. So fanden Moll et al. heraus, dass die Verwendung von sehr hohen Mengen an Mercaptoessigsäure auf UiO-66 zu einer Phasenumwandlung von fcu zu hcp führt.[90] Der Einsatz von Modulatoren zeigt aber nicht immer vorteilhafte Ergebnisse. So wurde von Defekten in MOFs berichtet, die eine unvollständige Aktivierung der Porosität bewirken. Dies führte zu einer Verstopfung der Poren durch Gastmoleküle, was sich negativ auf die Oberfläche und die Adsorptionskapazität auswirkte.[102,103]

Aluminiumbasierte MOFs wie MIL-53,[104] Aluminiumfumarat (Basolite A520),[44,105,106] CAU-10[107] oder MIL-160[108] können aufgrund ihrer chemischen und hydrothermalen Stabilität zu den vielversprechendsten MOFs für Anwendungen gezählt werden.[109,110,111,112,113] Aluminium ist ein weltweit reichlich vorhandenes und kostengünstiges Leichtmetall mit geringer Toxizität[111,112,114,115] Dieser Vorteil macht die

Al-MOFs besonders geeignet für Wärmetransformationsanwendungen.[54,55] Insbesondere MIL-160 ist aufgrund des Heteroatoms im Furan-Anteil des Linkers ein hydrophiles MOF. Dies führte zu einem sehr hydrothermal stabilen Material mit vielversprechenden Wassersorptionseigenschaften. Die Syntheseroute von MIL-160 ist umweltfreundlich, da der Linker aus erneuerbarer Biomasse über die Oxidation von 5-(Hydroxy-methyl)furfural (5-HMF) in industriellen Maßstab hergestellt werden kann und Wasser das einzige Lösungsmittel ist.[116,117] MIL-160 wurde auch von Cadiau et al. als das vielversprechendste Al-MOF für Wärmepumpenanwendungen bezeichnet, da es sowohl Aluminiumfumarat als auch CAU-10-H in Bezug auf gravimetrische Wasserbeladungen übertrifft.[109]

2 Motivation und Zielsetzung

In der Entwicklung der MOF-Forschung hat sich das Überwinden der Schwelle zur Anwendungsreife als eine essentielle Herausforderung erwiesen um das Potential dieser Materialklasse vollumfänglich auszuschöpfen. Ein Teilbereich dieser Potentiale ist die Verwendung von MOFs als Sorptionsmaterialien für Wärmetransformationsprozesse, im Gegensatz zu den bisher verwendeten klassischen Materialien. Die Literatur umfasst zu diesem Themenkomplex eine Vielfalt von Forschungsschwerpunkten. Darunter die Sorptions- und Desorptions Eigenschaften verschiedenster MOFs, ihre (Lösungs-) Stabilität, Hydro- und Lipophilie und ihre Sorptiv- Affinitäten. Anhand der Literatur soll im ersten Teil dieser Arbeit dieser Aspekt untersucht werden, indem die Sorptionseigenschaften für Wärmetransformationsprozesse verschiedener MOFs diskutiert werden und eine Übersicht des bisherigen Kenntnisstands zusammengestellt wird. Diese Übersicht soll helfen, die vorhandenen Potentiale von MOFs im Hinblick auf Wärmetransformationsprozesse zu erweitern und die Erschließung von Anwendungsmöglichkeiten zu verbessern.

Im zweiten Teil der Dissertation soll der Einfluss von Modulatormolekülen in der MOF-synthese untersucht werden. Der Einsatz von Modulatoren in der MOF-Synthese ist einer von mehreren Ansätzen des sogenannten MOF-Engineerings, welches bestimmte MOF-Eigenschaften gezielt in eine gewünschte Richtung verändern soll. Für zirkoniumbasierte MOFs wird die Modulation schon länger erfolgreich eingesetzt um zum Beispiel die Porosität und die Kristallinität zu verbessern.[118,119,120,121] Es sollen die Auswirkungen von Modulatoren auf ein aluminiumbasiertes MOF untersucht werden, um herauszufinden ob sich die Erkenntnisse zu den modulierten Zirkonium-MOFs auf aluminiumbasierte MOFs übertragen lassen. Ein vielversprechendes Al-MOF ist MIL-160, welches umweltfreundlich und kostengünstig herzustellen ist und

über ansprechende Sorptionscharakteristika verfügt. Um einen breiten Bereich an Modulatoreinflüssen abzudecken, soll MIL-160 mit Ameisensäure, Essigsäure, Oxalsäure und Salzsäure moduliert werden. Ameisen- und Essigsäure als Monocarbonsäuren verschiedener Kettenlänge, Oxalsäure als Dicarbonsäure und Salzsäure als anorganische Säure.

Die relevanten Ergebnisse dieser Arbeit sollten in internationalen wissenschaftlichen Journalen veröffentlicht werden.

3 Kumulativer Teil

Die folgenden Kapitel beinhalten die Ergebnisse der Dissertation, die in Form von Publikationen mit einer Erstautorenschaft in internationalen Journalen veröffentlicht, bzw. eingereicht, wurden. Die Publikationen werden in chronologischer Reihenfolge aufgeführt, beginnend mit der ersten Veröffentlichung als Erstautor. Jede Publikation steht mit eigenem Literaturverzeichnis für sich. Abbildungen, Schemata und Tabellen folgen nicht der Nummerierung des Haupttextes, sondern der Nummerierung der Publikation selbst. Jede Publikation wird durch ein kurzes Profil eingeleitet, das den Titel, den Namen der Autoren und des Journals sowie eine Kurzfassung und die Eigenanteile des Autors an den Publikationen beinhaltet.

3.1 Metal-Organic Frameworks as Sorption Materials for Heat Transformation Processes

Dominik Moritz Steinert, Sebastian-Johannes Ernst, Stefan K. Henninger, Christoph Janiak: "*Metal-Organic Frameworks as Sorption Materials for Heat Transformation Processes"*

Eur. J. Inorg. Chem. **2020**, 4502-4515. DOI: 10.1002/ejic.202000834

Kurzfassung:

Zyklische physikalische Adsorptions- und Desorptionsprozesse an porösen Materialien können für die Umwandlung von Wärme in Wärmetransformationsprozessen genutzt werden, was dem Arbeitsprinzip in Adsorptionswärmepumpen (AHP) entspricht. Umweltfreundliches Wasser mit seiner hohen Verdampfungsenthalpie ist das Arbeitsmittel der Wahl in AHPs. Metallorganische Gerüstverbindungen (MOFs) können große Mengen an Wasser oder Methanol bis zu ihrem eigenen Gewicht adsorbieren. MOFs könnten eine Alternative zu Kieselsäuregelen, Zeolithen oder Aluminiumphosphaten für Wärmeumwandlungen bei niedrigen Temperaturen in AHPs sein.

Anteile an der Publikation:

- Idee und Übergabe des Projekts erfolgte durch Herrn Prof. Dr. Christoph Janiak.
- Konzeption, Aufbau und Verschriftlichung des Reviews auf der Basis einer ausgiebigen Literaturrecherche erfolgte eigenständig.
- Herr Dr. Sebastian-Johannes Ernst und Herr Dr. Stefan Kai Henninger lieferten Informationen und Abbildungen für die Abschnitte „Application“ und „Open cycles“.
- Die Verschriftlichung der Abschnitte „Application“ und „Open cycles“ erfolgte in Abstimmung mit Herrn Dr. Sebastian-Johannes Ernst und Herrn Dr. Stefan Kai Henninger.
- Kommunikation und finale Abstimmung des Manuskripts mit den externen Kooperationspartnern Herrn Dr. Sebastian-Johannes Ernst und Herrn Dr. Stefan Kai Henninger.
- Die Korrekturen und die konstruktive Durchsicht des Manuskripts erfolgten durch Herrn Prof. Dr. Christoph Janiak.
- Das Einreichen in dem internationalen Journal „European Journal of Inorganic Chemistry“ und die finale Abstimmung, sowie der Revision des Manuskripts erfolgte in Zusammenarbeit mit Herrn Prof. Dr. Christoph Janiak.

EurJIC
European Journal of Inorganic Chemistry

Minireview
doi.org/10.1002/ejic.202000834

Check for updates
Chemistry Europe
European Chemical Societies Publishing

MOFs for Heat Transformation

Metal-Organic Frameworks as Sorption Materials for Heat Transformation Processes

Dominik Moritz Steinert,[a] Sebastian-Johannes Ernst,[b] Stefan K. Henninger,[b] and Christoph Janiak*[a]

Dedicated to Prof. Dr. Erwin Riedel on the occasion of his 90th birthday.

Abstract: Cyclic physical adsorption and desorption processes on porous materials can be used for the conversion of heat in heat transformation processes, which is the working principle in adsorption heat pumps (AHPs). Environmentally benign water with its high enthalpy of evaporation is the working fluid of choice in AHPs. Metal-organic frameworks, MOFs can adsorb large amounts of water or methanol, up to their own weight. MOFs could be alternative materials to silica gels, zeolites, or aluminum phosphates for low-temperature heat transformations in AHPs.

Introduction

Metal-organic frameworks (MOFs) are potentially porous coordination networks composed of metal nodes and organic linkers that self-assemble into an extended (crystalline) two- or three-dimensional network (Figure 1).[1–3] Their high internal surface area and a large pore volume, adjustable three-dimensional structure, and tunable inner and outer microenvironment let one envision MOFs for a myriad of applications,[4–7] most prominently in gas storage and separation,[8,9] as porous fillers in mixed-matrix membranes,[10–14] catalysis,[15] drug delivery,[16,17] enzyme immobilization, etc.[18] as filler in mixed-matrix membranes etc.

Since their discovery in the early 1990s, MOFs have proven to be more and more suitable for a task- and compound-specific adsorption of gases and vapors.[4–7] Compared to other sorption materials such as activated carbons, silica gels, or zeolites, the sorption properties of MOFs can be better tailored via the organic ligands. Due to the chemical robustness of MOFs, the ligands can be modified by organic-chemical reactions (substitutions, additions) even after MOF network synthesis. For this purpose, the term "post-synthetic modification" has been coined for MOFs.[19] In a simplified picture, zeolites and silica gels have only SiO_4 and AlO_4 building blocks which are connected via corners into networks. A modification of the assembly of these building blocks is only possible within relatively narrow limits when compared to MOFs. For the latter, the essentially infinite variety of organic chemistry is available for the modification of MOF ligands. MOFs are record holders for the size of the internal surface area. Specific inner surface areas of MOFs typically range from 1000–4000 m^2/g, but values above 6000 m^2/g have also been reported (MIL-210 or NU-100).[20] In contrast, the specific inner surface areas of zeolites and silica gels are at 1000 m^2/g and below. The pore openings or channel diameters in MOFs range from 0.3 to 3.4 nm, with specific pore volumes up to 1.5–2 cm^3/g. An advantage of MOFs over amorphous sorption materials such as activated carbon or silica gel is their perfectly identical pore size over the entire network structure. In contrast, activated carbons and silica gels are

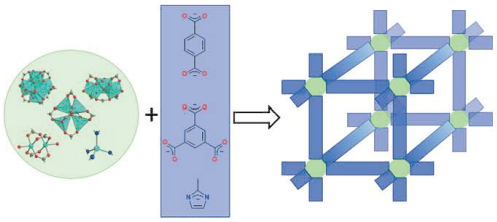

Figure 1. Construction principle of MOFs from metal clusters or metal atoms (examples shown with their attached donor atoms from ligands with carboxylate, $-CO_2$ or azolate, -N groups) and organic ligands (linkers) into a three-dimensional porous framework.

[a] D. M. Steinert, C. Janiak
Institut für Anorganische Chemie und Strukturchemie,
Heinrich-Heine-Universität,
40204 Düsseldorf, Germany
E-mail: janiak@hhu.de
https://www.ac1.hhu.de
[b] Dr. S.-J. Ernst, Dr. S. K. Henninger
Dept. Thermally Active Materials and Solar Cooling, Fraunhofer Institute for Solar Energy Systems ISE,
Heidenhofstr. 2, 79110 Freiburg, Germany
https://www.ise.fraunhofer.de
ORCID(s) from the author(s) for this article is/are available on the WWW under https://doi.org/10.1002/ejic.202000834.

Part of the German Chemical Society ADUC Prizewinner Collection

amorphous materials, so their microstructure is not precisely known.

In the last few years, water sorption has become an increasingly important research field.[21,22] This also includes the possible use of porous materials to adsorb and desorb water vapor under atmospheric conditions without external power sources as a promising methodology for the capture and release of water in arid or desert regions of the world. The potential of metal-organic frameworks as water harvesting materials for freshwater production in dry regions with medium or high humidity conditions during the night appears to have first been tested by Kim et al.[23] and Trapani et al. in 2016,[24] The possible generation of drinking water through the adsorption of moisture from the air was then followed-up by Yaghi and co-workers in 2017. The energy-efficient adsorption of atmospheric water and its separation for subsequent use still represents a technical and economic challenge.[25–29]

One obstacle on the way to broader applications of MOFs has long been their insufficient hydrothermal stability (see below).[30] However, in the meantime MOFs are known to be stable against prolonged contact with water, and not only because of their high hydrophobicity (as with ZIF-8). This has opened up the potential application of cyclic water sorption with water-stable MOFs in adsorption heat pumps (AHPs), including adsorption chillers.[31] Physical adsorption and desorption processes on inner surfaces of highly porous materials, can be used to convert heat in heat transformation processes.[32] Adsorption is a process of adhesion of atoms, molecules, or ions of a gas or liquid at the surface of a solid or liquid. Most research focuses on adsorption on the solid surface and physisorption, i.e. the process in which the adsorbed species do not form chemical bonds with the surface but only bind through physical forces (dispersion, electrostatic, etc.).

A simple setup illustrates the working cycle (Figure 2) in which cold is generated, which can be used for cooling processes, from the evaporation of water which is driven by adsorption into the activated porous sorption material.

Figure 3 depicts the underlying principle of closed cycling adsorption heat transformation systems. The heart of such systems is the working pair consisting of an adsorbent and a working fluid. During the first stage of this two-stage-process, the active (dry, porous) adsorbent physisorbs the working fluid that is evaporated by taking up heat (Q_{in}) and thereby generating useful cold. The released heat of adsorption in the adsorbent is led away or used as heat ($Q_{out,1}$). During the desorption stage, heat has to be applied to the filled (wet) adsorbent (Q_{drive}) in order to induce the desorption of the working fluid. The working fluid is condensed by leading away or using the heat of condensation ($Q_{out,2}$) on a medium temperature level. $Q_{out,1}$ and $Q_{out,2}$ can be applied as usable heats for heating purposes.

Dominik Moritz Steinert *studied Business Chemistry and Chemistry at the Heinrich-Heine-University Düsseldorf and received his Master degree in 2017. Since then he works as a PhD student at the Heinrich-Heine University within the section of Bioinorganic chemistry under the supervision of Prof. Christoph Janiak. His research focuses on the synthesis, characterization and development of metal organic frameworks (e.g. MOFs).*

Sebastian-Johannes Ernst *studied chemical engineering at the Karlsruhe Institute of Technology and received his Diploma degree in 2014. Since then, he works at Fraunhofer Institute for Solar Energy Systems within the Division Thermal Systems and Building Technologies and did his doctorate on the topic Development and Characterization of Advanced Materials for Heat Transformation Applications under supervision of Prof. Bart/TU Kaiserslautern. Since 2019 he is head of the group Service life and material analysis.*

Stefan Kai Henninger *studied physics at the University of Freiburg and received his Diploma degree in 2002. He did his PhD at the Freiburg Material Research Center (FMF) on the topic of new adsorbents for heat storage and transformation using Monte Carlo simulations. Since 2008, he worked at the Fraunhofer ISE on materials development and characterization being head of a research group until 2018. After being responsible for the IP management and strategy of a large project he switched his position to the department heating and cooling technologies as deputy head taking care of developments with focus on high temperature heat pumps for industrial applications.*

Christoph Janiak *is full professor at the Heinrich-Heine-University Düsseldorf since 2010, with research interests in porous materials (e.g. MOFs), mixed-matrix membranes, metal nanoparticles, ionic liquids and catalysis. Currently, he is a guest professor at the Hoffmann Institute of Advanced Materials at Shenzhen Polytechnic in China. He has (co-)authored about 530 research papers.*

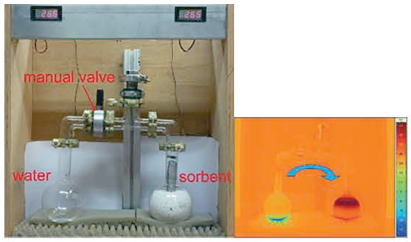

Figure 2. A simple experimental setup illustrates how the evaporation of water generates useful cold. After opening the manual valve, the water evaporates from the left-hand flask into the right-hand flask, driven by the adsorption into an empty, porous sorption material. Right: infrared image taken a few minutes after opening the manual valve. In the water flask the temperature drops to approx. –5 °C with the formation of ice; in the sorption material it rises to approx. 40 °C.[33,34] Reproduced from ref.[34]

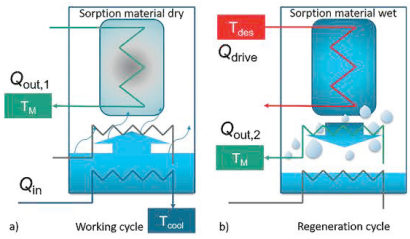

Figure 3. Schematic working principle of thermally-driven adsorption heat transformation. (a) In the working cycle, a working fluid (favorably water due to its high evaporation enthalpy and nontoxicity) is evaporated at a low-temperature level T_{cool} consuming the heat of evaporation Q_{in} which translates into useful cold. During adsorption into a porous material, heat of adsorption $Q_{out,1}$ is released at a medium temperature level T_M. (b) In the regeneration cycle, driving heat Q_{des} for desorption is applied at a high-temperature level T_{des} to regenerate the adsorbent. The released working fluid is collected in a condenser and releases condensation heat $Q_{out,2}$ at the medium temperature level T_M. The device can be used as a chiller or a heat pump.

By reversing the adsorption and regeneration in few-minute intervals, a heat pump, including an air conditioning system can be set up. In the heating mode, the heat of adsorption ($Q_{out,1}$) and heat of condensation ($Q_{out,2}$) are utilized and Q_{in} presents the additional energy gain from the environment to Q_{drive} (ideally $Q_{out,1} + Q_{out,2} = Q_{drive} + Q_{in}$), determining the coefficient of performance for heating (COP_{HP}) (see below).

In the cooling mode cold is generated essentially from heating and adsorption heat transformation (AHT) can therefore operate much more energy-efficiently than conventional air conditioning systems operated with compressors (using electrical energy), if there is the chance to use waste heat which is otherwise lost.[35] For both modes, driving heat (Q_{drive}) can be supplied by often readily available waste heat (below 100 °C) from industrial processes, solar heat, or direct heat from a gas burner.[36,37]

So far, the inorganic materials silica gels and zeolites are already used in commercial adsorption coolers and adsorption heat pumps. At low humidity, zeolites adsorb water well with up to 0.26 g of water per gram zeolite (0.26 g/g) (Figure 4), but also require a high temperature of over 200 °C for regeneration.[38,39] Silica gels bind water less well than zeolites and require only about 100 °C for regeneration (see also below). However, silica gels have only a low water adsorption capacity in the relevant vapor pressure range of 0.13 g/g (Figure 4).[40]

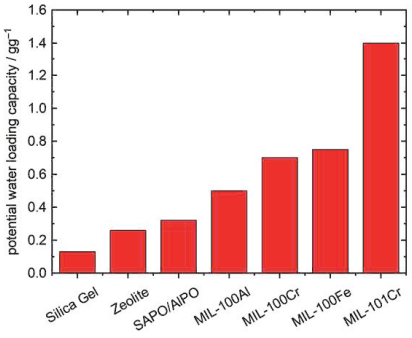

Figure 4. Comparison of typical water adsorption capacities of classical porous materials and MOFs of the MIL type,[68] for the possible use in adsorption driven heat pumps.[35] The loading capacity (in g of water/g of dry sorbent material) is the uptake or loading lift within an adsorption-desorption cycle. The water stability of some of the MIL networks was confirmed over a large number of adsorption and desorption cycles (MIL-100Al and MIL-100Fe,[67] MIL-100Cr,[66] MIL-101Cr[34]).

A sorption material for thermal adsorption chillers and adsorption heat pumps should have a high water adsorption capacity at low to medium relative humidity (5–35 %, that is 0.05 < p/p_0 < 0.35), release the water vapor below 80 °C and have a water uptake during each cycle of at least 0.3 g/g.[35,41] This value is two to three times higher than the mass-based g/g working capacity of silica gel within the stated boundaries.

A broad variety of different adsorbent-adsorbate working pairs is already investigated for sorption heat transformation.[37,42] Each one of these classes has its own distinct field of application, e.g. activated carbon-methanol for cooling, SAPO-34-water for heating, silica gel for certain cooling applications, zeolite 13X for heat storage, not to mention the vast variety of salt-based adsorbents and composites for any of these applications. Activated carbons are rather low-cost and hydrophobic materials and have high adsorption capacities for alcohol and ammonia.[43,44] Silica gel is one of the most used adsorbents in commercially available AHTs due to its low cost and stability, despite its less favorable linear water uptake curve instead of the S-shaped isotherm and low water uptake of 0.03 to 0.1 g/g.[45,46] The recently developed AHT technique "Heat from Cold" (HeCol) uses LiCl-silica gel/methanol as working pair.[47,48] LiBr-silica and $CaCl_2$-silica[49] appear to be superior composite adsorbents with the working fluid water for air conditioning and heat pumping. For refrigeration, where water freezes and cannot be used as adsorbate, LiBr-silica with methanol and ethanol was found as promising working pair.[50] One of the biggest disadvantages of standard zeolites for AHT is their quite high hydrophilicity, which necessitates desorption temperatures up to 120 °C.[51] Modified zeolites such as Mitsubishi's adsorbent

AQSOA®-FAM-Z02,[52–54] and the SAPO-34 zeolite[55] with water as adsorbate were similar in performance to the above-noted LiBr-silica and $CaCl_2$-silica.[50] Since the focus here is set to the use of MOFs, the reader is referred to a variety of publications for further reviewing and comparing different classes of adsorbents and adsorbent-adsorbate working pairs.[51,56–60]

Further, water is the natural choice as working fluid due to its non-toxicity and its high heat of evaporation (2258 kJ/kg). However, other working fluids even though inferior in the heat of evaporation come with advantages like higher pressure levels, less problems with hydrothermal stability (for the adsorbate), and a freezing point below 0 °C (to allow for refrigeration applications). These other working fluids are methanol (1100 kJ/kg), ethanol (838 kJ/kg), ammonia (1368 kJ/kg), and even difluoromethane (45 kJ/kg). The latter two have already been proposed and tested, e.g. with the working pair activated carbon/ammonia[32,61,62] and activated carbon/difluoromethane.[63] However, to the best of our knowledge ammonia and difluoromethane have not been tested with metal-organic frameworks with respect to their use in heat transformation. Regarding methanol, it has to be stated, that methanol itself showed instabilities (e.g. ether formation) at driving temperatures above 120 °C whereas there have been no such observations for ammonia.[51,64]

The group of late Prof. Gérard Férey from the Institute Lavoisier at the University of Versailles has produced highly porous, water-stable MOF materials called MILs (MIL = Materials of Institute Lavoisier).[65] MIL materials can adsorb significantly more water than zeolites (Figure 4).[33,35,66,67,68] The zeolite-like but inorganic-organic hybrid chromium terephthalate MOF MIL-101Cr can adsorb more than its own weight of water (Figure 4).[33–35,68] At the same time, the highly porous material MIL-101Cr is stable against water and heat for a long time. MIL-101Cr is among the MOF record holders for water uptake which however takes place at a slightly too high relative pressure of 0.4.[34]

How it Started

The development of cyclic water sorption in MOFs for heat transformation in the Janiak group started with the contact to Dr. Henninger in 2009 to employ the potential of MOFs with their high porosity as sorption material in heating and cooling applications. In the Janiak group, the doctoral student Hesham A. Habib had synthesized the MOF 3D-{[$Ni_3(\mu_3\text{-btc})_2(\mu_4\text{-btre})_2(\mu\text{-}H_2O)_2$]·ca. $22H_2O$} (Figure 5) in water as solvent. This MOF contained about 30 wt.-% of crystal water with about 22 disordered water molecules where the oxygen atoms with partially occupied position could be refined in the X-ray structure.[69] At the same time this MOF could be expected to be at least somewhat water stable, because it originated from this medium. When the cycling water sorption properties of this MOF were published,[70] the MOF was denoted as ISE-1 (ISE = [Fraunhofer] Institute for Solar Energy Systems). Using the MOF ISE-1, the possibility of using MOFs for cycling water sorption for heat transformation was experimentally demonstrated for the first time,[70] after a suggestion for MOFs for adsorptive heat pumping and storage had been put forward by Aristov.[71] Subsequently, Henninger and Janiak as well as other groups examined many aspects of this area. The main focus was on the hydrothermal stability of the MOFs in combination with uptake capacity, humidity region, and synthesis from inexpensive starting materials. Furthermore, shaping of the microcrystalline MOF powder became a focus that is extremely important for almost any industrial application.

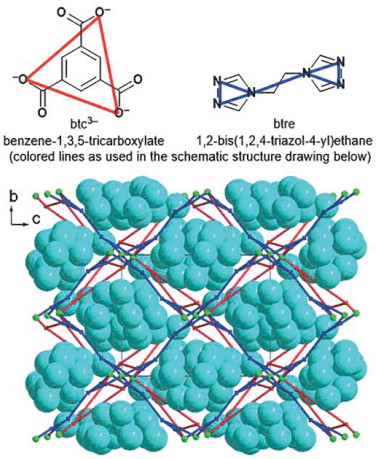

Figure 5. Schematic drawing of the 3D framework 3D-{[$Ni_3(\mu_3\text{-btc})_2(\mu_4\text{-btre})_2(\mu\text{-}H_2O)_2$]·ca. $22H_2O$} (btc ligand in red, btre ligand in dark blue, nickel atoms in green) with the oxygen atoms (light blue) of the water of crystallization in space-filling mode.[69,70] Reproduced from ref.[70] © (2009), with permission of the American Chemical Society.

Theory of Water Adsorption

The physisorption of water in porous materials can be described in two different parts, at first the attachment of layers or clusters of water molecules to surfaces or in pores until surface saturation. Subsequently, the continuous pore filling takes place, which occurs as capillary condensation in the case of small pore sizes.[72]

The capillary condensation depends on the so-called critical pore diameter (D_c), which in turn is temperature-dependent.[89] The variables included in the calculation are the van der Waals diameter of the adsorptive (σ), the measuring temperature (T), and the critical temperature of the adsorptive (T_c).[89]

$$D_c = \frac{4\sigma T_C}{(T_C - T)}$$

For water, D_c at 298 K is approximately 20 Å (2 nm). Porous materials are classified according to their pore size. According to IUPAC, microporous materials have pore sizes up to 2 nm, mesoporous ones between 2 to 50 nm, and macroporous ones have a pore diameter above 50 nm.[73] Up to the value of 2 nm the pore filling occurs continuously. At larger pore diameters the pore condensation leads to a hysteresis in the desorption isotherm.[72]

An S-shape of the sorption isotherm (IUPAC classification Type V)[74] is desirable which enables a large loading lift within a narrow relative pressure range and with the large uptake step, that is the steep rise and inflection point in the relative pressure range of $p/p_0 \approx 0.1–0.3$ for an effective usable adsorptive uptake.[75] The inflection point of the water sorption isotherms describes the relative hydrophilicity of the adsorbent. At this point, half of the maximum intake has been reached. The hydrophilicity of porous materials is a measure of the material's affinity for water, in a multi-component mixture. Hydrophilic linkers as well as small pore sizes move the inflection point to lower partial pressures.[89,76] For the uptake capacity, it is, however not the hydrophilicity, but the pore volume that is decisive.[89] The optimum inflection point and uptake pressure range should be tunable as they depend on the desired working conditions which can vary. Suitable for AHP applications are, in particular, those porous materials which have a high water uptake (adsorption) in a narrow partial pressure range and which show little to no hysteresis.[77,89] A hysteresis will reduce the usable part of the loading and lead to loss of sensible heat.[78,79] The partial pressure at which water adsorption takes place can be adjusted by pore size and hydrophilicity. These requirements make MOFs the most promising materials for further development of adsorbents for AHPs because of the easy fine-tuning of their hydrophilicity (see below). Figure 4 has already shown the advantage of MOFs in terms of water adsorption capacity.

The water sorption isotherm provides insight into the uptake mechanism and hydrophilicity/hydrophobicity of the material. Figure 6 shows five isothermal water adsorption profiles of adsorbents which differ in their hydrophilicity and porosity. A highly hydrophilic material, such as a zeolite but also a hydrophilic MOFs, such as HHU-1[80] with uniform micropores will have a steep uptake at very low p/p_0 due to strong adsorbent-adsorptive interactions in the narrow micropores from which a micropore filling at very low p/p_0 results (curve a in Figure 6). With lower hydrophilicity but still uniform microporosity, as in the MOFs NH_2-MIL-125,[81] aluminum fumarate (Alfum)[82] or CAU-10-H[78,83] the isotherm changes to an S-form with the uptake in the relative pressure range up to $p/p_0 \approx 0.3$ (curve b in 6).[84] If the material becomes more hydrophobic and may also include mesopores beside micropores, as MIL-101Cr[34] the steep S-rise shifts to higher p/p_0 (curve c in Figure 6) and may also become more gradual.[84] The isotherm curve d in Figure 6 is obtained with highly hydrophobic materials, such as activated carbons[85,86] or covalent triazine frameworks (CTFs).[87,88] There, the pores are only filled at high partial pressures. Silica gels lie with their hydrophilicity and amorphous micro-mesopore structure between these examples and show continuous water adsorption.[89]

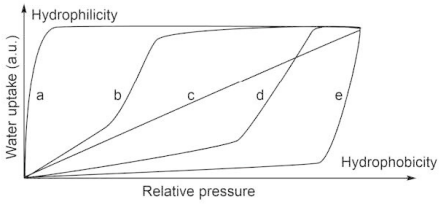

Figure 6. Comparison of different types of water adsorption isotherms. a: hydrophilic and microporous (e.g. zeolites); b: less hydrophilic, microporous (e.g. SAPO/AlPOs, hydrophilic MOFs); c) moderate hydrophilicity, amorphous micro up to mesoporous (e.g. mesoporous silica gels), d) hydrophobic, mesoporous; e) very hydrophobic (e.g. active carbon and related materials). For the version of this diagram with specific examples the reader is directed to Figure 4 in ref.[36] and to ref.[52] Noteworthy a microporous (regular density) silica gel has an isotherm of type I (a); however, less steep than a hydrophilic zeolite.

Stability of MOFs for Water Sorption

Water stability of MOFs is one of the necessary conditions for a sensible use in AHPs. For the use of MOFs in adsorption heat pumps, it is important to note that hydrothermal stability cannot be concluded by proving the structural integrity simply by immersing into and retrieving the MOF from an aqueous suspension. Instead, water stability needs to be verified through a larger number of water-vapor ad/desorption cycles (Figure 7).

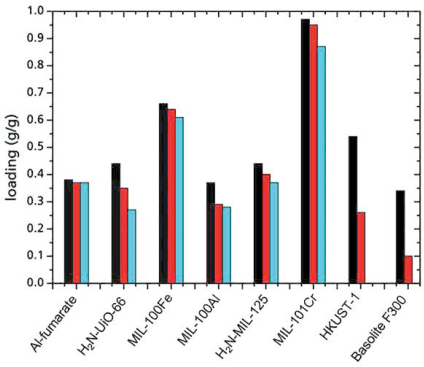

Figure 7. Water loading lift measured on Al fumarate,[82] H_2N-UiO-66,[81] MIL-100Fe,[67] MIL-100Al,[67] H_2N-MIL-125,[81] MIL-101Cr,[34] HKUST-1[35] and Basolite™ F300[35] after activation (black filled square), after 20 ad-/desorption cycles with water vapor (red filled square), and after 40 ad/desorption cycles (blue filled square). Graphic adapted from ref.[84] © (2014), with permission of the Royal Society of Chemistry.

Expected lifetimes in real adsorption-driven heat pumps are over 100,000 ad- and desorption-cycles.[35,77] The 100,000 cycles correspond to an estimate of ten years of operation in a heat pump.[77] Cycling water sorption over thousands of cycles will be impossible without very high water stability. The desired water stability depends on the metal and ligand building blocks. Stability is divided into thermodynamic and kinetic stability.[76,90,91] MOFs are 2- to 3-dimensional coordination compounds with the same stability principles which are known for molecular metal-ligand complexes. The coordinative metal-ligand bond can be viewed as a superposition of an ionic and a covalent bond. The ionic bond derives from the Coulomb interaction between a metal cation and a ligand anion or the negative end of a polar ligand molecule. A covalent metal-ligand sigma bond can be viewed as a Lewis acid (metal) –

Lewis base (ligand) (or acceptor–donor) interaction where a ligand donor atom donates its free electron pair into an empty metal orbital.

Water can react with metal-ligand complexes as a protic reagent (an acid) or as a ligand. Consequently, non-water-stable MOFs decompose either through hydrolysis or linker exchange. In the case of hydrolysis, the metal-ligand bond is broken with formation of the metal-hydroxide and the conjugated acid of the ligand.[92] During ligand exchange, a water molecule (an aqua ligand) replaces the original ligand.

$$M^{n+}\text{–}O_2C\text{-}R + H_2O \longrightarrow M^{n+}\text{–}OH + R\text{-}CO_2H$$

$$M^{n+}\text{–}O_2C\text{-}R + H_2O \longrightarrow M^{n+}\text{–}OH_2 + R\text{-}CO_2^-$$

The metal-ligand stability in terms of complex formation constant is determined by the metal cation and the ligand in equilibrium with the metal-ligand complex. The thermodynamic stability towards water can, in principle, be derived from this complex formation constant, the formation constant for the aqua-metal complex, the formation constant (or solubility product) for the hydroxido-metal complex (or metal hydroxide), and the pK_a value of the conjugated acid-base pair of the ligand. More practical, a higher covalency of the metal-ligand bonds is often viewed to go along with increased water stability. For example, azolates such as imidazolates have higher-lying nitrogen donor orbitals which are closer in energy to the empty metal orbitals and, thereby, give more covalent metal-nitrogen ligand bonds. Whereas carboxylates with their more electronegative oxygen donors yield to more ionic metal-ligand interactions. Consequently, ZIFs, where Zn2+ and imidazolate derivatives are combined, are rationalized more hydrolytically stable than MOF-5 analogs from Zn^{2+} and aryl-dicarboxylate ligands.[89,90,92] To a large extent the often noted hydrolytic stability of ZIF-8 is purely kinetic and due to the hydrophobicity of the material with almost no water uptake.[93,94] When the hydrophobicity/hydrophilicity of ZIF-8 was adjusted through linker modification as demonstrated by Zhang et al.[95] MAF-4 (ZIF-8, zinc 2-methylimidazolate) was tuned to become more hydrophilic by partial or full replacement of the linker with 3-methyl-1,2,4-triazolate in MAF-7. Replacing a C–H moiety with an isoelectronic N atom influenced the polarity of the resulting MOF strongly, where the additional N atom served as an extra adsorption site for polar water molecules.[35,95] This MAF-4 to –7 variation demonstrated the potential of MOF tailoring through partial isoreticular linker replacement (see below) but the more hydrophilic MAF-5 to –7 were no longer water stable. Figure 8 compares the water stability of different MOFs.

Qualitatively, also the HSAB concept allows a quick estimate of the bond strength. Soft acids, that are easily polarizable large metal cations in combination with low oxidation states will give stable combinations with soft bases, that are easily polarizable ligands.[89] Such soft acid–soft base interactions are orbital controlled and have a higher covalency than charge-controlled (more ionic) hard acid–hard base interactions between metal ions and ligand donor atoms of low polarizability.[76,89,90]

Besides or instead of thermodynamics, kinetics can be used to stabilize a material. In thermodynamics the Gibbs free energy (ΔG) determines stability/instability. Kinetic stability, that is inertness/lability of a compound, e.g. of a metal complex towards ligand exchange is concerned with the reaction rate (constant) and activation energy for the process. Even if a complex is thermodynamically unstable it can be kinetically inert. The well-known rate constants for the exchange of aqua ligands in aqua complexes $\{[M(H_2O)_n]^{c+} + H_2O^* - k(H_2O) \rightarrow [M(H_2O)_{n-1}(H_2O^*)]^{c+} + H_2O\}$ can be used to assess metal cations as inert or labile.[96–98] The divalent transition-metal cations from Mn^{2+} to Cu^{2+} have fast rate constants $k(H_2O)$ of over 10^6 s^{-1} for this exchange which renders their complexes rather labile. For trivalent Cr^{3+} $k(H_2O)$ is about 10^{-6} s^{-1} and Cr^{3+} complexes are generally viewed as inert. The most inert main-group metal-aqua complex is $[Al(H_2O)_6]^{3+}$ with $k(H_2O) = 1.3$ s^{-1}. Hence, Cr(III)- and Al(III)-MOFs are reasonably kinetically stable materials for AHPs. Along these lines, also Zr^{4+} and Ti^{4+} MOFs are among the more kinetically stable systems.

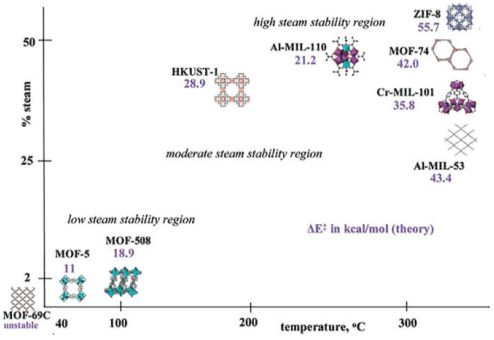

Figure 8. Hydrothermal stability of different MOFs against water vapor at different temperatures as a steam-temperature diagram. The corresponding activation energies for the MOFs, which are required for the exchange of a linker, are plotted as numerical values. Reproduced from ref.[92] © (2009), with permission from the American Chemical Society.

For MOFs, essentially three ways are discussed through which the hydrothermal decomposition can be kinetically inhibited. This includes steric shielding of the labile metal-donor atom bond, the increase of the material's hydrophobicity, and the use of rigid, inflexible linkers and metal-cluster secondary building units, SBUs.[89,76,90,92] Rigid linkers and SBUs significantly reduce linker exchange, while steric shielding makes the labile metal-linker bonds difficult to access for water molecules. The approach of hydrophobicity increase distinguishes between internal and external hydrophobicity. In the case of internal hydrophobicity, functionalization of the linker with e.g. fluorine atoms or alkyl chains slows down the approach of water molecules to the metal-linker bond. External hydrophobicity, on the other hand, prevents water molecules from penetrating into the pores of the material.[89,76]

The difference between the stability towards liquid water and towards water vapor in ad/desorption cycles can be explained by the water phase change enthalpy, the head of adsorption which is released at the adsorption site, i.e., in the MOF. Such adsorption enthalpies have been calculated to lie in the range of ligand displacement energies. In addition, water

molecules are constantly moved in and out of the porous material during cyclic ad/desorption processes. This increases the chance of metal-ligand bond hydrolysis and stresses the framework by the alternating forces created through cavitation (moving in) and capillary forces (moving out). For example, the Zr-MOF UiO-67 was shown to be stable towards linker hydrolysis in H_2O, but collapses during activation, that is desorption of H_2O from the pores through capillary-force-driven channel collapse.[99]

Linker Functionalization for Increased Hydrophilicity

A possibility to increase the hydrophilicity of a MOF is the functionalization of the aromatic spacer on the linker with an amino group. The amino-aryl function provides hydrogen-bond donor sites and thus an increased affinity of the MOF for water.[81,84] When UiO-66 and MIL-125 with their non-functionalized terephthalate linkers (O_2C-C_6H_4-CO_2) were compared to the analogs H_2N-UiO-66 and H_2N-MIL-125 with the 2-amino-terephthalate linker (O_2C-$C_6H_3(NH_2)$-CO_2)[81] the amino-functionalized MOFs showed a water uptake at lower p/p_0 (Figure 9). H_2N-MIL-125 also exhibited an extremely promising adsorption isotherm with the steep S-rise between 0.1 and 0.2 (p/p_0) being ideal for use in heat pumps. At the same time, H_2N-MIL-125 was shown to be stable to hydrolysis in over 40 water sorption cycles (Figure 9).

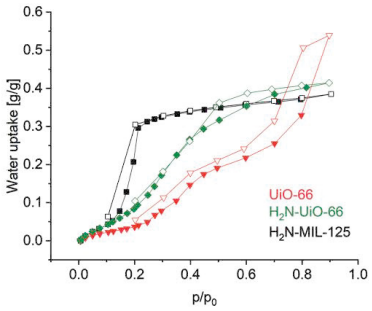

Figure 9. Water adsorption/desorption isotherms of UiO-66 (red), H_2N-UiO-66 (green) and H_2N-MIL-125 (black), acquired at T = 25 °C.[81] Adsorption: filled symbols; desorption: empty symbols.

Mixed Linker

In addition to functionalization, it is also possible to modulate the hydrophilicity or hydrophobicity of MOFs by using mixed linker systems. For example, Schlüsener et al. recently investigated a "solid solution" mixed-linker approach for aluminum MOFs.[100,101] Aluminum MOFs are particularly promising for industrial applications because aluminum salts are low cost and readily available starting materials, and their MOFs are rather hydrothermally robust materials which can also be manufactured in an environmentally friendly aqueous and even continuous route.[78,82,83,102,103] Schlüsener et al. were able to modulate the hydrophilicity between the two water-stable MOFs CAU-10-H and MIL-160 by varying the proportions of the two (commercially inexpensive) linkers (isophthalic acid and furandicarboxylic acid).

CAU-10-H[104] is currently the most realistic stable known MOF for hydrothermal cycling between 40 °C adsorption and 140 °C desorption temperature, with proven stability of 10,000 water adsorption-desorption cycles.[78] It has a BET surface area of over 1000 m^2/g and a water uptake of 0.33 g/g, even below the relative pressure of 0.2, which is significantly earlier than comparable MOFs.[105]

The tuning made it possible to continuously adjust the water adsorption in between the p/p_0 limits set by the two single-ligand MOFs. Figure 10 depicts the modulation of the hydrophilicity, i.e. the fine-tuning of the p/p_0 range of the water uptake step between MIL-160 and CAU-10-H thereby maintaining the single-step and high-uptake characteristics of the single-ligand starting MOFs.

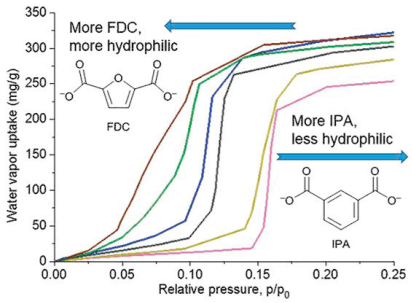

Figure 10. Fine-tuning of water adsorption curves with solid solution mixed-linker aluminum MOFs with varying furandicarboxylate and isophthalate linker proportions between (from left to right) neat MIL-160 (FDC-only, brown), IPA:FDC 22:78 (green), 53:47 (blue), 74:26 (grey), 85:15 (olive), neat CAU-10-H (IPA only, pink).[101] Reproduced from ref.[81] © (2019), with permission the American Chemical Society.

The above mixed-linker approach was only successful because of the very close isostructural MOF frameworks of MIL-160 and CAU-10-H. An only superfluous structural similarity may not be sufficient to yield such mixed-linker solid solution materials. Such was the case with the attempt to tune the water uptake between the MOFs CAU-23 (with 2,5-thiophenedicarboxylate, TDC) and MIL-160 (with FDC).[101] This attempt was made as CAU-23[106] and MIL-160[107,108] are seen as two of the most promising adsorbents for heat transformation.

All of the aforementioned Al-MOFs share fourfold helical chains of bis-OH and tetrakis-CO_2 bridged $\{Al(OH)_2(O–C–O)_4\}$-polyhedra as the inorganic building unit, which are interconnected by the linkers to the 3D framework structures with square-shaped one-dimensional channels. The slight and easily overlooked difference lies in the or *cis*-$(OH)_2$ and *trans*-$(OH)_2$ connection of the $\{Al(OH)_2(O–C–O)_4\}$ octahedra which in turn depends on the opening angle between the di-carboxyl groups (Scheme 1).

MIL-160 and CAU-10-H, which enable the formation of solid solution mixed-linker networks, share the *cis*-$(\mu\text{-}OH)_2$ connectiv-

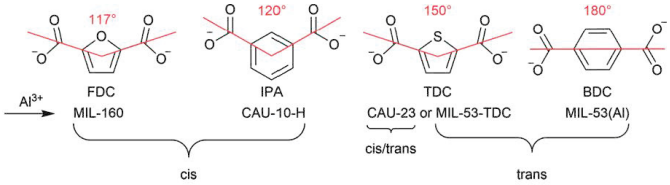

Scheme 1. Schematic illustration of linker molecules relevant in this work, their opening angles, and the resulting MOFs with their *cis*- and/or *trans*-$(\mu\text{-OH})_2$ connectivity of the $\{Al(OH)_2(O\text{–}C\text{–}O)_4\}$ octahedra.

ity of the $\{Al(OH)_2(O\text{–}C\text{–}O)_4\}$ octahedra. CAU-23 on the other hand features *cis*- and *trans*-connected $\{Al(OH)_2(O\text{–}C\text{–}O)_4\}$ along the chain. There is also a polymorph to CAU-23 in the form MIL-53-TDC with trans-only OH-bridges.[109] MIL-53-TDC also exhibits highly interesting water sorption properties with high hydrothermal stability and a favorable low isosteric heat of adsorption and a driving heat (for regeneration) below 65 °C.[110]

The different cis or trans connectivity of the infinite $\{Al(\mu\text{-OH})(O_2C\text{-})\}$ SBU apparently prevented the formation of clearly identifiable mixed-linker MOFs. Consequently, the three MOFs MIL-160, CAU-23, and MIL-53-TDC, which differ in *cis* and *trans* connectivity in their SBUs (Scheme 1), do not lead to a solid solution as in the case of CAU-10-H and MIL-160, but to mixed-MOF phases that are present side by side as in a physical mixture. The verification of mixed-MOF vs. mixed-linker proved, however, difficult since the differentiation via powder X-ray diffractometry (PXRD), IR-spectroscopy, and nitrogen sorption was either not conclusive enough or impossible, due to similarities (in PXRD) of the neat MOF phases. It was the curvature of the water sorption isotherms which indicated the simultaneous formation of the different MOF phases (albeit do not fully exclude mixed-linker MOFs which may form at low levels of substitution). Depending on the number and the position of the uptake steps, the different MOF phases could be discerned (Figure 11). Noteworthy, the MOF mixtures were obtained in-situ from one-pot syntheses of different linker mixtures. The resulting MOF mixtures then exhibited two or three uptake steps in their water sorption isotherms, corresponding to an overlay from the individual water sorption isotherms of MIL-160 (inflection point $p/p_0 \approx 0.07$), CAU-23 ($p/p_0 \approx 0.26$), and MIL-53-TDC ($p/p_0 \approx 0.33$) (Figure 11). The third water uptake step after 0.30 p/p_0 for MIL-53-TDC, was especially pronounced for the mixed-MOF material which was prepared from a 1:1 mixture of FDC and TDC. This was somewhat remarkable as the synthesis of MIL-53-TDC was hitherto unknown from purely aqueous synthesis conditions.[100]

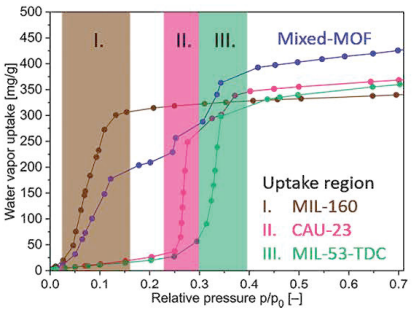

Figure 11. Comparison of uptake regions and water uptake from MIL-160, CAU-23, MIL-53-TDC, and the Mixed-MOF (purple-blue), containing a near 1:1 mixture of the TDC and FDC linker.[100] Reproduced from ref.[80] © (2019), with permission from the Royal Society of Chemistry.

Shaping

The shaping of the material is a necessary condition for the successful commercial application of MOFs. Traditionally, MOFs are obtained in the synthesis as microcrystalline powders, which in this form cannot be used or can only be used poorly in applications or devices. Suitable dosage forms for industrial applications are, for example, pellets, granules, monoliths, or membranes.[12,111–114]

The integration of porous materials in AHP devices requires close contact with a (metal) heat exchanger for the efficient and rapid dissipation of the heat of adsorption ($Q_{out,1}$) and the driving heat (Q_{drive}). Any increase in temperature within the sorption material during the working cycle (Figure 3) counteracts the desired uptake of the adsorbate. The close contact can be achieved by using a bulk of loose grains filled between the lamellae of a heat exchanger (Figure 12), by using monolayers of grains fixed/glued to the surface of the heat exchanger, by using binder coatings of small material particles or by using direct crystallization e.g. through partial support transformation into the porous material. For the latter three cases, the long-term mechanical stability is critical and must be ensured.[115,116] Although the latter three alternatives to fixed bed heat exchangers are more efficient, the fixed-bed technique is common because of its simplicity and its long-term mechanical stability.

In a proof-of-principle study, Gökpinar et al. prepared millimeter-scaled grains ca. 2 mm diameter of the Al-MOFs MIL-160 and Al-fumarate through the freeze granulation method (Figure 12) together with a pelleting device. Aluminum fumarate (Al-fum, commercially known as Basolite™ A520) is a very affordable MOF to manufacture. It is made at 60 °C from fumaric acid and (almost) any Al^{3+}salt sources in aqueous solution.[117] The BET surface area is around 1000 m^2/g and the water uptake is around 0.35 g/g. These properties, combined with an adsorption range at 0.2–0.3 relative pressure, make aluminum fumarate a suitable candidate for replacing silica gels in heat and cold applications. In addition, aluminum is stable over more

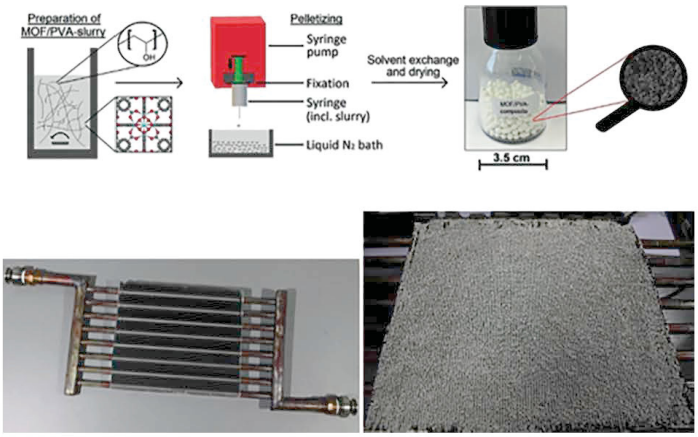

Figure 12. Top: freeze granulation process of MOF/polyvinyl alcohol (PVA) composites. Bottom: pipe-lamella heat exchanger unfilled (left) and filled (right) with pellets.[31] Reproduced from ref.[30] © (2019), with permission from the American Chemical Society.

than 4500 ad- and desorption cycles and has already been successfully tested in a heat pump prototype.[118] Poly(vinyl alcohol) (PVA) as binder gave highly mechanical and water stable, uniformly shaped MOF/PVA grains with 80 wt.-% MOF loading where the porosity properties of the MOFs were retained as verified by water adsorption isotherms, over 1000 water adsorption/desorption cycles and thermal and mechanical stability tests. The pellets withstood mechanical loads of up to 79 N. The Al-fumarate/PVA pellets were placed between the lamellae of a pipe-lamella heat exchanger, Dynamic adsorption and cooling performance testing provided specific cooling powers (SCP) from 349 up to 431 W/kg(adsorbent), which is better than current commercially used silica gel grains in AHPs under comparable operating conditions.[31]

Another promising shaping method for MOF/polymer monoliths was presented by Hastürk et al.[119,120] based on Sun's method of phase separation (Figure 13).[121] The Al-fum/PVA composites with a MOF loading of 50 to 80 wt.-% even exhibited an increased porosity. which was traced to additional mesopores from interfacial voids which were formed between Al-fum-particles and the PVA polymer. This additional interfacial volume leads in turn to an increase in water uptake capacity compared to the neat/pure MOF. The composites obtained had mechanical stability up to 63 N.

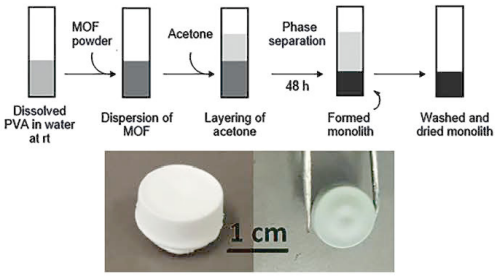

Figure 13. Top: schematic fabrication procedure of MOF/PVA monoliths via phase separation. Bottom: photographic images of Al-fum50/PVA2 (left) and MIL-101(Cr)40/PVA1 monolith (right).[120] Reproduced from ref.[100] © (2019), with permission from Elsevier.

Application

Meanwhile, many different methodologies have been envisioned for metal-organic frameworks suitable for water adsorption applications. These can roughly be divided into closed and open cycles.

Depending on the working mode (chiller or heat pump), different temperature levels are used and the efficiency, the so-called Coefficient of Performance (COP), can be defined differently. In both cases, the effort to spend is Q_{drive}. It is very important to note that the COP values vary with the working conditions, that is the adsorption temperature, condenser temperature, and evaporator temperature which in turn are chosen according to the sorption properties of the adsorbent-adsorbate working pair.[37]

In the heat pump mode, $Q_{out,1}$ and $Q_{out,2}$ are used for heating applications like floor heating or radiators. In this case, Q_{in} is the heat of evaporation that has been taken up from the environment, for instance by an earth probe.

The COP for the heat pump mode (COP_{HP}) is defined by:

$$COP_{HP} = \frac{-(Q_{out,1} + Q_{out,2})}{Q_{drive}}$$

In the chiller mode, a surrounding is cooled by evaporation of the working fluid and Q_{in} constitutes the useful cold, whereas the heat on medium temperature levels ($Q_{out,1}$ and

$Q_{out,2}$) has to be rejected to the environment. The COP for the chiller mode (COP_{Ch}) is defined by:

$$COP_{Ch} = \frac{Q_{in}}{Q_{drive}}$$

The COP_{Ch} values range from zero to less than 1 and COP_{HP} values range from one to less than two.[36] Chillers have already been commercialized, for instance by the companies Fahrenheit and Invensor. These systems reach COPs up to 0.75 (Invensor LTC 90e Plus). The adsorbents used in these systems are typically silica gel or a zeotype like SAPO-34.

Besides the efficiency or COP, the power and even more the power density of a heat transformation device is of major importance. Usually, the power *P* is defined as the ratio of mean heat gained over a half cycle (Q_{ads}) per half-cycle time (t_{cyc}):

$$P = \frac{Q_{ads}}{t_{cyc}}$$

The power density can be defined either with respect to the volume or to the mass. However, when presenting these values, the reference system (material, adsorber, module···) has to be provided.

Open Cycles

When it comes to open cycles, there are two major applications: In thermal heat storage, waste heat is used to charge the storage by desorption of the adsorbent. As soon as heat is to be used, the storage can be discharged by a humid air stream flowing through the adsorbent bed. The performance, ecological and economic efficiency is highly dependent on the number of cycles per year due to heat losses.[122,123]

The other main application is air conditioning, for instance, drying of industrial process air (e.g. clean room) or air conditioning in non-residential buildings. For the latter, a comfort zone is defined in DIN EN 12779. The minimum and maximum temperatures and humidities herein are 20 to 26 °C and 30 to 65 % r.h. This comfort zone is depicted in Figure 14 in a Mollier diagram (light blue area). The target state of the ingoing air is usually at around 18 °C and 8 g kg^{-1}. In conventional systems, emanating from typical summer conditions (red circle, 35 °C and 15 g kg^{-1}) this state is reached by first cooling the air to the saturation line, then dehumidifying the air by condensation and finally heating of the air.

A most elaborated adsorption air conditioning process is the so-called *desiccant and evaporative cooling* (DEC) process (Figure 14, dashed line). In such a process, the ingoing air is dehumidified by an adsorbent and simultaneously heated by the released heat of adsorption (1 → 2), precooled by the air that comes from the building (2 → 3) and then humidified and

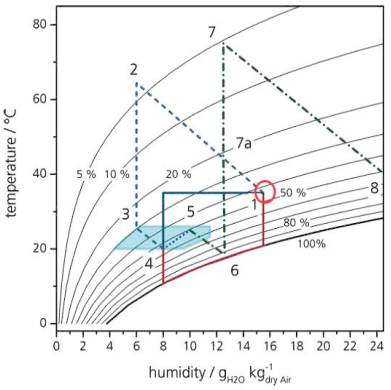

Figure 14. Process paths of a solid desiccant cooling (SDC) system (") and of a desiccant and evaporative cooling (DEC) system (·: ingoing air, —: outgoing air) are depicted in comparison to a conventional A/C system (") in a Mollier-diagram.

adiabatically cooled (3 → 4). The air coming from the building is first adiabatically cooled (5 → 6) and then used to precool the ingoing air (6 → 7a). In the last step the air is heated (7a → 7) and used for the regeneration of the adsorbent (7 → 8).[124] Power and efficiency of this process are mainly determined by the heat of adsorption and the necessary desorption temperature.[128]

In the aforementioned processes, the temperature boundaries are set by the application and humidities that are listed in Table 1 and plotted transferred to relative pressures in Figure 15. The colored areas show the working windows for the different applications. Therefore, an adsorbent has to be chosen according to the application. The necessary properties of an adsorbent are high uptake within the boundaries and stability against thermal and adsorption induced stress. The uptake capacity depends on geometrical parameters like pore volume and specific surface as well as on surface chemistry.

A great effort has been spent finding materials that match the different boundary conditions and has lately been exhaustingly reviewed.[76] Amongst the above mentioned metal-organic frameworks, MIL-160(Al) has been evaluated as a promising material for heat transformation and storage.[105,108] The work of Schlüsener and co-workers demonstrated the possibilities to tune the adsorption characteristics by a mixed linker approach varying the linker from furandicarboxylic acid to isophthalic acid yielding a mixture of MIL-160 and CAU-10-H structure.[101] These mixed-linker materials can be used at the standard conditions (evaporator temperature of 10 °C; mid. T of 40 °C) applying lower desorption temperatures. Therefore, these

Table 1. Boundary temperatures for open and closed thermally-driven applications.

	closed			open	
	Heat pump	Chiller	Server cooling	Heat storage	Dehumidification
Evaporator	−10–15 °C	−15–25 °C	18–22 °C	−10–22 °C	8–17 °C
Adsorber/Condenser	35–65 °C	20–37 °C	27–32 °C	25–100 °C	30–50 °C
Desorption	95–250 °C	55–95 °C	55–65 °C	100–250 °C	50–95 °C

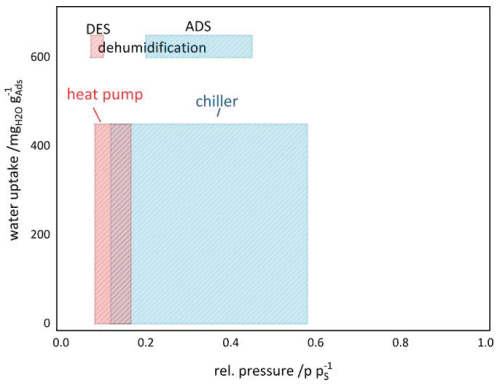

Figure 15. Working windows of possible application based on water adsorption.

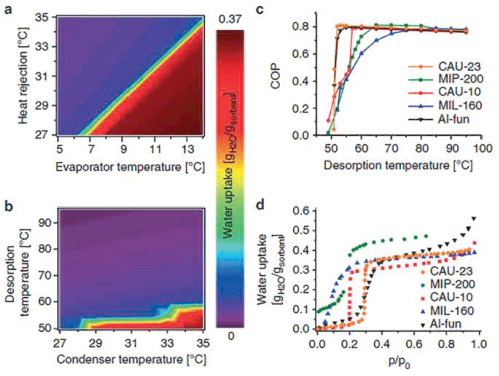

Figure 16. Calculation of adsorption driven chiller temperature boundaries for CAU-23 and coefficient of performance for cooling in comparison with selected state of the art materials. Calculated loading of CAU-23 for different temperatures used in an ADC setup for adsorption **a**, and desorption cycle **b**. Calculation of the COP values for different driving temperatures (assumed desired cooling of 10 °C and back cooling temperature of 30 °C). **d** Water adsorption curves at 40 °C of selected compounds. Reproduced from ref.[106] © (2019), with permission from Springer Nature.

materials show higher COP values at lower desorption temperatures.

Since water has the disadvantage of freezing at temperatures below 0 C, methanol has been investigated as a possible working fluid with HKUST-1 and MIL-101(Cr) showing COP-values higher than 1 for evaporator temperatures below 0 °C and adsorption temperatures between 40 °C and 50 °C. Later, MIL-53-muc was shown to yield a COP_{HP} of over 1.6 for evaporator temperatures of 0 °C and of almost 1.4 for evaporator temperatures of –10 °C by researchers of the Janiak group.[126–129]

The same MOF has also been evaluated for the use in adsorption chillers with a COP_{CH} of over 0.7 at ice-making conditions surpassing the performance of activated carbon/methanol.[129–134]

When it comes to adsorption chillers, metal-organic frameworks fully develop their potential due to their well-balanced hydrophilicity and the possibility to adjust the adsorption characteristics according to the application. An impressive example is the development of MIL-53-TDC showing sufficient water uptake capacities of 0.35 g·g^{-1} for comparably high evaporation temperatures of above 15 °C and/or heat rejection below 30 °C. At this condenser temperature, the MOF can be fully dried at desorption temperatures of only 60 °C.[110] This development pathed the way towards MOFs for ultra-low temperature-driven cooling yielding in the isostructural MOF CAU-23 As can be seen from Figure 16 this MOF yields a very high cooling COP_{Ch} of 0.8 at ultra-low temperature of less than 55 °C and typical cooling conditions of 10 °C and 30 °C.[106] (Figure 16).

Thermal batteries can be seen as a sub-category of thermal heat storage based on a closed cycle. The working principle is described in detail elsewhere.[135–137] The targeted performance as defined by the U.S. Department of Energy is a minimum heat storage capacity of 2.5 kW h with the condition of the maximum weight of the heat exchanger system of 35 kg.[138] Just recently, a composite material of LiCl@UiO-66 has been proven to be able to fulfil the capacity by use of only 10 kg of this material outperforming the benchmark material up to this date.[139]

Conclusions

With their high-water adsorption capacity, MOFs can significantly expand the existing inorganic sorption materials for heat transformation applications through the cycling ad- and desorption of water. The water adsorption behavior of MOFs can be controlled by the hydrophilic nature of the linker, i.e. the organic bridging ligand. On the way to a mature application, further optimizations of the kinetics of water sorption and the proof of hydrothermal stability for more than 100,000 adsorption and desorption cycles are necessary. In place of water, alcohols are also possible working fluids, thus extending the range of MOFs that can be used. Some MOFs are already industrially produced today (e.g. by BASF and marketed under the name Basolite™). A current challenge is still the processing of MOFs into shaped parts and the deposition and adherence of MOFs on surfaces. By solving these challenges, heat and mass transfer can be further improved, making MOFs sought-after new materials for numerous future tasks in heat transformation and storage, but also catalysis, gas separation, and storage.

Outlook and Future Challenges

As shown within this review, the development of materials made a great success, and a lot of great materials have been identified showing steep water uptake curves within the whole area of relative pressures, also techniques have been proposed to further shape the water uptake curves. To push these materials further towards the application, the research should be oriented on the application. New materials usually make it into the application when they either come with a new function or they fulfil a needed task better or cheaper as compared to state-of-the-art materials. In the case of MOFs for heat transformation, MOFs have to compete with activated carbon, silica

gel, and zeotypes, all well researched and developed materials. Although further work should be invested to decrease the synthesis effort of MOFs, they might never become competitive to silica gels or zeolites in terms of cost per mass of dry powder. Also, when it comes to comparing the volumetric loading (water mass uptake per *volume* of adsorbent, e.g. kg m^{-3}) or to power density (generated heating or cooling power per *volume* of adsorbent, e.g. kW m^{-3}) MOFs are only partly competitive to commercial silica gels due to the low specific density of MOFs.[140] Therefore, MOFs have to become more competitive in terms of cost per (volume) specific power. This may either be achieved by adjusting material characteristics in terms of higher uptake per volume of MOF or by improving heat and mass transfer by optimized shaping technologies. When it comes to shaping, it would be beneficial to provide a solution that can be employed in existing technologies easily, leading to either (directly) coated heat exchangers or granules in the size of silica gel granules that can be glued on heat exchanger structures with established approaches.

To further ensure the long time stability, the stability should be within the focus of further research not only in the case of hydrothermal cycles but also in the case of compatibility of the MOFs in combination with a supporting structure like the heat exchanger materials, binding agents, and the working fluids. Here, issues like outgassing, adhesion, fouling, corrosion, and decomposition have to be further understood and taken care of.

Last but not least, life cycle analyses are under-presented in this field, especially taking into account that the technology of heat transformation is intended to save CO_2. Profound LCA studies starting at the synthesis of MOFs and taking also into account the full operating lifetime will definitely be guiding further needs for research and development.

Acknowledgments

Funding by the German Federal Ministry of Economics (BMWi) for the project Nextsol under grant-# 0327851A/B and by the German Federal Ministry of Education and Research (BMFT) for the project Optimat under grant 03SF0492A/C is gratefully acknowledged. Open access funding enabled and organized by Projekt DEAL.

Keywords: Adsorption-driven heat pumps · Adsorption heat transformation · Metal-organic frameworks · Sorption materials · Water sorption

[1] S. R. Batten, N. R. Champness, X.-M. Chen, J. Garcia-Martinez, S. Kitagawa, L. Öhrström, M. O'Keeffe, M. Paik Suh, J. Reedijk, *Pure Appl. Chem.* **2013**, *85*, 1715–1724.
[2] C. Janiak, *Dalton Trans.* **2003**, 2781–2804.
[3] C. Janiak, J. K. Vieth, *New J. Chem.* **2010**, *34*, 2366–2388.
[4] A. Schoedel, S. Rajeh, *Top. Curr. Chem.* **2020**, *378*, 19.
[5] J. D. Evans, B. Garai, H. Reinsch, W. Li, S. Dissegna, V. Bon, I. Senkovska, R. A. Fischer, S. Kaskel, C. Janiak, N. Stock, D. Volkmer, *Coord. Chem. Rev.* **2019**, *380*, 378–418.
[6] H.-C. Zhou, S. Kitagawa, *Chem. Soc. Rev.* **2014**, *43*, 5415–5418.
[7] J. R. Long, O. M. Yaghi, *Chem. Soc. Rev.* **2009**, *38*, 1213–1214.
[8] R. B. Getman, Y.-S. Bae, C. E. Wilmer, R. Q. Snurr, *Chem. Rev.* **2012**, *112*, 703–723.
[9] K. Adil, Y. Belmabkhout, R. S. Pillai, A. Cadiau, P. M. Bhatt, A. H. Assen, G. Maurin, M. Eddaoudi, *Chem. Soc. Rev.* **2017**, *46*, 3402–3430.
[10] J. Dechnik, C. J. Sumby, C. Janiak, *Cryst. Growth Des.* **2017**, *17*, 4467–4488.
[11] J. Dechnik, J. Gascon, C. J. Doonan, C. Janiak, C. J. Sumby, *Angew. Chem. Int. Ed.* **2017**, *56*, 9292–9310; *Angew. Chem.* **2017**, *129*, 9420.
[12] H. B. Tanh Jeazet, C. Staudt, C. Janiak, *Dalton Trans.* **2012**, *41*, 14003–14027.
[13] A. Nuhnen, D. Dietrich, S. Millan, C. Janiak, *ACS Appl. Mater. Interfaces* **2018**, *10*, 33589–33600.
[14] M. A. Carreon, S. R. Venna *"Metal Organic Framework Membranes for Molecular Gas Separations"*. Vol 6, World Scientific. **2020**.
[15] S. M. J. Rogge, A. Bavykina, J. Hajek, H. Garcia, A. I. Olivos-Suarez, A. Sepúlveda-Escribano, A. Vimont, G. Clet, P. Bazin, F. Kapteijn, M. Daturi, E. V. Ramos-Fernandez, F. X. Llabrés i Xamena, V. Van Speybroeck, J. Gascon, *Chem. Soc. Rev.* **2017**, *46*, 3134–3184.
[16] L. Wang, M. Zheng, Z. Xie, *J. Mater. Chem. B* **2018**, *6*, 707–717.
[17] W. Chen, C. Wu, *Dalton Trans.* **2018**, *47*, 2114–2133.
[18] X. Lian, Y. Fang, E. Joseph, Q. Wang, J. Li, S. Banerjee, C. Lollar, X. Wang, H.-C. Zhou, *Chem. Soc. Rev.* **2017**, *46*, 3386–3401.
[19] S. Cohen, *Chem. Sci.* **2010**, *1*, 32–36.
[20] O. K. Farha, A. Ö. Yazaydin, I. Eryazici, C. D. Malliakas, B. G. Hauser, M. G. Kanatzidis, S. T. Nguyen, R. Q. Snurr, J. T. Hupp, *Nat. Chem.* **2010**, *2*, 944–948.
[21] *World Economic Forum, Global Risks **2015***, 10th Edition (World Economic Forum, Geneva, Switzerland, **2015**, accessed Aug, 2020. http://www3.weforum.org/docs/WEF_Global_Risks_2015_Report15.pdf.
[22] M. M. Mekonnen, A. Y. Hoekstra, *Sci. Adv.* **2016**, *2*, 1500323.
[23] S.-I. Kim, T.-U. Yoon, M.-B. Kim, S.-J. Lee, Y. K. Hwang, J.-S. Chang, H.-J. Kim, H.-N. Lee, U.-H. Lee, Y.-S. Bae, *Chem. Eng. J.* **2016**, *286*, 467–475.
[24] F. Trapani, A. Polyzoidis, S. Loebbecke, C. G. Piscopo, *Microporous Mesoporous Mater.* **2016**, *230*, 20–24.
[25] H. Kim, S. Yang, S. R. Rao, S. Narayanan, E. A. Kapustin, H. Furukawa, A. S. Umans, O. M. Yaghi, E. N. Wang, *Science* **2017**, *356*, 430-434.</jnl>
[26] M. S. Hanikel, F. Prevot, E. A. Fathieh, H. Kapustin, H. Lyu, H. Wang, N. J. Diercks, T. G. Glover, O. M. Yaghi, *ACS Cent. Sci.* **2019**, *5*, 1699–1706.
[27] A. J. Rieth, A. M. Wright, S. Rao, H. Kim, A. D. LaPotin, E. N. Wang, M. Dinca, *J. Am. Chem. Soc.* **2018**, *140*, 17591–17596.
[28] E. Elsayed, R. Al-Dadah, S. Mahmoud, A. Elsayed, P. A. Anderson, *Appl. Therm. Eng.* **2016**, *99*, 802–812.
[29] R. Al-Dadah, S. Mahmoud, E. Elsayed, P. Youssef, F. Al-Mousawi, *Energy* **2020**, *190*, 116356.
[30] K. Leus, T. Bogaerts, J. De Decker, H. Depauw, K. Hendrickx, H. Vrielinck, V. Van Speybroeck, P. Van Der Voort, *Microporous Mesoporous Mater.* **2016**, *226*, 110–116.
[31] S. Gökpinar, S.-J. Ernst, E. Hastürk, M. Möllers, I. El Aita, R. Wiedey, N. Tannert, S. Nießing, S. Abdpour, A. Schmitz, J. Quodbach, G. Füldner, S. K. Henninger, C. Janiak, *Ind. Eng. Chem. Res.* **2019**, *58*, 21493–21503.
[32] S. K. Henninger, F. P. Schmidt, H. M. Henning, *Appl. Therm. Eng.* **2010**, *30*, 1692–1702.
[33] C. Janiak, S. K. Henninger, *Chimia* **2013**, *67*, 419–424.
[34] J. Ehrenmann, S. K. Henninger, C. Janiak, *Eur. J. Inorg. Chem.* **2011**, 471–474.
[35] S. K. Henninger, F. Jeremias, H. Kummer, C. Janiak, *Eur. J. Inorg. Chem.* **2012**, *2012*, 2625–2634.
[36] M. F. de Lange, K. J. F. M. Verouden, T. J. H. Vlugt, J. Gascon, F. Kapteijn, *Chem. Rev.* **2015**, *115*, 12205–12250.
[37] D. B. Boman, D. C. Hoysall, D. G. Pahinkar, M. K. J. Ponkala, S. Garimella, *Appl. Therm. Eng.* **2017**, *123*, 422–434.
[38] J. Jänchen, D. Ackermann, H. Stach, W. Brosicke, *Solar Energy* **2004**, *76*, 339–344.
[39] F. P. Schmidt, S. K. Henninger, H. Stach, J. Jänchen, H.-M. Henning, *NoVel adsorbents for solar cooling applications*, Proceedings of the International Conference on Solar Air-Conditioning; OTTI Technology Kolleg: Staffelstein, **2005** (October 6/7); pp. 39–44.
[40] K. C. Ng, H. T. Chua, C. Y. Chung, C. H. Loke, T. Kashiwagi, A. Akisawa, B. B. Saha, *Appl. Therm. Eng.* **2001**, *21*, 1631–1642.

[41] S. K. Henninger, F. Jeremias, H. Kummer, P. Schossig, H.-M. Henning, *Energy Procedia* **2012**, *30*, 279–288.
[42] M. M. Younes, I. I: El-Sharkawy, A. E. Kabeel, B. B. Saha, *Appl. Therm. Eng.* **2017**, *114*, 394-414.
[43] A. Pal, K. Thu, S. Mitra, I. I. El-Sharkawy, B. B. Saha, H.-S. Kil, S.-H. Yoon, J. Miyawaki, *Int. J. Heat Mass Transfer* **2017**, *110*, 7–19.
[44] I. I. El-Sharkawy, K. Uddin, T. Miyazaki, B. B. Saha, S. Koyama, H.-S. Kil, S.-H. Yoon, J. Miyawaki, *Int. J. Heat Mass Transfer* **2015**, *81*, 171–178.
[45] S. Vasta, V. Brancato, D. La Rosa, V. Palomba, G. Restuccia, A. Sapienza, A. Frazzica, *Nanomaterials* **2018**, *8*, 522.
[46] H. T. Chua, K. C. Ng, A. Chakraborty, N. M. Oo, M. A. Othman, *J. Chem. Eng. Data* **2002**, *47*, 1177–1181.
[47] N. M. Voskresenskii, B. N. Okunev, L. G. Gordeeva, *Therm. Eng.* **2018**, *65*, 524–530.
[48] L. G. Gordeeva, A. Freni, T. A. Krieger, G. Restuccia, Y. I. Aristov, *Microporous Mesoporous Mater.* **2008**, *112*, 254–261.
[49] Y. I. Aristov, G. Restuccia, G. Cacciola, V. N. Parmon, *Appl. Therm. Eng.* **2002**, *22*, 191–204.
[50] A. Freni, G. Maggio, A. Sapienza, A. Frazzica, G. Restuccia, S. Vasta, *Appl. Therm. Eng.* **2016**, *104*, 85–95.
[51] S. K. Henninger, S.-J. Ernst, L. Gordeeva, P. Bendix, D. Fröhlich, A. D. Grekova, L. Bonaccorsi, Y. Aristov, J. Jaenchen, *Renewable Energy* **2017**, *110*, 59–68.
[52] Mitsubishi Plastics. Zeolitic Water Vapor Adsorbent: AQSOA. http://www.aaasaveenergy.com/products/001/pdf/AQSOA_1210E.pdf (accessed 05–12–2018).
[53] H. Kakiuchi S. Shimooka M. Iwade K. Oshima M. Yamazaki S. Terada, H. Watanabe, T. Takewaki, *Kagaku Kogaku Ronbunshu* **2005**, *31*, 273–277.
[54] H. Kakiuchi S. Shimooka M. Iwade K. Oshima, M. Yamazaki, S. Terada, H. Watanabe, T. Takewaki, *Kagaku Kogaku Ronbunshu* **2005**, *31*, 361–364.
[55] Y. H. H. Luo, J. L. Funke, R. D. Falconer, *Ind. Eng. Chem. Res.* **2016**, *55*, 9749–9757.
[56] B. B. Saha, E. C. Boelman, T. Kashiwagi, *ASHRAE Trans.* **1995**, *101*, 348–357.
[57] H. Wu, F. Salles, J. Zajac, *Molecules* **2019**, *24*, 945.
[58] J. M. S. Dias, V. A. F. Costa, *Renewable Sustainable Energy Rev.* **2018**, *98*, 317–327.
[59] F. Kuznik, K. Johannes, C. Obrecht, D. David, *Renewable Sustainable Energy Rev.* **2018**, *94*, 576–586.
[60] F. Shabir, M. Sultan, T. Miyazaki, B. B. Saha, A. Askalany, I. Ali, Y. Zhou, R. Ahmad, R. R. Shamshiri, *Renewable Sustainable Energy Rev.* **2020**, *119*, 109630.
[61] Z. Tamainot-Telto, S. J. Metcalf, R. E. Critoph, Y. Zhong, R. Thorpe, *Int. J. Refrig.* **2009**, *32*, 1212–1229.
[62] A. A. Askalany, B. B. Saha, *Heat Mass Transfer* **2017**, *53*, 107–114.
[63] A. A. Askalany, B. B. Saha, M. S. Ahmed, I. M. Ismail, *Int. J. Refrig.* **2013**, *36*, 1037–1044.
[64] E. J. A. Hu, *Sol. Energy* **1998**, *62*, 325–329.
[65] G. Férey, *Dalton Trans.* **2009**, 4400–4415.
[66] G. Akiyama, R. Matsuda, S. Kitagawa, *Chem. Lett.* **2010**, *39*, 360–361.
[67] F. Jeremias, A. Khutia, S. K. Henninger, C. Janiak, *J. Mater. Chem.* **2012**, *22*, 10148–10151.
[68] C. Janiak, S. K. Henninger, *Nachr. Chem.* **2013**, *61*, 520–523.
[69] H. A. Habib, J. Sanchiz, C. Janiak, *Dalton Trans.* **2008**, 1734–1744.
[70] S. K. Henninger, H. A. Habib, C. Janiak, *J. Am. Chem. Soc.* **2009**, *131*, 2776–2777.
[71] Y. Aristov, *J. Chem. Eng. Jpn.* **2007**, *40*, 1242–1251.
[72] J. Canivet, A. Fateeva, Y. Guo, B. Coasne, D. Farrusseng, *Chem. Soc. Rev.* **2014**, *43*, 5594–5617.
[73] J. Rouquerol, D. Avnir, C. W. Fairbridge, D. H. Everett, J. M. Haynes, N. Pernicone, J. D. F. Ramsay, K. S. W. Sing, K. K. Unger, *Pure Appl. Chem.* **1994**, *66*, 1739–1758.
[74] M. Thommes, K. Kaneko, A. V. Neimark, J. P. Olivier, F. Rodriguez-Reinoso, J. Rouquerol, K. S. W. Sing, *Pure Appl. Chem.* **2015**, *87*, 1051–1069.
[75] Y. I. Aristov, *Appl. Therm. Eng.* **2013**, *50*, 1610–1618.
[76] X. Liu, X. Wang, F. Kapteijn, *Chem. Rev.* **2020**, *120*, 8303–8377.
[77] E. Hastürk, S.-J. Ernst, C. Janiak, *Curr. Opin. Chem. Eng.* **2019**, *24*, 26–36.
[78] D. Fröhlich, E. Pantatosaki, P. D. Kolokathis, K. Markey, H. Reinsch, M. Baumgartner, M. A. van der Veen, D. E. De Vos, N. Stock, G. K. Papadopoulos, S. K. Henninger, C. Janiak, *J. Mater. Chem. A* **2016**, *4*, 11859–11869.
[79] A. Khutia, H. U. Rammelberg, T. Schmidt, S. Henninger, C. Janiak, *Chem. Mater.* **2013**, *25*, 790–798.
[80] T. J. Matemb Ma Ntep, H. Reinsch, B. Moll, E. Hastürk, S. Gökpinar, H. Breitzke, C. Schlüsener, L. Schmolke, G. Buntkowsky, C. Janiak, *Chem. Eur. J.* **2018**, *24*, 14048–14053.
[81] F. Jeremias, V. Lozan, S. K. Henninger, C. Janiak, *Dalton Trans.* **2013**, *42*, 15967–15973.
[82] F. Jeremias, D. Fröhlich, C. Janiak, S. K. Henninger, *RSC Adv.* **2014**, *4*, 24073–24082.
[83] D. Fröhlich, S. K. Henninger, C. Janiak, *Dalton Trans.* **2014**, *43*, 15300–15304.
[84] F. Jeremias, D. Fröhlich, C. Janiak, S. Henninger, *New J. Chem.* **2014**, *38*, 1846–1852.
[85] P. Kim, S. Agnihotri, *J. Colloid Interface Sci.* **2008**, *325*, 64–73.
[86] G. Wang, K. Leus, H. S. Jena, C. Krishnaraj, S. Zhao, H. Depauw, N. Tahir, Y.-Y. Liu, P. van der Voort, *J. Mater. Chem. A* **2018**, *6*, 6370.
[87] S. Dey, A. Bhunia, I. Boldog, C. Janiak, *Microporous Mesoporous Mater.* **2017**, *241*, 303–315.
[88] S. Dey, A. Bhunia, H. Breitzke, P. B. Groszewicz, G. Buntkowsky, C. Janiak, *J. Mater. Chem. A* **2017**, *5*, 3609–3620.
[89] O. M. Yaghi, M. J. Kalmutzki, C. S. Diercks, *Introduction to Reticular Chemistry. Metal-organic frameworks and covalent organic frameworks*, Wiley, Weinheim, **2019**.
[90] M. J. Kalmutzki, C. S. Diercks, O. M. Yaghi, *Adv. Mater.* **2018**, *30*, 1704304.
[91] N. C. Burtch, H. Jasuja, K. S. Walton, *Chem. Rev.* **2014**, *114*, 10575–10612.
[92] J. J. Low, A. I. Benin, P. Jakubczak, J. F. Abrahamian, S. A. Faheem, R. R. Willis, *J. Am. Chem. Soc.* **2009**, *131*, 15834–15842.
[93] K. Zhang, R. P. Lively, C. Zhang, W. J. Koros, R. R. Chance, *J. Phys. Chem. C* **2013**, *117*, 7214–7225.
[94] S. Tanaka, Y. Tanaka, *ACS Omega* **2019**, *4*, 19905–19912.
[95] J.-P. Zhang, A.-X. Zhu, R.-B. Lin, X.-L. Qi, X.-M. Chen, *Adv. Mater.* **2011**, *23*, 1268–1271.
[96] L. Helm, A. E. Merbach, *Coord. Chem. Rev.* **1999**, *187*, 151–181.
[97] L. Helm, G. M. Nicolle, A. E. Merbach, *Adv. Inorg. Chem.* **2005**, *57*, 327–379.
[98] S. E. Lincoln, *Helv. Chim. Acta* **2005**, *88*, 523–545.
[99] J. E. Mondloch, M. J. Katz, N. Planas, D. Semrouni, L. Gagliardi, J. T. Hupp, O. K. Farha, *Chem. Commun.* **2014**, *50*, 8944–8946.
[100] C. Schlüsener, D. N. Jordan, M. Xhinovci, T. J. Matemb, M. Nteb, A. Schmitz, B. Giesen, C. Janiak, *Dalton Trans.* **2020**, *49*, 7373–7383.
[101] C. Schlüsener, M. Xhinovci, S.-J. Ernst, A. Schmitz, N. Tannert, C. Janiak, *Chem. Mater.* **2019**, *31*, 4051–4062.
[102] N. Tannert, C. Jansen, S. Nießing, C. Janiak, *Dalton Trans.* **2019**, *48*, 2967–2976.
[103] M. Gaab, N. Trukhan, S. Maurer, R. Gummaraju, U. Müller, *Microporous Mesoporous Mater.* **2012**, *157*, 131–136.
[104] H. Reinsch, M. A. van der Veen, B. Gil, B. Marszalek, T. Verbiest, D. de Vos, S. Norbert, *Chem. Mater.* **2013**, *25*, 17–26.
[105] A. Cadiau, J. S. Lee, D. D. Borges, P. Fabry, T. Devic, M. T. Wharmby, C. Martineau, D. Foucher, F. T. Taulelle, C.-H. Jun, Y. K. Hwang, N. Stock, M. F. De Lange, F. Kapteijn, J. Gascon, G. Maurin, J.-S. Chang, C. Serre, *Adv. Mater.* **2015**, *27*, 4775–4780.
[106] D. Lenzen, J. Zhao, S.-J. Ernst, M. Wahiduzzaman, A. Ken Inge, D. Fröhlich, H. Xu, H.-J. Bart, C. Janiak, S. Henninger, G. Maurin, X. Zou, N. Stock, *Nat. Commun.* **2019**, *10*, 3025.
[107] A. Permyakova, O. Skrylnyk, E. Courbon, M. Affram, S. Wang, U.-H. Lee, A. H. Valekar, F. Nouar, G. Mouchaham, T. Devic, G. de Weireld, J.-S. Chang, N. Steunou, M. Frère, C. Serre, *ChemSusChem* **2017**, *10*, 1419–1426.
[108] A. Permyakova, S. J. Wang, E. Courbon, F. Nouar, N. Heymans, P. D'Ans, N. Barrier, P. Billemont, G. DeWeireld, N. Steunou, M. Frere, C. Serre, *J. Mater. Chem. A* **2017**, *5*, 12889–12898.
[109] C. B. L. Tschense, N. Reimer, C.-W. Hsu, H. Reinsch, R. Siegel, W.-J. Chen, C.-H. Lin, A. Cadiau, C. Serre, J. Senker, N. Stock, *Z. Anorg. Allg. Chem.* **2017**, *643*, 1600–1608.
[110] N. Tannert, S.-J. Ernst, C. Jansen, H.-J. Bart, S. K. Henninger, C. Janiak, *J. Mater. Chem. A* **2018**, *6*, 17706–17712.
[111] S. Kaskel, U.-H. Lee, A. H. Valekar, Y. K. Hwang, J.-S. Chang, *The Chemistry of Metal-Organic Frameworks, Synthesis, Characterization, and Application*, Wiley-VCH, Weinheim, **2017**, pp. 551–571.

[112] L. D. O'Neill, H. Zhang, D. J. Bradshaw, *J. Mater. Chem.* **2010**, *20*, 5720–5726.
[113] R. Ostermann, J. Cravillon, C. Weidmann, M. Wiebcke, B. M. Smarsly, *Chem. Commun.* **2011**, *47*, 442–444.
[114] S. Qiu, M. Xue, G. Zhu, *Chem. Soc. Rev.* **2014**, *43*, 6116–6140.
[115] A. Freni, L. Bonaccorsi, L. Calabrese, A. Caprì, A. Frazzica, A. Sapienza, *Appl. Therm. Eng.* **2015**, *82*, 1–7.
[116] A. Freni, B. Dawoud, L. Bonaccorsi, S. Chmielewski, A. Frazzica, L. Calabrese, G. Restuccia, *Characterization of Zeolite-Based Coatings for Adsorption Heat Pumps*; SpringerBriefs in *Applied Sciences and Technology* (Chapter 4); Springer, **2015**.
[117] E. Leung, U. Müller, N. Trukhan, H. Mattenheimer, G. Cox, S. Blei, Process for preparing porous metal-organic frameworks based on aluminum fumarate, US20120082864A1, **2012**.
[118] H. Kummer, F. Jeremias, A. Warlo, G. Füldner, D. Fröhlich, C. Janiak, R. Gläser, S. K. Henninger, *Ind. Eng. Chem. Res.* **2017**, *56*, 8393–8398.
[119] E. Hastürk, C. Schlüsener, J. Quodbach, A. Schmitz, C. Janiak, *Microporous Mesoporous Mater.* **2019**, *280*, 277–287.
[120] E. Hastürk, S.-P. Höfert, B. Topalli, C. Schlüsener, C. Janiak, *Microporous Mesoporous Mater.* **2020**, *295*, 109907.
[121] X. Sun, T. Fujimoto, H. Uyama, *Polym. J.* **2013**, *45*, 1101–1106.
[122] C. Rathgeber, E. Lavemann, A. Hauer, *J. Energy Storage* **2015**, *2*, 43–46.
[123] H. Schreiber, F. Lanzerath, C. Reinert, C. Gruntgens, A. Bardow, *Appl. Therm. Eng.* **2016**, *106*, 981–991.
[124] H.-M. Henning, T. Urbaneck, A. Morgenstern, T. Nunez, E. Wiemken, E. Thümmler, U. Uhlig, *Kühlen und Klimatisieren mit Wärme*, 2nd ed., Fraunhofer-IRB-Verlag, Stuttgart, **2015**.
[125] T. S. Ge, Y. J. Dai, R. Z. Wang, Y. Li, *Appl. Therm. Eng.* **2013**, *58*, 281–290.
[126] M. F. de Lange, B. L. van Velzen, C. P. Ottevanger, K. J. F. M. Verouden, L.-C. Lin, T. J. H. Vlugt, J. Gascon, F. Kapteijn, *Langmuir* **2015**, *31*, 12783–12796.
[127] S.-J. Ernst, F. Jeremias, H.-J. Bart, S. K. Henninger, *Ind. Eng. Chem. Res.* **2016**, *55*, 13094–13101.
[128] H. Kummer, M. Baumgartner, P. Hügenell, D. Fröhlich, S. K. Henninger, R. Gläser, *Appl. Therm. Eng.* **2017**, *117*, 689–697.
[129] T. J. Matemb Ma Nteb, H. Reinsch, P. P. C. Hügenell, S.-J. Ernst, E. Hastürk, C. Janiak, *J. Mater. Chem. A* **2019**, *7*, 24973–24981.
[130] R. E. Critoph, *Sol. Energy* **1988**, *41*, 21–31.
[131] R. E. Critoph, *Carbon* **1989**, *27*, 63–70.
[132] M. Pons, J. J. Guilleminot, *J. Sol. Energy Eng.* **1986**, *108*, 332–337.
[133] L. W. Wang, J. Y. Wu, R. Z. Wang, Y. X. Xu, S. G. Wang, X. R. Li, *Appl. Therm. Eng.* **2003**, *23*, 1605–1617.
[134] L. W. Wang, R. Z. Wang, Z. S. Lu, C. J. Chen, K. Wang, J. Y. Wu, *Carbon* **2006**, *44*, 2671–2680.
[135] L. Garzon-Tovar, J. Perez-Carvajal, I. Imaz, D. Maspoch, *Adv. Funct. Mater.* **2017**, *27*, 1606424.
[136] I. S. Girnik, A. D. Grekova, T. X. Li, R. Z. Wang, P. Dutta, S. P. S. Murthy, Y. I. Aristov, *Renewable Sustainable Energy Rev.* **2020**, *123*, 109748.
[137] T. X. Li, R. Z. Wang, T. Yan, *Energy* **2015**, *84*, 745–758.
[138] Advanced Research Projects Agency-DOE, HEATS Program Overview, https://arpa-e.energy.gov/sites/default/files/documents/files/HEATS_ProgramOverview.pdf, accessed Aug, **2020**.
[139] Y. Sun, A. Spieß, C. Jansen, A. Nuhnen, S. Gökpinar, R. Wiedey, S.-J. Ernst, C. Janiak, *J. Mater. Chem. A* **2020**, *8*, 13364.
[140] S. Graf, F. Redder, U. Bau, M. de Lange, F. Kapteijn, A. Bardow, *Energy Technol.* **2020**, *8*, 1900617.

Received: September 3, 2020

3.2 A caveat on the effect of modulators in the synthesis of the aluminum furandicarboxylate metal-organic framework MIL-160

Dominik Moritz Steinert, Alexa Schmitz, Marcus Fetzer, Philipp Seiffert, Christoph Janiak:

“A caveat on the effect of modulators in the synthesis of the aluminum furandicarboxylate metal-organic framework MIL-160“

Z. Allg. Anorg. Chem. **2022**, e202100380 DOI: 10.1002/zaac.202100380

Kurzfassung:

Modulatoren werden häufig bei der Synthese von metallorganischen Gerüstverbindungen (MOFs) zur Verbesserung der Porosität und Morphologie eingesetzt. Für Aluminium-MOFs wurde bisher selten über Modulationen berichtet, und wie hier am Beispiel des Aluminium-Furandicarboxylat-MOFs MIL-160 gezeigt wird, sind die positiven Auswirkungen von Modulatoren gering und nachteilige Auswirkungen wahrscheinlicher. Ameisensäure als Modulator kann die BET-Oberfläche und das Porenvolumen von MIL-160 bis zu einem Modulator:Linker-Verhältnis von 1.25:1 leicht erhöhen. Essigsäure zeigt nur beim kleinsten getesteten Verhältnis von 0.125:1 eine gewisse Zunahme der Oberfläche und des Porenvolumens. Die stärkeren Säuren Oxalsäure und Salzsäure mit den ebenfalls stärker aluminiumkoordinierenden Anionen haben keinen positiven Porositätseffekt und vermindern Oberfläche und Porenvolumen schon bei kleinen zugesetzten Mengen. Bei einem Modulator:Linker-Verhältnis von 1:1 für Oxalsäure und 0.75:1 für Salzsäure bildet sich nach der Analyse durch Pulverröntgenbeugung und Stickstoffsorption kein poröses MOF mehr. Die thermogravimetrische Analyse und die Rasterelektronenmikroskopie legen nahe, dass keiner der getesteten Modulatoren

einen merklichen positiven Einfluss auf das Entstehen von Linkerdefekten oder die Verbesserung der Kristallinität oder Kristallitgröße hat.

Anteile an der Publikation:

- Eigenständige Konzipierung und Verschriftlichung der experimentellen Ergebnisse und theoretischen Zusammenhänge in Form einer wissenschaftlichen Publikation. Umfassende und eigenständige Literaturrecherche. Kontinuierliche Bearbeitung des Manuskripts und Durchführung weiterer Experimente.
- Frau Dr. Alexa Schmitz führte die Analyse der TG durch
- Herr Marcus Fetzer führte die SEM Messungen durch.
- Herr Philipp Seiffert führte BET und PXRD von Reproduktionen durch.
- Die Korrekturen und die konstruktive Durchsicht des Manuskripts erfolgten durch Herrn Prof. Dr. Christoph Janiak.
- Die Einreichung in dem internationalen Journal „Zeitschrift für anorganische und allgemeine Chemie“ und die finale Abstimmung des Manuskripts erfolgte in Zusammenarbeit mit Herrn Prof. Dr. Christoph Janiak.

Journal of Inorganic and General Chemistry

ZAAC

Zeitschrift für anorganische und allgemeine Chemie

Accepted Article

Title: A caveat on the effect of modulators in the synthesis of the aluminum furandicarboylate metal-organic framework MIL-160

Authors: Dominik Moritz Steinert, Alexa Schmitz, Marcus Fetzer, Philipp Seifert, and Christoph Janiak

To be cited as: *Z. anorg. allg. Chem.* **2022**, e202100380

Link to VoR: https://doi.org/10.1002/zaac.202100380

WILEY-VCH www.zaac.wiley-vch.de

10.1002/zaac.202100380

WILEY-VCH

ARTICLE

A caveat on the effect of modulators in the synthesis of the aluminum furandicarboylate metal-organic framework MIL-160

Dominik Moritz Steinert,[a] Alexa Schmitz,[a] Marcus Fetzer,[a] Philipp Seifert,[a] Christoph Janiak*[a]

Dedicated to Prof. Dr. Caroline Röhr on the occasion of her 60th birthday

Modulators are widely used in the synthesis of metal-organic frameworks (MOFs) for improving the porosity and morphology. For aluminum MOFs modulation has been seldom reported and as is shown here for the example of the aluminum furandicarboylate MOF MIL-160 the positive effects of modulators are small and disadvantageous effects will be more likely. Formic acid as modulator can slightly increase the BET surface area and pore volume of MIL-160 up to a modulator:linker ratio of 1.25:1. Acetic acid only shows some increase in both surface area and pore volume at the smallest tested ratio of 0.125:1. The stronger acids oxalic acid and hydrochloric acid with the also more aluminum-coordinating anions have no positive porosity effect and decrease surface area and pore volume already at small amounts. At a 1:1 modulator:linker ratio for oxalic acid and at 0.75:1 for hydrochloric acid no porous MOF is formed anymore from the analysis by powder X-ray diffraction and nitrogen sorption. Further, thermogravimetric analysis and scanning electron microscopy suggests that none of the tested modulators has any noticeable positive effect on the introduction of linker defects or the improvement of crystallinity or crystal size.

Introduction

Metal-organic frameworks (MOFs) are crystalline and porous metal-ligand coordination networks.[1, 2, 3, 4] MOFs are designable in their properties[5] in many different dimensions, which leads to a still rising scientific and commercial interest in promising applications, such as useful heat transformation,[6, 7, 8] catalysis,[9] gas and liquid separation[10, 11] and natural gas.[12] and methane storage.[13] For applications like ethanol dehydration,[14] or the isosteric heat of adsorption of water[15] it can be necessary to tailor the characteristics of MOFs with respect to morphology, crystal size, porosity and defects,[16, 17, 18] e.g., through the use of modulators in their synthesis.[19, 20]

The kinetics of the framework formation can be influenced by modulating ligands which bind to the metal ion or cluster with a weaker binding energy than the linker. Thereby, the modulator competes with the linker and, for example, slows the crystal growth process or can in part remain in the MOF and induces linker defects.[3, 17, 18, 21, 22, 23, 24] Often used modulators are hydrochloric acid and organic monocarboxylic acids, such as benzoic acid, formic acid, acetic acid or trifluoroacetic acid. In UiO-type Zr-MOFs the increase of linker defects by monocarboxylic acid modulators is used to enhance the porosity and yield.[25] Gökpinar *et al.* observed an increase in BET surface areas, as well as increasing yields when HCl was used as modulator in UiOs.[26] Lazaro *et al.* for example used a MOF with modulation-increased defects for anti-cancer drug delivery and Liao *et al.* were able to induce desired types of porosity with templating modulators.[27, 28]

The modulation effects on the Al-MOF MIL-160, which is considered here, are derived from the kinetic and thermodynamic reaction behavior of solvated Al^{3+} cation and not necessarily by the MOF which is formed. Hence, different modulation effects are to be expected for MOFs with other metal ions, for example, for the Zr^{4+}-MOFs in the UiO series. The kinetic stability, that is inertness/lability of an existing metal-ligand bond towards ligand exchange will be fundamental in the modulation process, especially if both the modulator and linker feature the same (e.g. carboxylate) donor groups. The kinetic stability correlates with the reaction rate (constant) and activation energy for the process.[29]

An estimate of the lability of a metal ion towards ligand exchange can be obtained from the well-known *Merbach* series of rate constants for the exchange of aqua ligands in aqua complexes $\{[M(H_2O)_n]^{c+} + H_2O^* - k(H_2O) \rightarrow [M(H_2O)_{n-1}(H_2O^*)]^{c+} + H_2O\}$.[30, 31, 32] The most inert main-group metal ion is Al^{3+} with a rate constant for exchange in the $[Al(H_2O)_6]^{3+}$ complex of $k(H_2O)$ = 1.3 s^{-1}. Thereby, Al^{3+} occupies a middle position in the inert-to-labile classification. Among the three-valent metal ions Al^{3+} is more labile than for example Cr^{3+} ($k(H_2O) = 2.4 \cdot 10^{-6}$ s^{-1}) but less so than Fe^{3+} ($k(H_2O)$ = 180 s^{-1}) and especially Ti^{3+} ($k(H_2O) = 1.8 \cdot 10^{+5}$ s^{-1}) or the divalent transition-metal cations from Mn^{2+} to Cu^{2+}. The latter have fast rate constants $k(H_2O)$ of over 10^{+6} s^{-1}. Unfortunately, the rate constant for the aqua ligand exchange in Ti^{4+} has not been determined. Qualitatively, Ti^{4+} may be regarded as more labile than Al^{3+} because of its larger size and thereby more open coordination sphere for attacks towards nucleophilic substitution through an associative mechanism. Thermodynamically, the high-valent metal atoms Zr^{4+}, Cr^{3+} and Al^{3+} form stronger metal–carboxylate ligand bonds than divalent metal ions, simply from the Coulomb energy where the product of cation and anion charge enters in the nominator. Hence, Zr^{4+} may give a higher ionic bond strength by its increased charge than Al^{3+}, although this may be augmented by the high charge density of the smaller Al^{3+} (ionic radius 57 pm) over Zr^{4+} (87 pm).[29]

Thus, the action of modulators is difficult to predict. For example, Zhao *et al.* showed for MIL-101(Cr) that the addition of nitric acid improves both the yield and the porosity of the MOF, compared to the use of problematic hydrofluoric acid, while acetic acid enabled the MOF to be synthesized at lower temperatures and still acceptable surface area.[33] Furthermore, it was found that MIL-101(Cr) crystal growth was suppressed when acetic acid was

[a] D. M. Steinert, A. Schmitz, M. Fetzer, P. Seifert, Prof. C. Janiak
Institut für Anorganische Chemie und Strukturchemie
Heinrich-Heine-Universität Düsseldorf
40204 Düsseldorf, Germany
E-mail: janiak@uni-duesseldorf.de

Supporting information for this article is available on the WWW under https://doi.org/10.1002/zaac.xxxxxxxx

10.1002/zaac.202100380

used as a modulator, which led to smaller particle size.[34,35] Large amounts of acetic acid even changed the crystal phase of the MOF, as was demonstrated by Yang *et al.* with the formation of MIL-88B(Cr) instead of MIL101(Cr).[36] Moll *et al.* found that the use of very high amounts of mercaptoacetic acid in the synthesis of UiO-66 leads to a phase change from face-centered cubic, fcu to hexagonal close-packed, hcp phase with a different framework structure.[20]

The use of modulators does not even always show beneficial results. Bennett *et al.* discussed decreasing structure flexibility of UiO-66 with rising defect amounts, introduced by the use of monocarboxylic acids as modulator.[37] Even lowered nitrogen sorption abilities were reported based on the use of modulator in aluminum fumarate.[38]

Aluminum-based MOFs like MIL-53,[39] Alfum (Basolite A520),[40,41,42] CAU-10[43] or MIL-160[44] are among the most promising MOFs for applications due to their chemical and hydrothermal stability.[45,46,47,48,49] Aluminum is an abundant and inexpensive light metal with low toxicity.[46,47,50,51] MIL-160 in particular is a hydrophilic, highly hydrothermally stable Al-MOF (see Section S1, Figure S1 for structure description) with promising water sorption characteristics. MIL-160 was noted as the most promising Al-MOF for heat pump applications as it outperforms both Alfum and CAU-10-H in terms of gravimetric water loadings.[44] MIL-160 is also a highly promising material for adsorptive SO_2 separation and flue gas desulfurization, especially under application orientated conditions, and features excellent SO_2/CO_2 selectivities and $SO_2/N_2/CO_2$ breakthrough performance with high onset time, combined with high stability under both humid and dry SO_2 exposure.[52] The synthesis route of MIL-160 is environmentally friendly, since the linker can be produced from renewable biomass *via* oxidation of 5-(hydroxy-methyl)furfural (5-HMF) on a very large industrial scale and water is the single solvent.[53,54] Permyakova *et al.* investigated MIL-160 with resp1.ect to shaping into granules and heat reallocation underlining the suitability of the material for heat transformation application.[55]

Modulated Al-MOFs have been very rarely reported. Canossa *et al.* described the influence of oxalic acid for the synthesis of crystalline Al-MOFs and observed an increased particle size. from ~5 nm to ~40 nm.[56] Teo *et al.* presented formic acid modulated Alfum for improved water adsorption. Alfum particles elongate and the synthesis time could be reduced with the addition of formic acid.[57]

In this work we report the influence of the four modulators oxalic acid, formic and acetic acid as well as HCl in the synthesis of MIL-160. To the best of our knowledge there exists no systematic study on the influence of different modulators for aluminum MOFs yet.

Results and Discussion

The synthesis of MIL-160 was carried out following the synthesis from Permyakova *et. al.*[63] by combining basic aluminum diacetate and furandicarboxylic acid in a 1:1 molar ratio in the presence of formic acid, acetic acid, oxalic acid, and hydrochloric acid as modulators in water. The molar ratio of modulator:metal/linker ranged from 0:0625 to 2:1. Higher modulator to linker ratios were not investigated as it became evident that ratios of ~1:1 already induced significant disadvantageous and undesired phase and porosity changes.

The effect of modulation was assessed and followed by powder X-ray diffractometry (PXRD) (Figure 1) and porosity characterization through N_2 sorption measurements (Figure S2-S5, Supp. Info.). The PXRD pattern for the formic acid and acetic acid modulated MIL-160 show no significant change in crystal phase even at modulator:metal/linker ratios up to 2:1 (Figure 1a,b). With oxalic acid modulation the PXRD pattern exhibits reflexes for both MOF and crystalline linker at a modulator:metal/linker ratio of 1:1 (Figure 1c). At a ratio of 1.5:1 only the crystalline phase of the linker could be identified. With hydrochloric acid modulation, residual linker is already apparent at a modulator:metal/linker ratio of 0.5:1 (Figure 1d) with its PXRD reflexes and at 1.5:1 only linker reflexes remain.

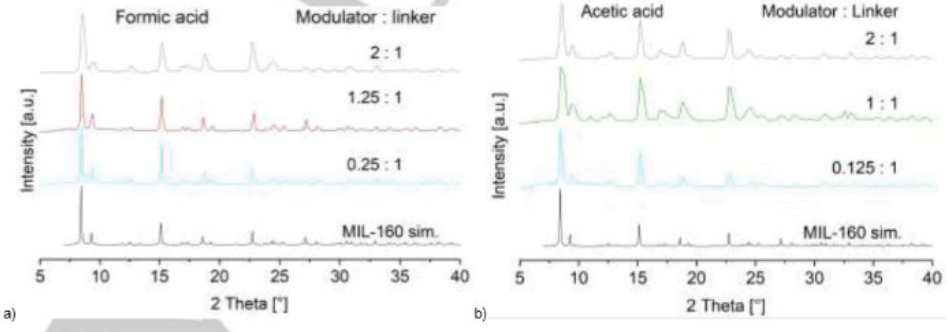

10.1002/zaac.202100380

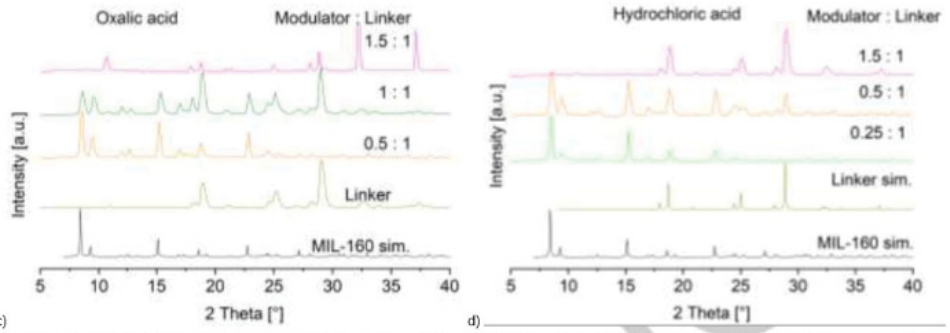

Figure 1. Selected powder X-ray diffraction patterns of MIL-160 synthesized with different modulators and molar modulators:linker ratios as indicated. The simulated diffractogram for MIL-160 is based on the deposited cif file with CCDC no. 1828694, Refcode PIBZOS.[58] The simulated diffractogram for the linker is based on the deposited cif file with CCDC no.11611468, Refcode FURDCA.[59] For diffraction patterns for all used modulator:linker ratios see Fig. S6-S9, SI.

The BET-surface areas increase slightly only with the modulator formic acid and very low amounts of acetic acid in modulator ratio, albeit at a different extent for each modulator (Table 1, Figure 2 and Table S2-S5). The pore volumes tend to first increase and go through a maximum with added formic and acetic acid modulator before decreasing again (Table 1, Figure 3). With oxalic and hydrochloric acid the pore volumes decrease right away.

Table 1. BET surface area and pore volume of modulated MIL-160.[a,b]

BET surface [$m^2\ g^{-1}$] (at molar modulator:linker ratio)
1105 (0:1, no modulator)

Formic acid	Acetic acid	Oxalic acid	Hydrochloric acid
1117 (0.125:1)	1197 (0.125:1)	1028 (0.0625:1)	743 (0.25:1)
1210 (1.25:1)	952 (0.75:1)	747 (0.625:1)	531 (0.5:1)
874 (1.75:1)	926 (2:1)	749 (0.875:1)	71 (0.75:1)

Total pore volume [$cm^3\ g^{-1}$] (at molar modulator:linker ratio)
0.43 (0:1, no modulator)

Formic acid	Acetic acid	Oxalic acid	Hydrochloric acid
0.45 (0.125:1)	0.51 (0.125:1)	0.42 (0.0625:1)	0.33 (0.25:1)
0.50 (1.25:1)	0.41 (0.75:1)	0.30 (0.625:1)	0.24 (0.5:1)
0.34 (1.75:1)	0.44 (2:1)	0.28 (0.875:1)	0.06 (0.75:1)

For formic acid the BET surface area increases up to a modulator-to-linker ratio of 1.25:1 or at the most increases only very slightly from 1105 $m^2\ g^{-1}$ to 1210 $m^2\ g^{-1}$. Upon further increase of modulator to 2:1 the surface area drops sharply to 442 $m^2\ g^{-1}$. For the acetic acid modulated series, the surface area only increased at a ratio of 0.125:1 and then drops to 900-800 $m^2\ g^{-1}$. Oxalic acid modulation starts with an immediate decrease at a low ratio of 0.0625:1 already, which continues to about 700 $m^2\ g^{-1}$ at a modulator:linker ratio of 0.875:1. At a 1:1 ratio a substantial amount of linker remains unreacted (cf. Figure 1c) and the product mixture is essentially non-porous (9 $m^2\ g^{-1}$). The concomitant pore volume of 0.01 $cm^3\ g^{-1}$ is due to interparticle voids. The modulator HCl induces also an immediate decrease of the surface area. At a ratio of 0.25:1 the BET surface is already reduced to 743 $m^2\ g^{-1}$. With a 0.5:1 ratio the BET surface decreases further to 531 $m^2\ g^{-1}$ and for ratios higher than 0.5:1 the BET surface area is little more than the outer surface area of a fine powder.

The total pore volume of formic acid modulated MIL-160 starts from 0.47 $cm^3\ g^{-1}$ at 0.125:1 and goes through a maximum of 0.52 $cm^3\ g^{-1}$ for 0.5:1 before decreasing with progressing modulator ratio down to 0.43 $cm^3\ g^{-1}$ at 1.5:1 and even below with higher ratios. For acetic acid the pore volume varies somewhat in a range from 0.51 to 0.37 $cm^3\ g^{-1}$ over the different modulator to linker ratios up to 2:1. For oxalic acid the pore volume decreases from 0.46 at 0.125:1 to 0.28 up to a modulator to linker ratio of 0.875:1. At the 1:1 ratio here, there is no longer a MOF synthesized, just residual linker is present with no BET surface and an only small measured pore volume of 0.01 $cm^3\ g^{-1}$. With hydrochloric acid the pore volume decreases from 0.33 $cm^3\ g^{-1}$ at a 0.25:1 modulator to linker ratio to 0.24 $cm^3\ g^{-1}$ at a 0.5:1 ratio. With higher ratios the pore volume goes down to nearly zero.

Thus, a small amount of modulator can advantageously increase the surface area and pore volume. Formic acid would be the best modulator choice at and up to a modulator:linker ratio of 1.25:1. Acetic acid only shows some increase in both surface area and pore volume at the smallest ratio of 0.125:1, whereas oxalic acid decreases both, the pore volume and the surface area considerably. The mineral acid HCl has no positive porosity effect.

10.1002/zaac.202100380

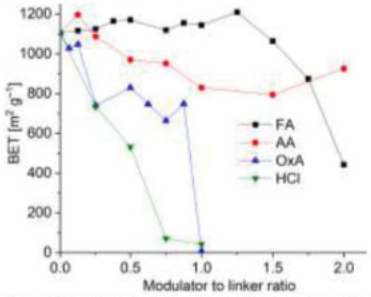

Figure 2. Trends of the BET surface of MIL-160, depending on the modulator to linker ratio of the different modulators.The numbers on the x-axis are always in relation to 1 with respect to the linker amount. The graphs include the values from all tested modulator:linker ratios as given in Table S2-S5, SI.

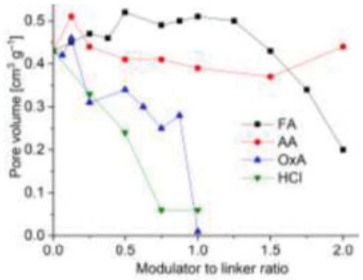

Figure 3. Trends of the total pore volume of MIL-160, depending on the modulator to linker ratio of the different modulators. The numbers on the x-axis are always in relation to 1 with respect to the linker amount. The graphs include the values from all tested modulator:linker ratios as given in Table S2-S5, SI.

Digestion NMR was used to test for the incorporation of modulator into the MOF. Selected samples which had been synthesized in the presence of high modulator:metal/linker ratio were dissolved und decomposed in 5% NaOD in D_2O. Samples from 2:1 ratios for formic and acetic acid and at a 1:1 ratio for oxalic acid showed no significant remnants of modulator in the samples (Figures S10-13, Supp. Info.).

Thermogravimetric analysis (TGA) was used to test for defects from linkers which were replaced by modulator or H_2O/OH ligands. The method for calculating missing linker-defect sites was adapted from the work of Shearer *et al.*[25,60] for UiO-66 (Section S5, Supp. Info.) Analysis of the TGA curve profiles (Fig. S16-23) led to the conclusion that these modulators do not induce significant amounts of missing linker defects in MIL-160 (see Supp. Info. for details). TGA shows in accordance with N_2 sorption and PXRD that at sufficiently high modulator quantities no more MOF is formed. At the above noted modulator-to-linker ratios almost exclusively linker is present in the solid products because the modulator kept the aluminum in solution during the synthesis and thus prevents the formation of the framework. Details are given in the Supp. Info.

The microcrystals of the formic acid and to some extent also the acetic acid modulated series seem to be fused to larger aggregates with increase of modulator (Figure S21, S22, Supp. Info).

The slightly positive effect of small amounts of the organic acid modulators formic acid and acetic acid on the porosity of MIL-160 is probably due to their similarity to the organic acid linker, e.g., in terms of pK_a values (formic acid 3.77, acetic acid 4.75, furandicarboxylic acid 4.38, 5.85[61]). Oxalic and hydrochloric acid are not only stronger acids (pK_a oxalic acid 1.25, hydrochloric acid –7) but also give rise to the formation of oxalato and chlorido complexes with aluminum, e.g., $[Al(ox)_3]^{3-}$ and $[AlCl_4]^-$. The formation of such relatively stable complexes will prevent the MOF formation as was evident in the powder X-ray diffractograms with remaining crystalline linker at a modulator:metal/linker ratio of 1:1 upon oxalic and hydrochloric acid modulation (Figure 1c,d).

Conclusions

The modulators formic acid and acetic acid, show only limited positive effects in the synthesis of the aluminum MOF MIL-160. This adds to the still rather small number of studies on the modulation of aluminum MOFs where also no strong effects could be observed, profoundly different from the significant modulator consequences in zirconium MOFs. For MIL-160 none of the tested modulators has any noticeable positive effect on the introduction of linker defects, the improvement of yield, crystallinity or crystal size. Formic acid up to a modulator:meta/linker ratio of 1.25:1 and acetic acid at the very small ratio of 0.125:1 yielded a small improvement in porosity, that is, BET surface area and pore volume. Above these ratios the BET surface area and eventually the pore volume started to decrease. For the modulators oxalic acid and hydrochloric acid, which interact more strongly with aluminum through complex formation, there was no positive effect on the porosity even for small amounts of modulator. The results do not rule out modulator effects for aluminum MOFs in general but caution for a careful evaluation before claiming an influence. The effects from the modulator comparison in this study suggest that monocarboxylic acids of similar binding strength to aluminum as the linker should be most promising.

To put these results in context with other studies on the modulation of MOFs, the comparatively small amount of modulator should be noted. The ratio of modulator to linker in this work is below 2, due to side-product formation etc. Whereas, in the modulation of UiO-66 modulator equivalents up to 100 are often used.[20,25] Thus, direct comparison between modulation reactions for Al-based and Zr-based MOFs do not seem appropriate. The difference in modulator amount may be seen as a manifestation of the different lability/inertness of Al^{3+} versus Zr^{4+} (cf. Introduction). It may be concluded that for the more inert Al^{3+} small amounts of modulator can already prevent the MOF formation, leaving unreacted linker as the only identifiable phase.

Experimental Section

Materials and Methods

10.1002/zaac.202100380

Basic aluminum diacetate, $Al(OH)(CH_3COO)_2$ was obtained from ChemPur, 2,5-furandicarboxylic acid (97%) from Apollo Scientific, oxalic acid (99.5%) from Acros Organics, formic acid (99%) from VWR Chemicals, acetic acid (99.8%) from Sigma Aldrich and hydrochloric acid (37%) from Fisher Chemicals and used without further purification.

Powder X-ray diffractograms (PXRD), were obtained with a *Bruker D2 Phaser* diffractometer using a flat silicon, low background sample holder and Cu-K_α radiation (λ= 1.54184 Å) at 30 kV and 0.04° s^{-1}in the 2θ = 5-50° range.

Brunauer-Emmett-Teller[62] (BET) surface areas were determined by nitrogen (N_2) (99.999%) sorption at T = 77 K on a *Quantachrome NOVA-4200e or* Autosorb-6 instrument with a relative pressure range of $pp_0^{-1} = 10^{-3} - 1$. Each sample (20 – 50 mg) was degassed under vacuum (<10^{-2} mbar) at 120 °C for at least 4 h prior to measurement. All BET surface areas were calculated from at least three adsorption data points in the pressure range $0.05 < pp_0 < 0.2$, applying Roquerol plots ($r > 0.998$). The total pore volume was determined at $pp_0^{-1} = 0.95$.

Thermogravimetric analysis (TGA) was measured on a *Netzsch TG 209 F3 Tarsus* under synthetic air atmosphere (20.5 % O_2 in N_2). The samples were measured with a heating rate of 5 K/min up to a temperature of 1000 °C in an aluminum oxide crucible.

Scanning electron microscope (SEM) images were taken on a JSM-6510LV QSEM with a LaB6 or with a tungsten cathode at 5–20 kV. The EDX measurements were performed with a Bruker Xflash 410 silicon drift detector with a Si(Li) semiconductor detector.

Nuclear magnetic resonance spectroscopy (NMR) were measured on a Bruker Avance III-600 or a Bruker Avance III-300 NMR spectrometer at 298 K. ^{1}H NMR Spectra were referenced to the residual proton solvent signal in D_2O/NaOD, set at 4.79 ppm. Approximately 10 mg of each sample was dissolved under decomposition in 5% NaOD/D_2O. The subsequently filtered solution, using a syringe filter, was transferred into an NMR tube. NMR spectra are shown in Section S4 in the Supp. Info.

Elemental analyses were measured on an ELEMENTAR vario MICRO cube.

Synthesis of MIL-160

The synthesis of MIL-160(Al) was performed using the synthesis recently reported from Permyakova *et al*.[63] In a typical reaction 2,5-furandicarboxylic acid ($C_4OH_2(COOH)_2$, 624 mg, 4.0 mmol) and basic aluminum diacetate ($Al(OH)(CH_3COO)_2$, 648 mg, 4.0 mmol) were dissolved in 4 mL of deionized Millipore water and refluxed (100 °C) for 24 h. Different amounts of modulator were added to the batches before refluxing in molar modulator:metal/linker ratios up to 2:1 (see Table S1, Supp. Info. for details). Formic acid, acetic acid, oxalic acid and hydrochloric acid were used as modulators. After 24 h the precipitated product was separated by centrifugation and washed three times each with water (3 x 35mL) and ethanol (3 x 35 mL). Subsequently, the product was dried under air for 12 h at 80 °C. Yields are given in the Supp. Info. in Table S1.

Acknowledgements

Funding by the German Federal Ministry of Education and Research (BMFT) for the project Optimat under grant 03SF0492C is gratefully acknowledged.

Keywords: MOF-modulation, metal-organic-framework, MIL-160, modulator, aluminum MOF

10.1002/zaac.202100380

WILEY-VCH

ARTICLE

Entry for the Table of Contents (Please choose one layout)

Layout 1:

FULL PAPER

Modulation of MIL-160 with formic acid, acetic acid slightly increased the porosity whereas oxalic acid and hydrochloric acid quickly prevented formation of the MOF.

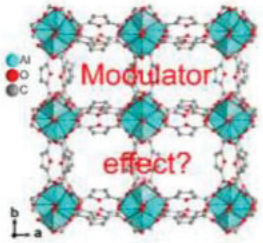

Dominik Moritz Steinert, Alexa Schmitz, Marcus Fetzer, Philipp Seifert, Christoph Janiak*

Page No. – Page No.

A caveat on the effect of modulators in the synthesis of the aluminum furandicarboylate metal-organic framework MIL-160

Layout 2:

FULL PAPER

((Insert TOC Graphic here; max. width: 11.5 cm; max. height: 2.5 cm))

*Author(s), Corresponding Author(s)**

Page No. – Page No.

Title

Text for Table of Contents

WILEY-VCH

ARTICLE

Additional Author information for the electronic version of the article.

Dominik Moritz Steinert: ORCID 0000-0002-5449-5809
Christoph Janiak: ORCID 0000-0002-6288-9605

[1] S. R. Batten, N. R. Champness, X.-M. Chen, J. Garcia-Martinez, S. Kitagawa, L. Öhrström, M. O'Keeffe, M. Paik Suh, J. Reedijk, *Pure Appl. Chem.* **2013**, *85*, 1715-1724.
[2] H.-C. Zhou, J. R. Long, O. M. Yaghi, *Chem. Rev.* **2012**, *112*, 673-674.
[3] A. Kirchon, L. Feng, H. F. Drake, E. A. Joseph, H-C. Zhou, *Chem. Soc. Rev.* **2018**, *47*, 8611-8638.
[4] C. Janiak, J. K. Vieth, *New J. Chem.* **2010**, *34*, 2366-2388.
[5] M. Taddei, *Coord. Chem. Rev.*, **2017**, *343*, 1–24.
[6] X. Liu, X. Wang, F. Kapteijn, *Chem. Rev.* **2020**, *120*, 8303-8377.
[7] D. M. Steinert, S.-J. Ernst, S. K. Henninger, C. Janiak, *Eur. J. Inorg. Chem.* **2020**, 4502-4515.
[8] F. Jeremias, D. Fröhlich, C. Janiak, S. Henninger, *New J. Chem.* **2014**, *38*, 1846-1852.
[9] S. M. J. Rogge, A. Bavykina, J. Hajek, H. Garcia, A. I. Olivos-Suarez, A. Sepúlveda-Escribano, A. Vimont, G. Clet, P. Bazin, F. Kapteijn, M. Daturi, E. V. Ramos-Fernandez, F. X. Llabrés i Xamena, V. Van Speybroeck, J. Gascon, *Chem. Soc. Rev.* **2017**, *46*, 3134-3184.
[10] K. Adil, Y. Belmabkhout, R. S. Pillai, A. Cadiau, P. M. Bhatt, A. H. Assen, G. Maurin, M. Eddaoudi, *Chem. Soc. Rev.* **2017**, *46*, 3402-3430.
[11] J. Dechnik, J. Gascon, C. J. Doonan, C. Janiak, C. J. Sumby, *Angew. Chem. Int. Ed.* **2017**, *56*, 9292-9310.
[12] J. A. Mason, M. Veenstra, J. R. Long, *Chem. Sci.* **2014**, *5*, 32-51.
[13] Y. He, W. Zhou, G. Qian, B. Chen, *Chem. Soc. Rev.* **2014**, *43*, 5657-5678.
[14] E. Alvarez, N. Guillou, C. Martineau, B. Bueken, B. Van de Voorde, C. Le Guillouzer, P. Fabry, F. Nouar, F. Taulelle, D. de Vos, J.-S. Chang, K. H. Cho, N. Ramsahye, T. Devic, M. Daturi, G. Maurin, C. Serre, *Angew. Chem. Int. Ed.* **2015**, *54*, 3664–3668.
[15] D. S. Sholl, R. P. Lively, *J. Phys. Chem. Lett.* **2015**, *6*, 3437– 3444.
[16] Z. Fang, B. Bueken, D. de Vos, R. A. Fischer, *Angew. Chem. Int. Ed.* **2015**, *54*, 7234–7254.
[17] S. Dissegna, K. Epp, W. R. Heinz, G. Kieslich, R. Fischer, *Adv. Mater.* **2018**, *30*, 1704501.
[18] J. Ren, M. Ledwaba, N. M. Musyoka, H. W. Langmi, M. Mathe, S. Liao, W. Pang, *Coord. Chem. Rev.* **2017**, *349*, 169–197.
[19] G. Wißmann, A. Schaate, S. Lilienthal, I. Bremer. A.A. Schneider. P. Behrens, *Microporous Mesoporous Mater.* **2011**, *152*, 64-70.
[20] B. Moll, T. Müller, C. Schlüsener, A. Schmitz, P. Brandt, S. Öztürk, C. janiak, *Mater. Adv.* **2021**, *2*, 804-812.
[21] M. Kalaj, K. C. bentz, S. Ayala Jr., J. M. Palomba, K. S. Barcus, Y. Katayama, S. M. Cohen, *Chem. Rev.* **2020**, *120*, 16, 8267–8302.
[22] T. Tsuruoka, S. Furukawa, Y.Takashima, K. Yoshida, S. Isoda, S. Kitagawa, *Angew. Chem. Int. Ed.* **2009**, *48*, 4739–4743
[23] A. Umemura, S. Diring, S. Furukawa, H. Uehara, T. Tsuruoka, S. Kitagawa *J. Am. Chem. Soc.* **2011**, *133*, 15506–15513
[24] S. Diring, S. Furukawa, Y. Takashima. T. Tsuruoka, S. Kitagawa, *Chem. Mater.* **2010**, *22*, 16, 4531–4538
[25] G. C. Shearer, S. Chavan, S. Bordiga, S. Svelle, U. Olsbye, K. P. Lillerud, *Chem. Mater.* 2016, **28**, 3749−3761.
[26] S. Gökpinar, T. Diment, C. Janiak, *Dalton Trans.* **2017**, *46*, 9895-9900.
[27] I. A. Lazaro, C. J. R. Wells, R. S. Forgan, *Angew.Chem. Int.Ed.* **2020**, *59*, 5211 –5217.
[28] Y. Liao, Zhang, M. H. Weston, W. Morris, J. T. Hupp, O. K. Farha, *Chem.Commun.* **2017**,*53*,9376.
[29] A. J. Rieth, A. M. Wright, M. Dincă, *Nat. Rev. Mater.* **2019**, *4*, 708-725.
[30] L. Helm, A. E. Merbach, *Coord. Chem. Rev.* **1999**, *187*, 151-181.
[31] L. Helm. G. M. Nicolle, A. E. Merbach, *Adv. Inorg. Chem.* **2005**, *57*, 327-379.
[32] S. E. Lincoln, *Helv. Chim. Acta* **2005**, *88*, 523-545.
[33] T. Zhao, F. Jeremias, I. Boldog, B. Nguyen, St. K. Henninger, C. Janiak, *Dalton Trans.* **2015**, *44*, 16791.
[34] T. Zhao, L. Yang, P. Feng, I. Gruber, C. Janiak, Y, Liu, *Inorg. Chim. Acta* **2018**, *471*, 440–445.
[35] T. Zhao, S. Li, Y-X. Xiao, C. Janiak, G. Chang, G. Tian, X.-Y. Yang, *Sci China Mater.* **2021**, *64*, 252–258.
[36] L. Yang, T. Zhao, I. Boldog, C. Janiak, X.-Y. Q. Li, Y.-J. Zhou, Y. Xia, D -W. Lai, Y.-J. Liu, *Dalton Trans.* **2019**, *48*, 989–996.
[37] T. D. Bennett, A. K. Cheetham, A. H. Fuchs, F.-X. Coudert, *Nat. Chem.* **2016**, *9*, 11–16.
[38] H.W. B. Teo, A. Chakraborty, S. Kayal, *Microporous Mesoporous Mater.* **2018**, *272*, 109–116.
[39] T. Loiseau, C. Serre, C. Huguenard, G. Fink, F. Taulelle, M. Henry, T. Bataille, G. Férey, *Chem. Eur. J.* **2004**, *10*, 1373-1382.
[40] C. Kiener, U. Müller and M. Schubert, Germany Pat. WO2007/118841 A2, BASF SE, **2007**.
[41] C. Kiener, U. Müller and M. Schubert, US Pat. 12/297,666, BASF SE, **2012**.
[42] E. Leung, U. Müller, N. Trukhan, H. Mattenheimer and G. Cox, US Pat. 13/249,943, BASF SE, **2012**.
[43] H. Reinsch, M. A. van der Veen, B. Gil, B. Marszalek, T. Verbiest, D. de Vos, N. Stock, *Chem. Mater.* **2013**, *25*, 17-26.
[44] A. Cadiau, J. S. Lee, D. D. Borges, P. Fabry, T. Devic, M. T. Wharmby, C. Martineau, D. Foucher, F. Taulelle, C.-H. Jun, Y. K. Hwang, N. Stock, M. F. De Lange, F. Kapteijn, J. Gascon, G. Maurin, J.-S. Chang, C. Serre, *Adv. Mater.* **2015**, *27*, 4775-4780.
[45] M. Gaab, N. Trukhan, S. Maurer, R. Gummaraju, U. Müller, *Microporous. Mesoporous. Mater.* **2012**, *157*, 131-136
[46] F. Jeremias, D. Fröhlich, C. Janiak, S. K. Henninger, *RSC Adv.* **2014**, *4*, 24073-24082.
[47] D. Fröhlich, S. K. Henninger, C. Janiak, *Dalton Trans.* **2014**, *43*, 15300-15304.
[48] D. Fröhlich, E. Pantatosaki, P. D. Kolokathis, K. Markey, H. Reinsch, M. Baumgartner, M. A. van der Veen, D. E. de Vos, N. Stock, G. K. Papadopoulos, S. K. Henninger, C. Janiak, *J. Mater. Chem. A* **2016**, *4*, 11859-11869.
[49] P. Brandt, S.-H. Xing, J. Liang, G. Kurt, A. Nuhnen, O. Weingart, C. Janiak, *ACS Appl. Mater. Interfaces* **2021**, *13*, 29137-29149.
[50] F. Jeremias, A. Khutia, S. K. Henninger, C. Janiak, *J. Mater. Chem.* **2012**, *22*, 10148–10151.
[51] A. Samokhvalov, *Coord. Chem. Rev.* **2018**, *374*, 236–253.
[52] P. Brandt, A. Nuhnen, M. Lange, J. Möllmer, O. Weingart, C. Janiak, *ACS Appl. Mater. Interfaces* **2019**, *11*, 17350-17358.
[53] http://avantium.com/yxy/yxy-technology.html; accessed 01.08.**2017**, 01:54 h.
[54] Press releases: 'Synvina: Jointventure of BASF and Avantium established', **2016**.
[55] M. Wahiduzzaman, D. Lenzen, G. Maurin, N. Stock, M. T. Wharmby, Eur. *J. Inorg. Chem.* **2018**, 3626-3632

[56] S. Canossa, A. Gonzalez-Nelson, L. Shupletsov, M del Carmen Martin, M. A. van der Veen, *Chem. Eur. J.* **2020**, *26*, 3564-3570.
[57] H.W. B. Teo, A. Chakraborty, S. Kayal, *Microporous Mesoporous Mater.* **2018**, *272*, 109–116.
[58] M. Wahiduzzaman, D. Lenzen, G. Maurin, N. Stock, M. T. Wharmby, *Eur. J. Inorg. Chem.* **2018**, 3626-3632.
[59] E. Martuscelli, C. Pedone, *Acta Cryst. B* **1968**, *24*, 175.
[60] G. C. Shearer, S. Chavan, J. Ethiraj, J. G. Vitillo, S. Svelle, U. Olsbye, C. Lamberti, S. Bordiga, K. P. Lillerud, *Chem. Mater.* **2014**, *26*, 4068-4071
[61] H. Hopff, A. Krieger, *Helv. Chim. Acta* **1961**, *44*: 1058-1063.
[62] M. Tommes, K. Kaneko, A. V. Neimark, J. P. Olivier, F. Rodriguez-Reinoso, J. Rouquerol, K. S. W. Sing, *Pure Appl. Chem.* **2015**, *87*, 1051-1069.
[63] A. Permyakova, O. Skrylnyk, E. Courbon, M. Affram, S. Wang, U-H. Lee, A. H. Valekar, F. Nouar, G. Mouchaham, T. Devic, G. De Weireld, J.-S. Chang, N. Steunou, M. Frère, C. Serre, *ChemSusChem.* **2017**, *10*, 1419-1426.

Supporting information (SI)

A caveat on the effect of modulators in the synthesis of the aluminum furandicarboylate metal-organic framework MIL-160

Dominik Moritz Steinert, Alexa Schmitz, Marcus Fetzer, Philipp Seifert, Christoph Janiak*

Institut für Anorganische Chemie und Strukturchemie, Heinrich-Heine-Universität Düsseldorf, D-40204 Düsseldorf, Germany. Fax: +49-211-81-12287; Tel: +49-211-81-12286.

Email addresses: moritz.steinert@hhu.de, alexa.schmitz@hhu.de, marcus.fetzer@hhu.de, philipp.seiffert@hhu.de, janiak@hhu.de

Content

S1: Structure and syntheses parameters of MIL-160

MIL-160 (MIL = *Matériaux Institut Lavoisier*) was first described by Cadiau *et al.* in 2015.[1] The MOF was initially synthesized from aqueous solutions of 2,5-furandicarboxylic acid, sodium hydroxide and aluminum chloride under reflux. MIL-160 is constructed from {AlO_6} octahedra which share vertices by bridging (μ-)OH with adjacent μ-OH cis to each other. The {AlO_6} octahedra form helical chains, which are then joined by the linker 2,5-furandicarboxylate (Figure S1).

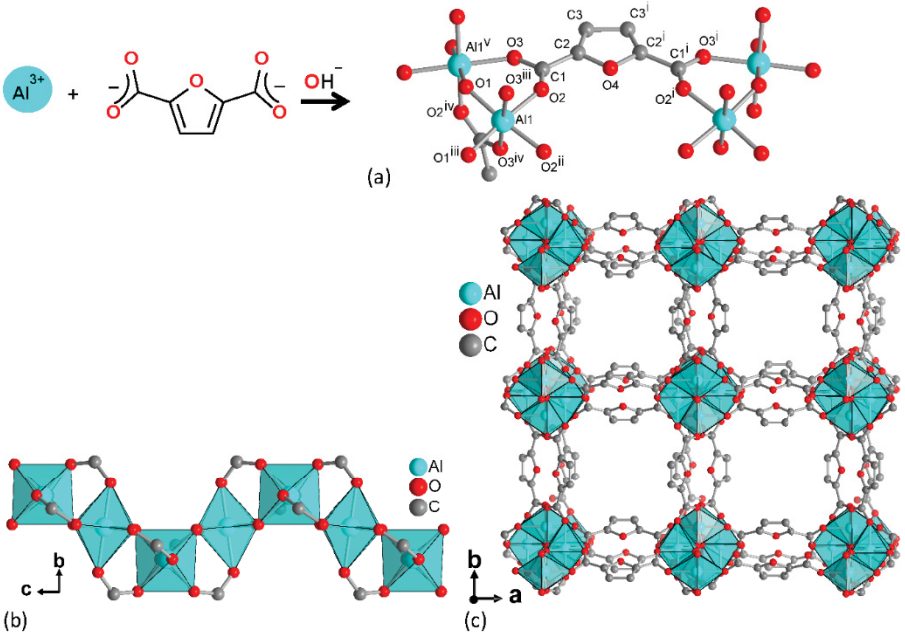

Figure S1. Structural elements in the framework of MIL-160: (a) Extended asymmetric unit with full Al coordination spheres and full ligand bridging mode. Symmetry transformations i = 1–x, y, z; ii = x, –y, –z; iii = 0.25+y, 0.25–x, –0.25+z; iv = 0.25+y, –0.25+x, 0.25–z; v = 0.25–y, –0.25+x, 0.25+z. (b) Helical chains of cis OH-bridged {AlO_6} octahedra in polyhedral presentation and (c) section of the packing diagram with square-shaped one dimensional channels along the crystallographic *c* axis. Graphic produced by software Diamond (Version 4.6)[2] from cif-file for MIL-160 (CSD-Refcode PIBZOS).[3]

MIL-160 has the chemical formula of $[Al(OH)(O_2C\text{-}C_4H_2O\text{-}CO_2) \cdot n\ H_2O]_m$ and microporous square-shaped channels of 5 Å edge length.[1,4] The material exhibits a surface area of 1070 $m^2\ g^{-1}$ and a pore volume of 0.40 $cm^3\ g^{-1}$ from $AlCl_3$ and NaOH (theoretically: 1250 $m^2\ g^{-1}$, 0.48 $cm^3\ g^{-1}$),[1] respectively 1150 $m^2\ g^{-1}$ and 0.46 $cm^3\ g^{-1}$, from $Al(OH)(CH_3COO)_2$,[4] although theoretical calculations suggested a surface area of 776 $m^2\ g^{-1}$ and a pore volume of 0.45 $cm^3\ g^{-1}$.[5]

Table S1. Syntheses parameters of MIL-160 samples.

Molar modulator to linker ratio	Basic aluminum diacetate [mg] (mmol)	2,5-Furandicarboxylic acid [mg] (mmol)	Modulator [mg] (mmol)	Yield [g]	Yield [%]
Non-modulated MIL-160					
0:1	650 (4.0)	624 (4.0)	0 (0)	0.747	94
Formic acid modulated MIL-160					
0.125:1	650 (4.0)	625 (4.0)	23 (0.5)	0.313	39
0.25:1			46 (1.0)	0.721	91
0.375:1			69 (1.5)	0.747	94
0.5:1			92 (2.0)	0.696	87
0.75:1			138 (3.0)	0.691	87
0.875:1			161 (3.5)	0.626	79
1:1			184 (4.0)	0.720	91
1.25:1			230 (5.0)	0.705	89
1.5:1			276 (6.0)	0.668	84
1.75:1			322 (7.0)	0.599	76
2:1			368 (8.0)	0.684	86
Acetic acid modulated MIL-160					
0.125:1	650 (4.0)	625 (4.0)	30 (0.5)	0.762	96
0.25:1			60 (1.0)	0.717	90
0.5:1			120 (2.0)	0.722	91
0.75:1			180 (3.0)	0.726	92
1:1			240 (4.0)	0.712	89
1.5:1			360 (6.0)	0.712	90
2:1			480 (8.0)	0.710	89
Oxalic acid modulated MIL-160					
0.0625:1	650 (4.0)	625 (4.0)	33 (0.25)	0.753	95
0.125:1			64 (0.5)	0.706	89
0.25:1			127 (1.0)	0.742	94
0.5:1			252 (2.0)	0.769	97
0.625:1			315 (2.5)	0.324	41
0.75:1			379 (3.0)	0.572	72
0.825:1			441 (3.5)	0.165	21
1:1			503 (4.0)	0.463	58
1.5:1			758 (6.0)	0	0

2:1			1006 (8.0)	0	0
Hydrochloric acid modulated MIL-160					
0.25:1	650 (4.0)	625 (4.0)	99 (1.0)	0.761	96
0.5:1			197 (2.0)	0.694	87
0.75:1			296 (3.0)	0.699	88
1:1			394 (4.0)	0.659	83
1.5:1			591 (6.0)	0.473	60
2:1			788 (8.0)	0.586	73

S2: BET surfaces and pore volumes

BET surface and pore volume of MIL-160 without modulator: 1105 $m^2 g^{-1}$, 0.43 $cm^3 g^{-1}$

Formic acid modulated MIL-160

Table S2. BET surface area and pore volume for formic acid modulated MIL-160.

Molar modulator to linker ratio	BET surface [$m^2 g^{-1}$]	Pore volume [$cm^3 g^{-1}$]	Reproduced BET surface [$m^2 g^{-1}$] [a]	Reproduced Pore volume [$cm^3 g^{-1}$] [a]
0:1	1105	0.43	-	-
0.125:1	1117	0.45	-	-
0.25:1	1125	0.47	1065 [a]	n.a. [a,b]
0.375:1	1140	0.63	1165 [a]	0.46 [a,c]
0.5:1	1171	0.52	-	-
0.75:1	1119	0.49	1252[a]	0.57[a]
0.875:1	1155	0.50	1228[a]	0.58[a]
1:1	1144	0.51	-	-
1.25:1	1210	0.50	-	-
1.5:1	1064	0.43	-	-
1.75:1	874	0.34	-	-
2:1	442	0.20	-	-

[a] Replicated synthesis experiments with N_2 sorption analysis on an Autosorb-6 device instead of a Nova 4200e. [b] This sample was analyzed in short measurement, just to confirm the surface. The covered pressure range is insufficient for calculating the total pore volume. [c] This isothertherm is shown in Fig. S2 and S2.1.

Acetic acid modulated MIL-160

Table S3. BET surface area and pore volume for acetic acid modulated MIL-160.

Molar modulator to linker ratio	BET surface [$m^2 g^{-1}$]	Pore volume [$cm^3 g^{-1}$]	Reproduced BET surface [$m^2 g^{-1}$] [a]	Reproduced Pore volume [$cm^3 g^{-1}$] [a]
0:1	1105	0.43	-	-
0.125:1	1197	0.51	-	-
0.25:1	1087	0.44	-	-
0.5:1	970	0.41	990 [a]	0.41 [a]
0.75:1	952	0.41	-	-
1:1	830	0.39	-	-
1.5:1	794	0.37	-	-
2:1	926	0.44	-	-

[a] Replicated synthesis experiment with N_2 sorption analysis on an Autosorb-6 device instead of a Nova 4200e.

Oxalic acid modulated MIL-160

Table S4. BET surface area and pore volume for oxalic acid modulated MIL-160.

Molar modulator to linker ratio	BET surface [$m^2 g^{-1}$]	Pore volume [$cm^3 g^{-1}$]	Reproduced BET surface [$m^2 g^{-1}$]	Reproduced Pore volume [$cm^3 g^{-1}$]
0:1	1105	0.43	-	-
0.0625:1	1028	0.42	1047 [a]	0.42 [a]
0.125:1	1048	0.46	-	-
0.25:1	742	0.31	-	-
0.5:1	830	0.34	869 [a]	0.37 [a, c]
0.625:1	747	0.30	-	-
0.75:1	664	0.25	-	-
0.875:1	749	0.28	-	-
1:1	9	0.01	-	-

[a] Replicated synthesis experiment with N_2 sorption analysis on an Autosorb-6 device instead of a Nova 4200e. [c] This isothertherm is shown in Fig. S2 and S2.1.

Hydrochloric acid modulated MIL-160

Table S5. BET surface area and pore volume for hydrochloric acid acid modulated MIL-160.

Molar modulator to linker ratio	BET surface [$m^2\ g^{-1}$]	Pore volume [$cm^3\ g^{-1}$]	Reproduced BET surface [$m^2\ g^{-1}$]	Reproduced Pore volume [$cm^3\ g^{-1}$]
0:1	1105	0.43	-	-
0.25:1	743	0.33	-	-
0.5:1	531	0.24	-	-
0.75:1	71	0.06	85 [a]	0.10 [a, c]
1:1	42	0.06	85 [a]	0.09 [a]

[a] Replicated synthesis experiments with N_2 sorption analysis on an Autosorb-6 device instead of a Nova 4200e. [c] This isothertherm is shown in Fig. S2 and S2.1.

S3: Nitrogen sorption isotherms

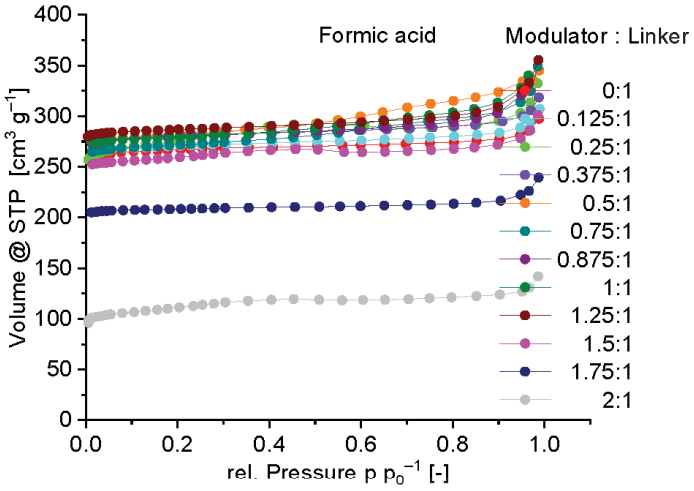

Figure S2. Nitrogen adsorption isotherms of formic acid modulated MIL-160 at 77 K. For clarity, the desorption isotherms are not shown.

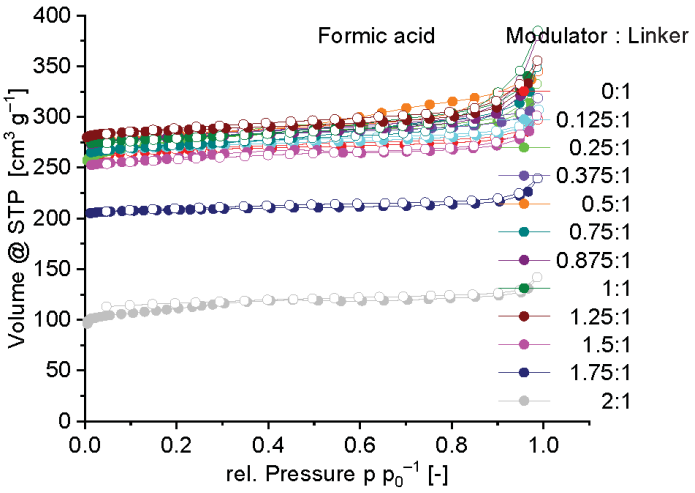

FigureS2.1. Nitrogen sorption isotherms of formic acid modulated MIL-160 at 77 K. Desorption is shown as empty dots of the same color as the sorption.

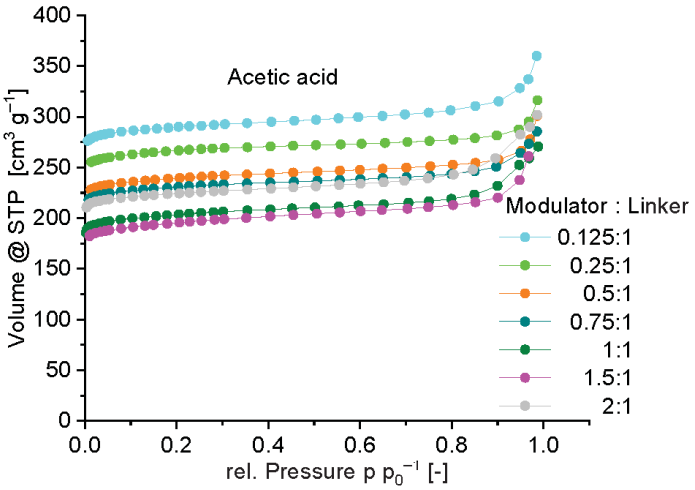

Figure S3. Nitrogen adsorption isotherms of acetic acid modulated MIL-160 at 77 K. For clarity, the desorption isotherms are not shown.

7

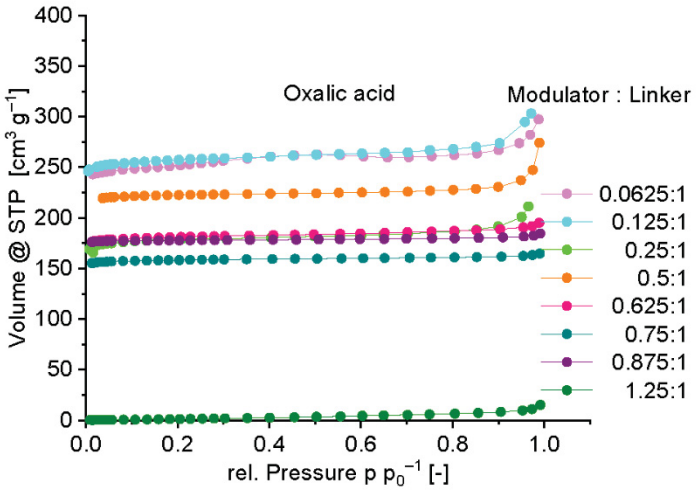

Figure S4. Nitrogen adsorption isotherms of oxalic acid modulated MIL-160 at 77 K. For clarity, the desorption isotherms are not shown.

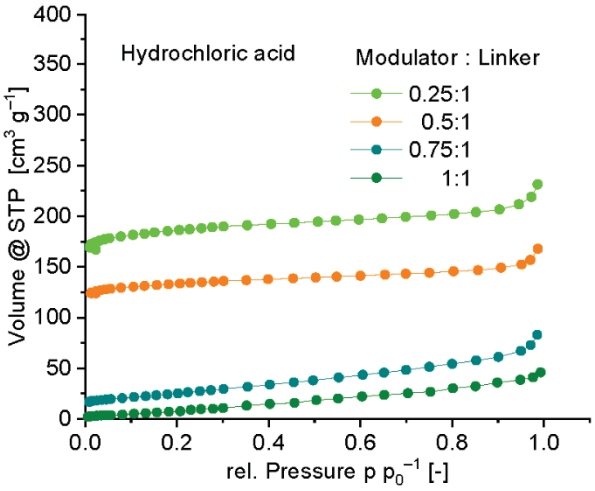

Figure S5. Nitrogen adsorption isotherms of hydrochloric acid modulated MIL-160 at 77 K. For clarity, the desorption isotherms are not shown.

S4: Powder X-ray diffractometry

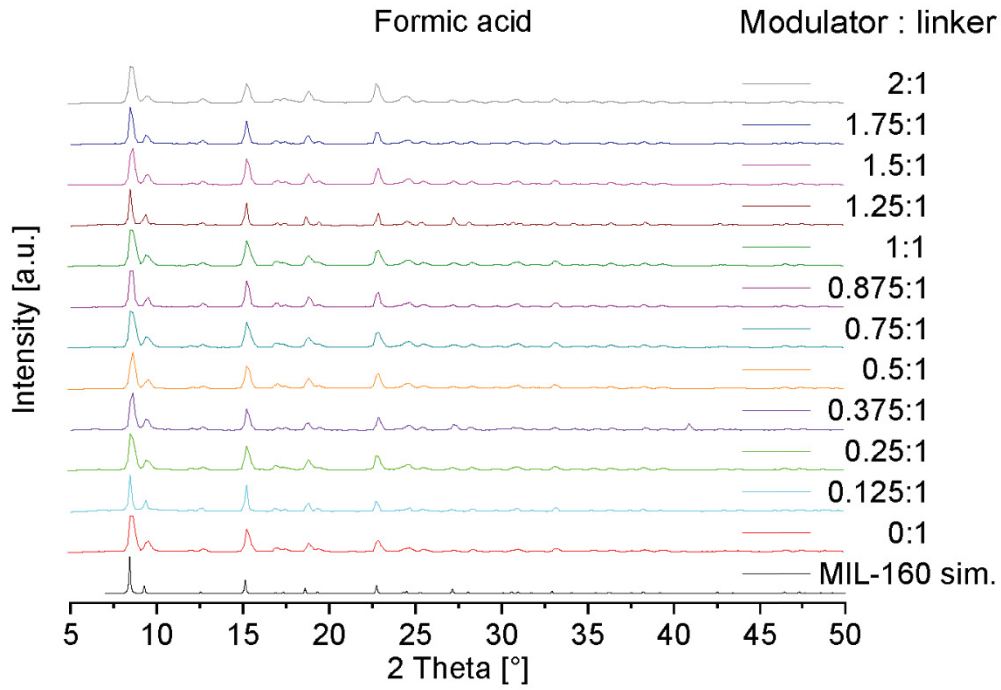

Figure S6. PXRDs of formic acid modulated MIL-160 for different molar modulator:linker. The simulated diffractogram for MIL-160 is based on the deposited cif file with CCDC no. 1828694, Refcode *PIBZOS*.[6]

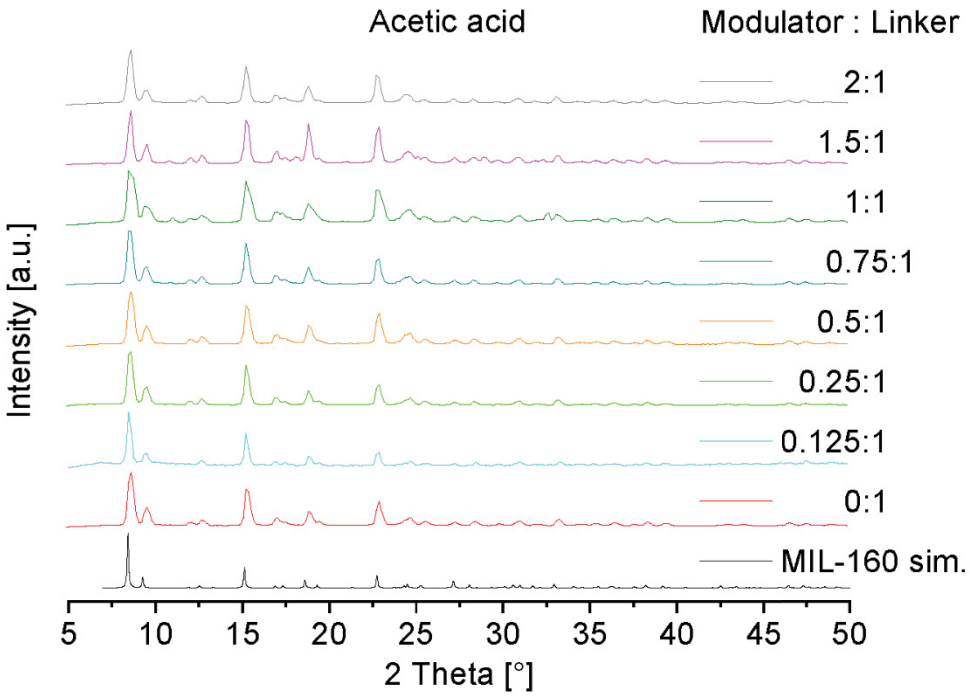

Figure S7. PXRDs of acetic acid modulated MIL-160 for different molar modulator:linker. The simulated diffractogram for MIL-160 is based on the deposited cif file with CCDC no. 1828694, Refcode *PIBZOS*.[6]

10

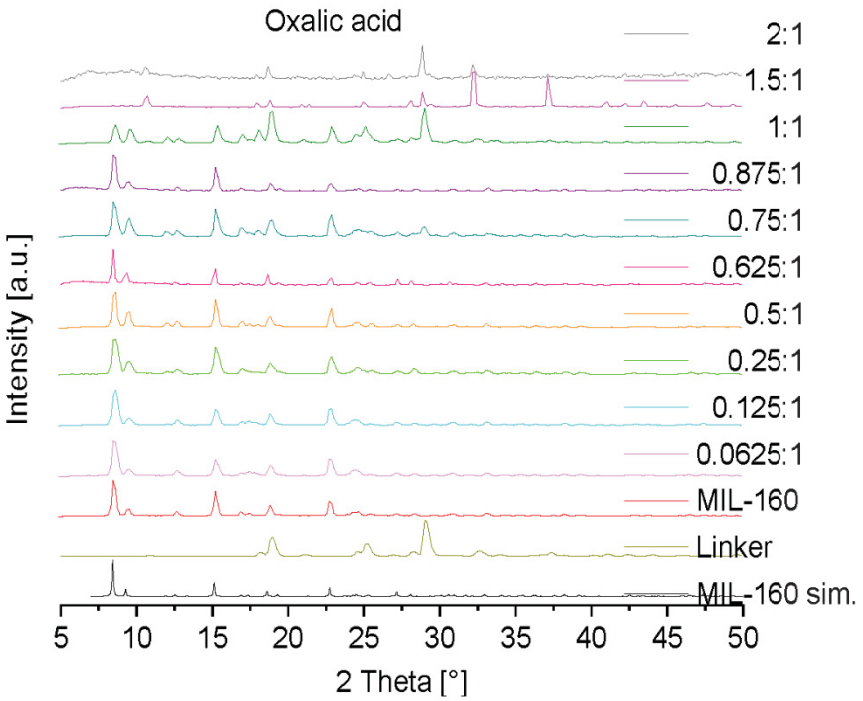

Figure S8. PXRDs of oxalic acid modulated MIL-160 for different molar modulator:linker. The simulated diffractogram for MIL-160 is based on the deposited cif file with CCDC no. 1828694, Refcode *PIBZOS*.[6]

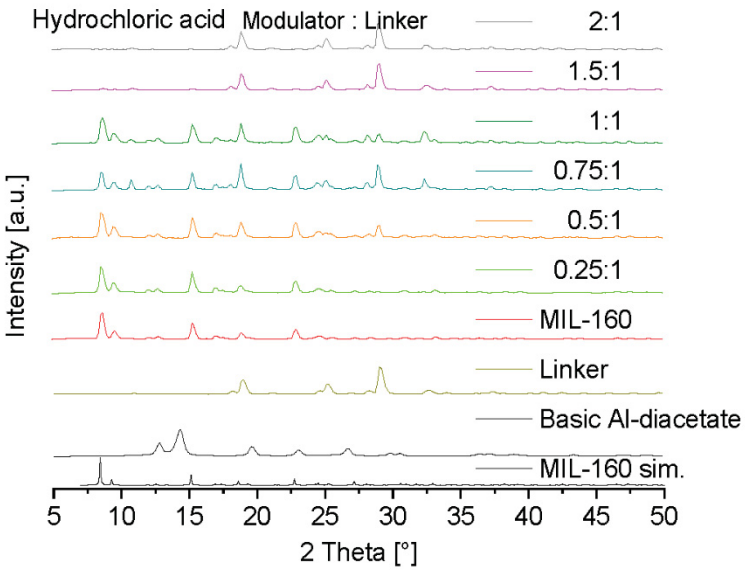

Figure S9. PXRDs of hydrochloric acid modulated MIL-160 for different molar modulator:linker. The simulated diffractogram for MIL-160 is based on the deposited cif file with CCDC no. 1828694, Refcode *PIBZOS*.[6]

S5: NMR measurements

With exception of the formic acid modulated MOF, the dissolution NMRs show no residual modulators in the samples. Figures s10 show the respective ^{13}C NMR of MIL-160 with the highest amount of oxalic acid as well as the ^{1}H NMR of acetic acid without any detectable modulator. Figure S12 shows MIL-160 with the only observable amount of modulator.

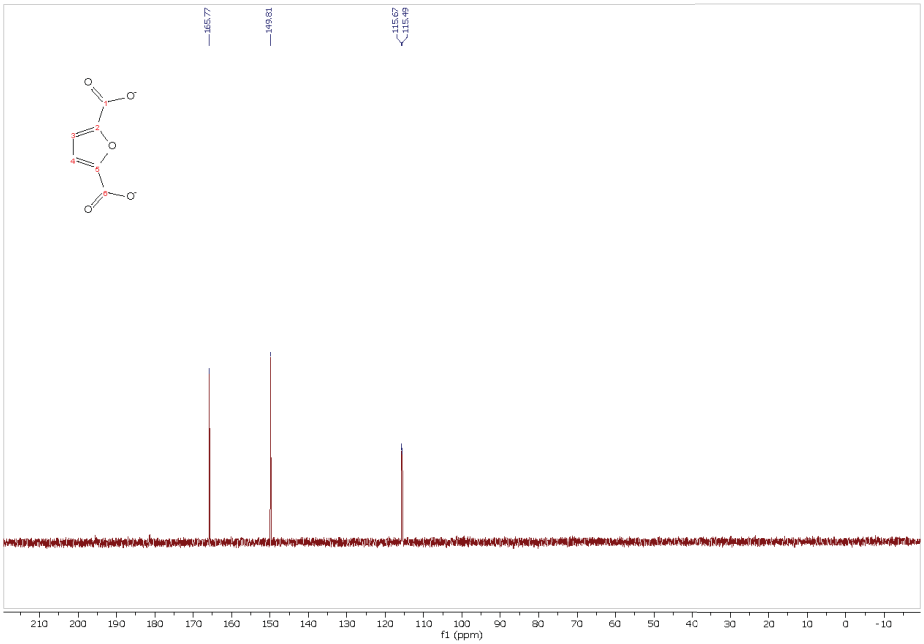

Figure S10.· Proton-decoupled ^{13}C NMR spectrum of "digested" MIL-160, modulated with oxalic acid at a molar modulator:metal/linker ratio of 2:1, after decomposition with 5% NaOD/D_2O, in D_2O at 300 MHz. The furandicarboxylate linker signals appear at 165.9 (C^1,C^6), 149.8 (C^2,C^5) and 115.6 (C^3,C^4) ppm.

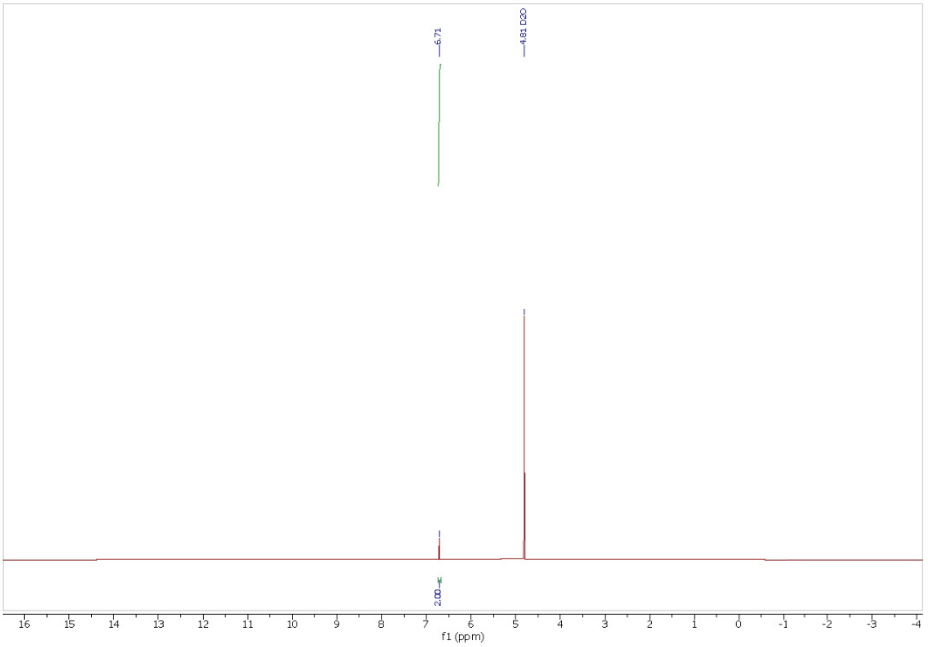

Figure S11. ^{1}H NMR spectrum of "digested" MIL-160, modulated with acetic acid at a molar modulator:metal/linker ratio of 2:1, after decomposition with 5% $NaOD/D_2O$, in D_2O. The furandicarboxylate linker signal appears at 6.59 ppm (normalized to two protons), the solvent signal at 4.79 ppm.

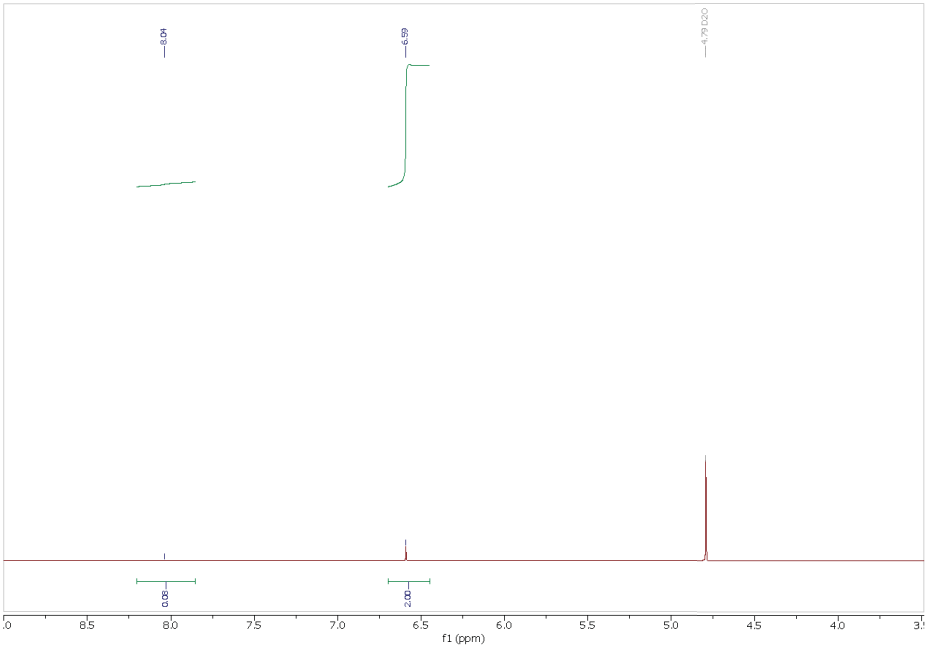

Figure S12. ^{1}H NMR spectrum of "digested" MIL-160, modulated with acetic acid at a molar modulator:metal/linker ratio of 2:1, after decomposition with 5% NaOD/D_2O. The furandicarboxylate linker signal appears at 6.59 ppm (normalized to two protons), the formate signal at 8.04 ppm, the solvent signal at 4.79 ppm.

The dissolution NMR measurement of formic acid modulated MIL-160 showed the presence of only 4% formic acid, compared to the amount of linker in the sample with the highest amount of formic acid (8 mmol, modulator to linker ratio 2:1). Smaller amounts of formic acid did not reach the detection limit. This also applies to the acetic acid and oxalic acid as modulators, which were not observable via NMR measurements. The amount of modulator was calculated for formic acid according to:

$$\frac{Integral\ linker}{protons\ linker} = x = \frac{2}{2} = 1$$

$$\frac{Integral\ modulator}{protons\ modulator} = y = \frac{0.04}{1} = 0.04$$

$$\frac{y}{x+y}100\% = \frac{0.04}{1.04}100\% = 4\%$$

A is the MIL-160 linker signal, b is the formic acid signal.

To ensure that the formate proton in HCO_2^- will not be exchanged against D in NaOD/D_2O, formic acid and methanol (2.5 mmol each), where examined in NMR under the same conditions

as the MOF batches. The signal remains visible and the intensity are approximately 1:3 as expected, which rules out the exchange.

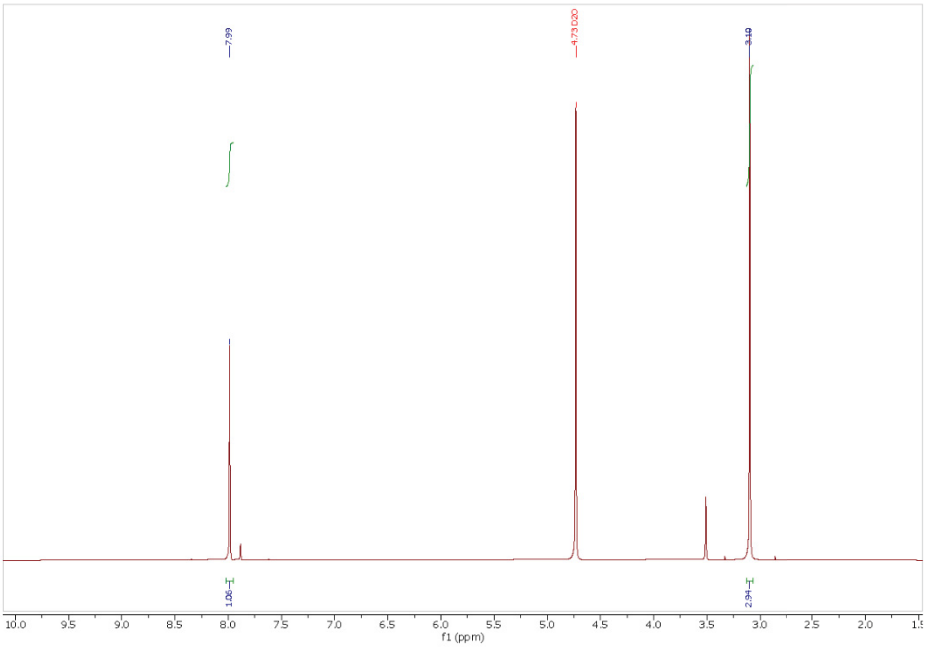

Figure S13. ^{1}H NMR spectrum of formic acid and methanol at a molar ratio of 1:1 after decomposition with 5% NaOD, in D_2O, the formate signal appears at 8.04 ppm, the methanolate signal at 3.10 ppm, the solvent signal at 4.79 ppm.

S5: Thermogravimetric analysis for possible defect calculation

The samples were investigated by thermogravimetric analysis (TGA) to quantify the possible defects from missing linkers. The TGA measurements where done under synthetic air through slow heating (5 K / min) to 1000 °C, to fully oxidize the linker and to obtain the metal component as its metal oxide, here Al_2O_3. A powder diffractogram of the remaining powder at 1000 °C matched the pattern of eta- Al_2O_3 (Figure S14).

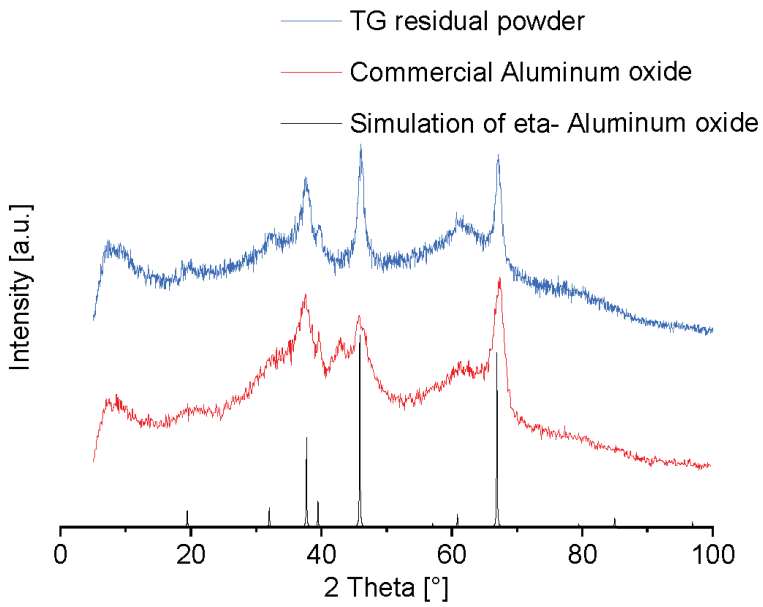

Figure S14. Comparison of the residue of MIL-160 after combustion in the TGA crucible, a commercial Al_2O_3 sample and a simulation of eta- Al_2O_3.[7]

When heating the MOFs to over 1000°C, beside the oxide (Al_2O_3) also the carbide (Al_4C_3) can be formed. Therefore, the residue from the TG measurement was analyzed by elemental analysis to give C 0.00%, H 0.6 %, N 0.00%, S 0.00%). The result excludes the presence of a carbide.

The end mass of Al_2O_3 can then be compared to the last weight plateau before the sample decomposed, as described by *Shearer et al.* for the zirconium MOFs of the UiO-66 series.[8] In this method it is assumed that the final product is the pure metal oxide (ZrO_2).

In the method of Shearer *et al.* on modulated UiO-66 it was also assumed that after guest adsorbate volatilization (in this case H_2O) any monocarboxylate modulator ligands (in this case

formate) were removed and the bridging OH groups in the Zr_6 building units were dehydroxylated in the temperature range of ca. 200-350 °C. From ideal UiO-66 with the formula $[Zr_6(\mu_3\text{-}O)_4(\mu_3\text{-}OH)_4(BDC)_6]$ (BDC = terephthalate, benzene-1,4-dicarboxylate) the dehydroxylation with the loss of 2 H_2O then gave $[Zr_6(O)_6(BDC)_6]$. The final framework decomposition with the combustion of the BDC linker then occurred over the range of 390-525 °C for the dehydroxylated UiO-66.

From the digestion NMR analysis of modulated MIL-160 in Section S5 we can exclude a replacement of missing linkers by modulator for formic acid, acetic acid or oxalic acid. Still a missing linker cannot leave an open metal site, hence for a saturated metal site and for charge neutrality, a missing linker must at least be replaced by aqua and hydroxido ligands.

In the MIL-53-type structure of MIL-160, each furandicarboxylate linker coordinates to four Al atoms, with each carboxylate group bridging between two Al atoms of the infinite $\{Al(\mu\text{-}OH)(O_2C\text{-})_2\}$ chain building unit. Thus, a defect MIL-160 will have a missing furandicarboxylate linker replaced by two H_2O and two OH^- ligands.

For the quantification, the reaction equation during linker combustion is considered, after the solvent guest molecules have already been evaporated. If we transfer the dehydroxylation of UiO-66 to MIL-160, the reaction equation of ideal MIL-160, $[Al(OH)(C_6H_2O_5)]$ is as follows, with the temperatures taken from the TGA results in Figure S16-S19:

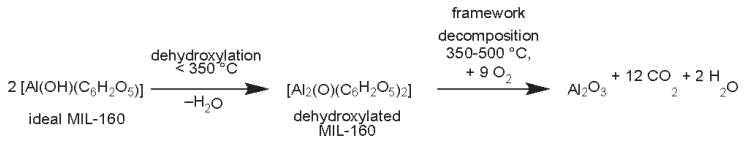

Free furandicarboxylate linker which may have remained in the pores without being removed through washing should have been decomposed at below 350 °C. Also, any left-over basic aluminum acetate starting material, $Al(OH)(O_2CCH_3)_2$ should have been largely decomposed to aluminum oxide (theor. 31.5%) at 400 °C (Figure S15).

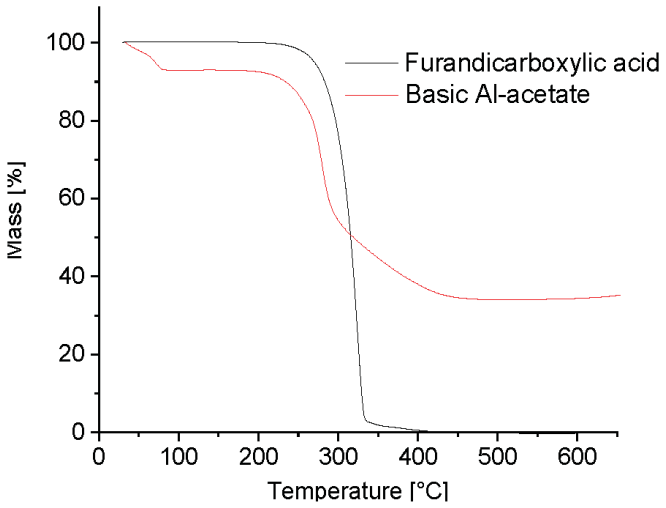

Figure S15. TG measurement of the MIL-160 educts.

Two resolved weight losses are observed in the TGA traces (end weight normalized to 100%). The losses are assigned to the following processes: (1) Adsorbate volatilization (in this case H_2O). This occurs over a temperature range of ca. 25−120 °C. (2) Removal of monocarboxylate ligands[9] (in this case formate) and dehydroxylation of the Al- cornerstones. These two weight loss events occur over a similar temperature range. The following figures 16-13 show the all samples from the four modulation series. The deviations of the initial masses are due to the non-homogeneity of MOFs in the case of smaller displacements, and to excess ligand in the case of the sometimes very large displacements, which is present in the sample and in some cases also blocks the pores. Since displacements can have diametral effects on the surface area and pore volume, the evaluation is limited to some extent.[10,11,12] As shown in figure 15 above, the mass loss between 300°C-350°C from the FDC linker is significantly stronger than the one from the Aluminum compound. This effect is also noticeably in the measured MIL-160 samples. With higher modulator to Linker ratios the difference is raising even to extraordinary dimensions in some cases. For a better understanding the not normalized TG figures are also shown below (figure S17, S19, S21, S23) That can be a hint of residual linker inside the MOF pores. That blocked pores may led to the observed decreasing BET-surfaces with higher modulator to linker ratios. The found deviations in the values of $W_{Exp\ Plat}$ and $W_{Theo.Plat}$, e.g the amount of linker in the four series do not allow a clear conclusion to be drawn as to the extent to which the modulator quantity induces linker defects. The trends of the calculated linker amounts are shown in figure S24 as an overview from selected samples. The selected temperature for each $W_{Exp.Plat}$ is shown in table S7-S9.

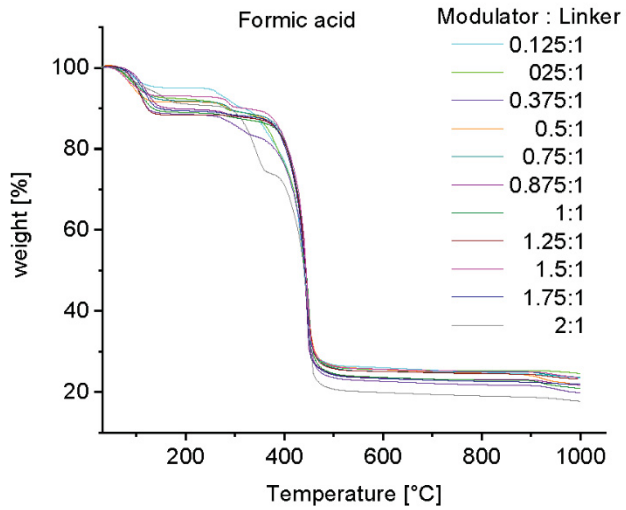

Figure S16. TGA measurements of MIL-160 with formic acid as modulator and different modulator: metal/linker ratios.

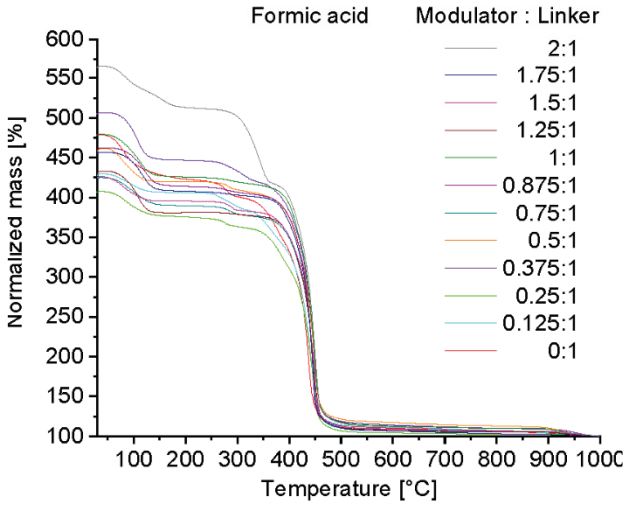

Figure S17. TGA measurements of MIL-160 with formic acid as modulator and different modulator : metal/linker ratios. The TGA traces are normalized such that the end mass is 100%.

20

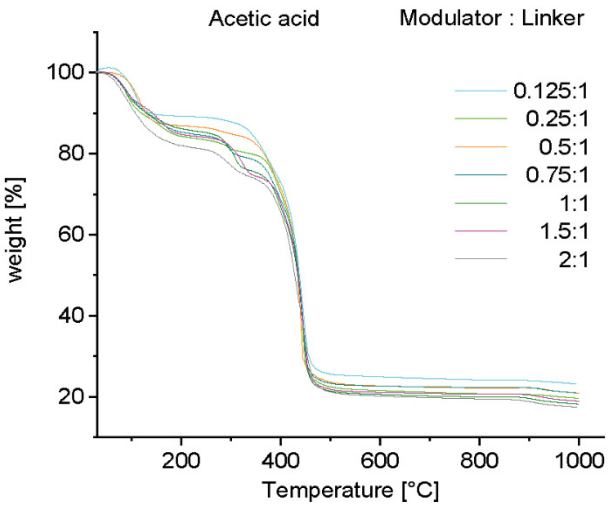

Figure S18. TGA measurements of MIL-160 with acetic acid as modulator and different modulator:metal/linker ratios.

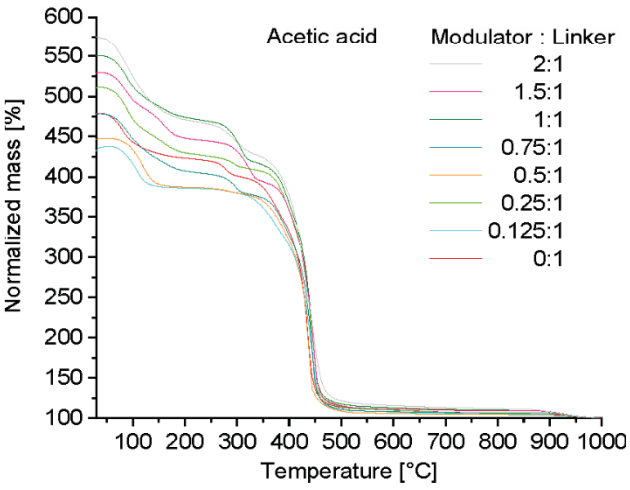

Figure S19. TGA measurements of MIL-160 with acetic acid as modulator and different modulator:metal/linker ratios. The TGA traces are normalized such that the end mass is 100%.

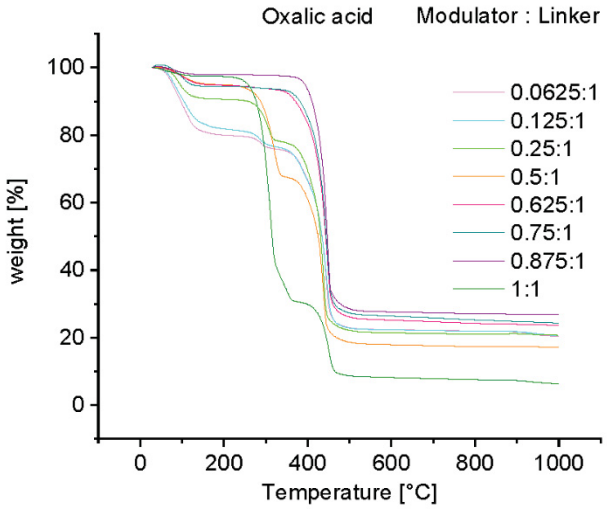

Figure S20. TGA measurements of MIL-160 with oxalic acid as modulator and different modulator:metal/linker ratios.

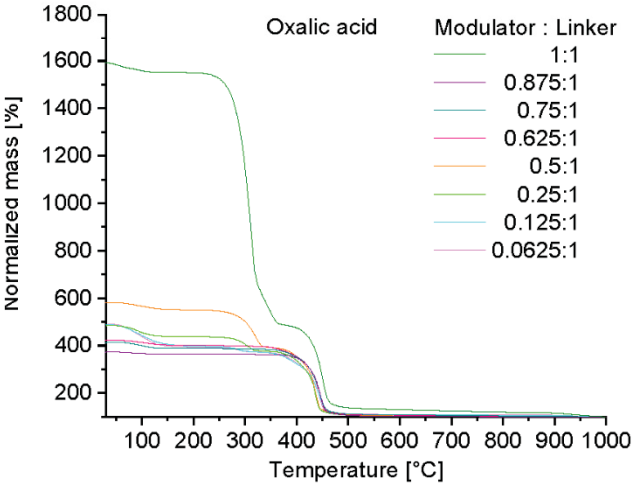

Figure S21. TGA measurements of MIL-160 with oxalic acid as modulator and different modulator:metal/linker ratios. The TGA traces are normalized such that the end mass is 100%.

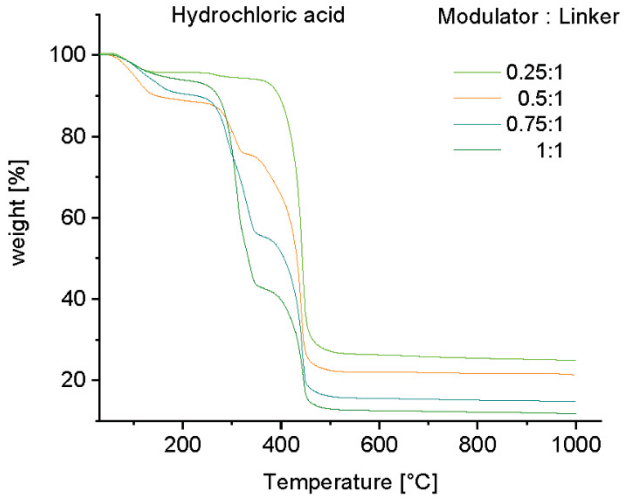

Figure S22. TGA measurements of MIL-160 with hydrochloric acid as modulator and different modulator:metal/linker ratios.

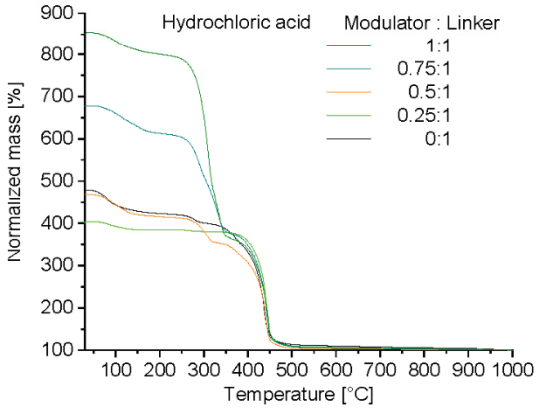

Figure S23. TGA measurements of MIL-160 with hydrochloric acid as modulator and different modulator:metal/linker ratios. The TGA traces are normalized such that the end mass is 100%.

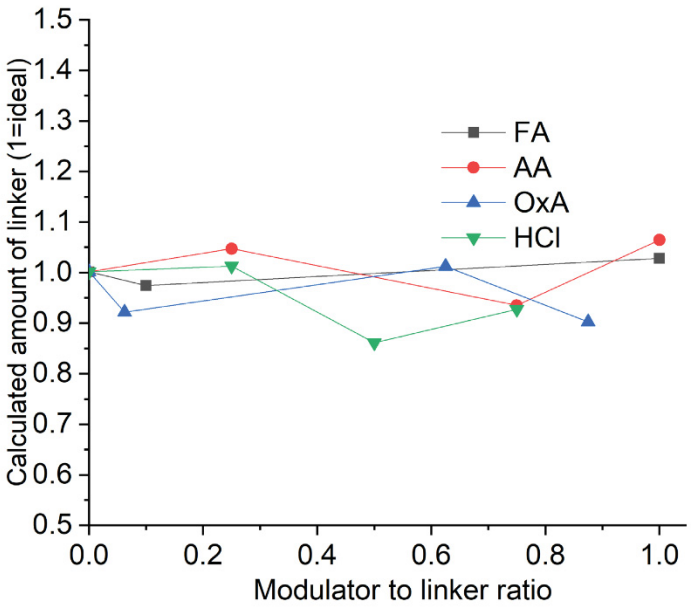

Figure S24. Trends of the linker amounts of MIL-160, depending on the modulator to linker ratio of the different modulators. The numbers on the x-axis are always in relation to 1 with respect to the linker amount.

Using this reaction equation from above, the theoretical TGA plateau weight ($W_{Theo.Plat.}$) after guest removal can now be calculated. This is the ratio of the molar masses of the MOFs used and the metal oxide, which is Al_2O_3.

The weight ratio of the molar mass of the final product is then compared to the molar mass of the respective MOF with its ideal molecular formula. The molar mass of the final product is normalized to 100%. Based on this, a theoretical weight plateau of the ideal MOF in relation to its residual mass after complete oxidation is calculated. Shearer *et al.*[8] have established the following equations:

$$W_{Theo.Plat.} = \left(\frac{M_{Comp.}}{M_{MO_2}}\right) * W_{End}$$

At, W_{End} this is the final mass of the TGA data. It is normalized to 100% for this evaluation. This means that in the application of the curves the start is above 100 % and the mass decreases more and more to 100 % in the course of the measurement.

$W_{Theo.Plat.}$ is the determined theoretical weight of the ideal MOF.

$M_{Comp.}$ is the molar mass of the measured MOF sample to be determined.

W_{End} is the final weight of the TG measurement, which is normalized to 100%.

Since each of these MOFs has a ratio of one linker per metal atom, the direct loss of mass per linker can be abbreviated to $Wt.PL_{Theo.}$ for easy determination. For more complex compositions of MOFs, the following formula can be used.

$$Wt.PL_{Theo.} = \left(\frac{W_{Theo.Plat.} - W_{End}}{Number\ of\ linker}\right)$$

Since W_{End} is 100% and the number of linkers is only 1 for each of the MOFs, in the cases given here only 100% of the values given above as $W_{Theo.Plat.}$ must be subtracted, so that the following $Wt.PL_{Theo.}$ results:

MIL-160:

$$\frac{198{,}07\frac{g}{mol}}{50{,}98\frac{g}{mol}} \times 100\% = 388\% - 100\% = 288\%$$

$$W_{Theo.Plat.} = 388\%$$

$$Wt.PL_{Theo.} = 289\%$$

The determination of the exact number of defects is carried out for non-modified MIL-160 in detail exemplary.

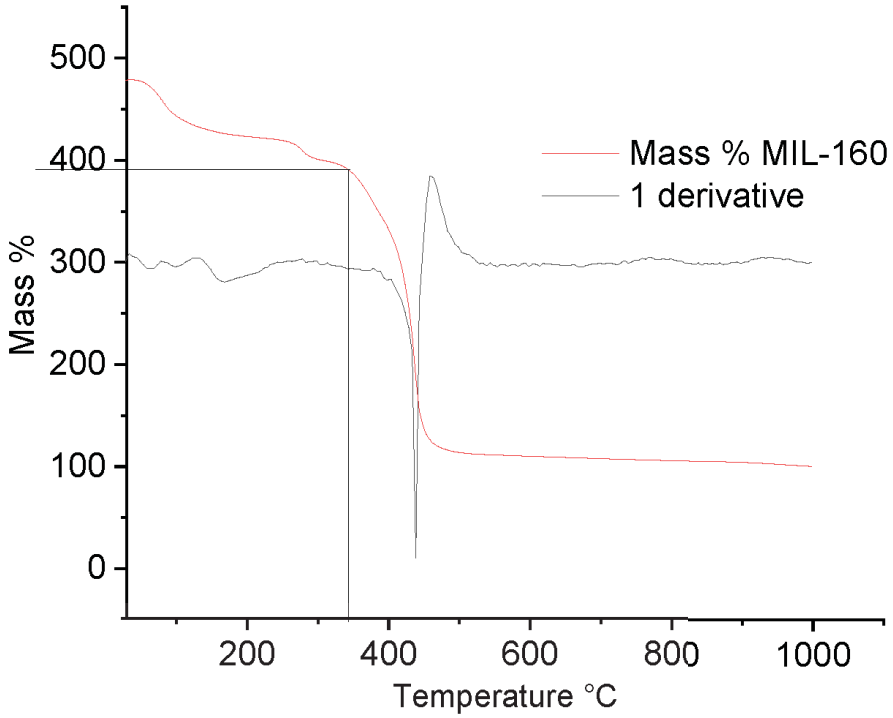

Figure S20. TGA measurement of MIL-160. The black lines show the chosen point for defect determination.

With the TGA curves, different areas can be determined. In the curve shown here, a slight loss of mass can be seen up to 100 °C. This can be attributed to solvents still contained in the pores of the MOF. This loss of mass can be expected, since the sample was dried before the measurement, but no further degassing step is performed as before a sorption measurement. A plateau can be detected after the mass loss. Here the mass remains constant up to about 400 °C. This means that the MOF does not decompose at these temperatures. Afterwards, another strong loss of mass can be detected. This is the mass loss that is interesting for the evaluation, since this is the oxidation of the organic linker to CO_2 and H_2O. After this loss of mass, a plateau is reached again. To determine the exact number of defects, the mass at the end of the second plateau is needed, i.e. in the example given above at about 350 °C. For the calculations this value is called $W_{Exp.Plat}$. In order to be able to determine this end of the plateau comparably over all measurements, the derivative was formed. It was defined that the end of the plateau used for evaluation is determined according to the following conditions. Starting from the lowest point of the derivative in the direction of low temperatures, it was checked whether the derivative at one point either reaches 0 or begins to assume more negative values again. If neither of the two cases occurred, the first value was chosen where the change in the derivative between two points was no more than 0.01. After determining the exact temperature at which the end of the plateau is located, the corresponding percentage mass normalized to the mass of Al_2O_3 could be read. In the example of the non-modulated MIL-160, this is the temperature 348 °C with the corresponding weight of 387 %. The exact number of linkers in this sample, abbreviated as $NL_{Exp.}$, can now be calculated with the following formula:

$$NL_{Exp.} = \frac{W_{Exp.Plat.} - W_{End}}{Wt.PL_{Theo}}$$

In the chosen example this results in a number of linkers of:

$$NL_{Exp.} = \frac{387\ \% - 100\ \%}{289\ \%} = 0.99$$

It could be determined that the sum formula of this sample has 0.99 linker per aluminum instead of one. The same calculation was performed for each additional TGA evaluation listed above. The following Tables S6-S9 show the calculated results of all four MIL.160 series in detail.

Table S6. Calculated defects of formic acid modulated MIL-160

Molar modulator to linker ratio	$W_{Exp.Plat.}$	Selected temperature for $W_{Exp.Plat.}$ [°C]	Calculated amount of Linker (1 = ideal)
0:1	387	345	1.00
0.125:1	382	331	0.97
0.25:1	357	347	0.89
0.375:1	401	356	1.09
0.5:1	397	371	1.03
0.75:1	370	372	0.93
0.875:1	396.	376	1.02
1:1	408	381	1.06
1.25:1	370	376	0.93
1.5:1	377	366	0.96
1.75:1	397	367	1.03
2:1	413	385	1.08

Table S7. Calculated defects of acetic acid modulated MIL-160

Molar modulator to linker ratio	$W_{Exp.Plat.}$	Selected temperature for $W_{Exp.Plat.}$ [°C]	Calculated amount of Linker (1 = ideal)
0.125:1	370	337	0.94
0.25:1	402	365	1.05
0.5:1	401	341	1.04
0.75:1	369	361	0.94
1:1	407	369	1.06
1.5:1	386	377	0.99
2:1	412	377	1.08

Table S8. Calculated defects of oxalic acid modulated MIL-160

Molar modulator to linker ratio	$W_{Exp.Plat.}$	Selected temperature for $W_{Exp.Plat.}$ [°C]	Calculated amount of Linker (1 = ideal)
0.0625:1	367	362	0.92
0.125:1	363	364	0.91
0.25:1	370	369	0.93
0.5:1	385	375	0.98
0.625:1	392	351	1.01
0.75:1	380	367	0.97
0.875:1	360	375	0.90
1:1	479	396	1.31

Table S9. Calculated defects of hydrochloric acid modulated MIL-160

Molar modulator to linker ratio	$W_{Exp.Plat.}$	Selected temperature for $W_{Exp.Plat.}$ [°C]	Calculated amount of Linker (1 = ideal)
0.25:1	376	372	1.01
0.5:1	349	353	0.86
0.75:1	369	352	0.93
1:1	350	391	1.01

S6: SEM analysis of particle sizes

The following Figures S21 to S24 show the scanning electron microscopy (SEM) images of all four modulator series. The scale bar is always 1 µm.

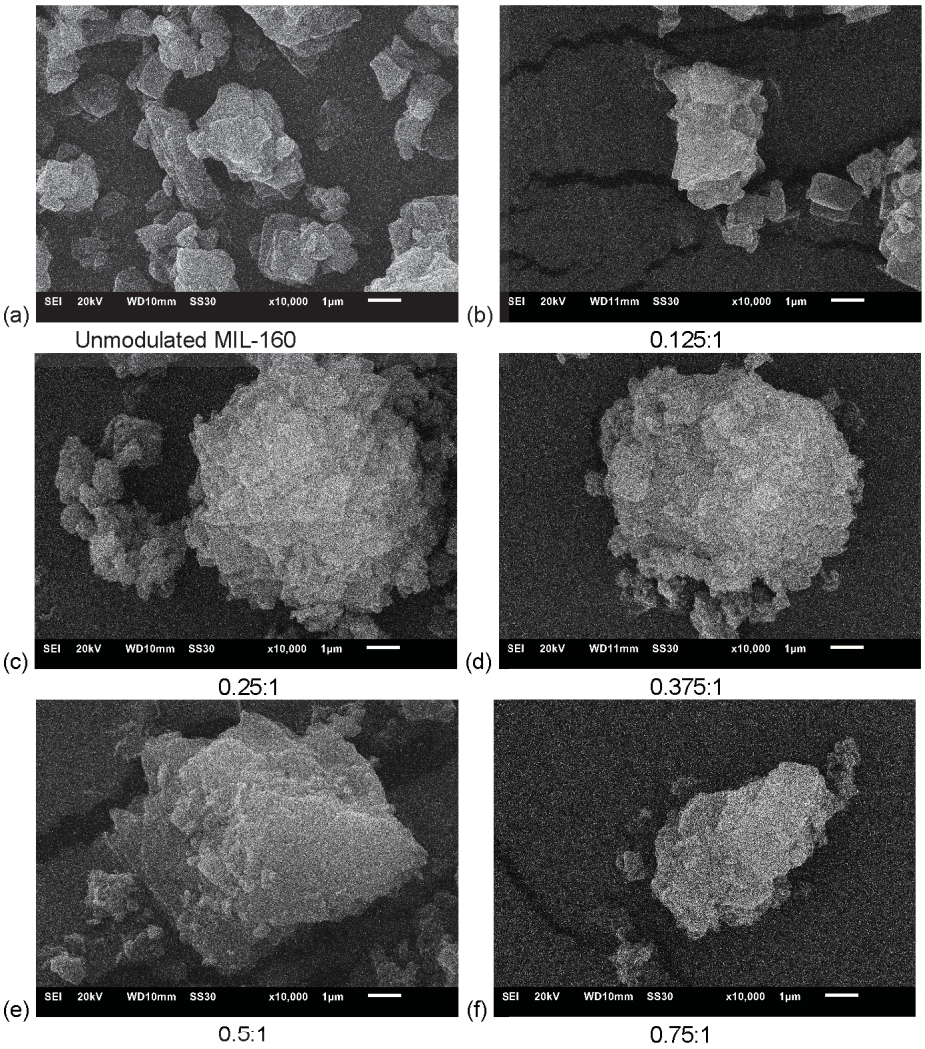

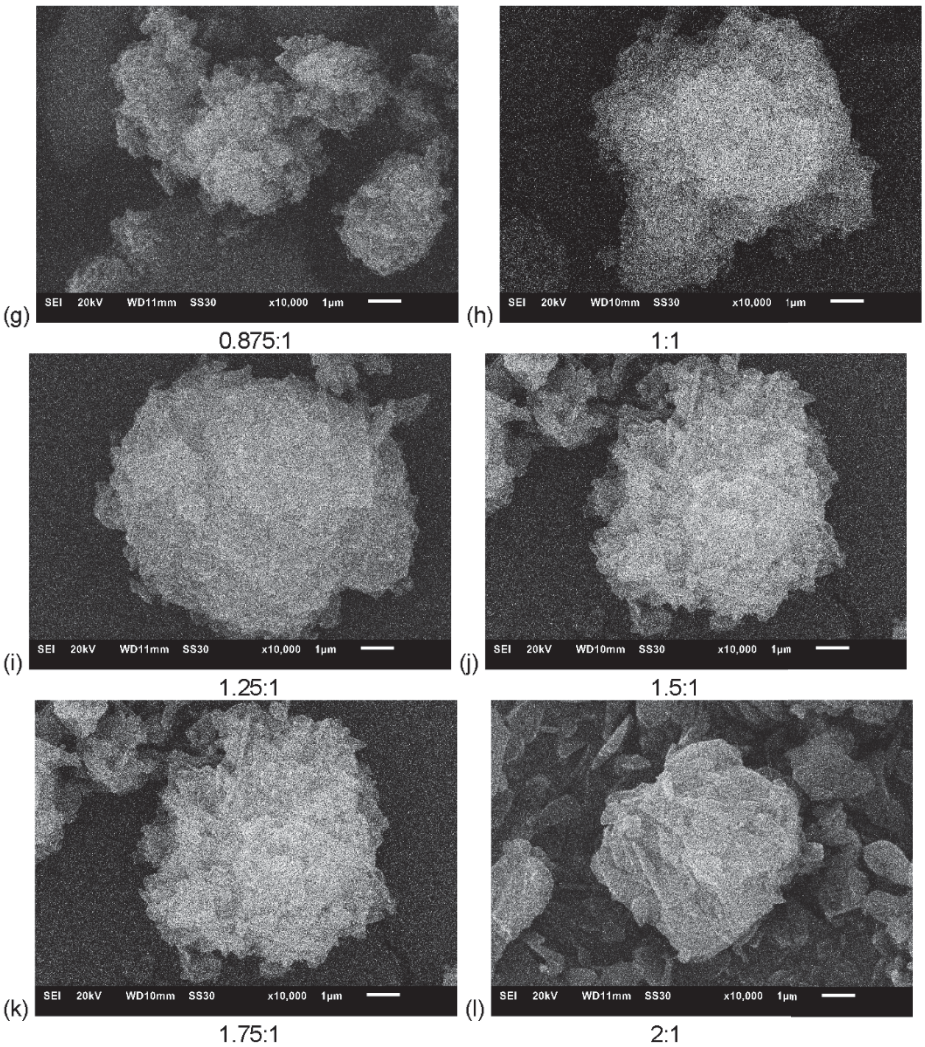

Figure 21. Formic acid modulated MIL-160 series with modulator to linker ratios of (a) unmodulated MIL-160, (b) 0.125:1, (c) 0.25:1, (d) 0.375:1, (e) 0.5:1, (f) 0.775:1, (g) 0.875:1, (h) 1:1, (i) 1.25:1, (j) 1.5:1, (k) 1.75:1 and (l) 2:1. The ratios are also given under each SEM picture.

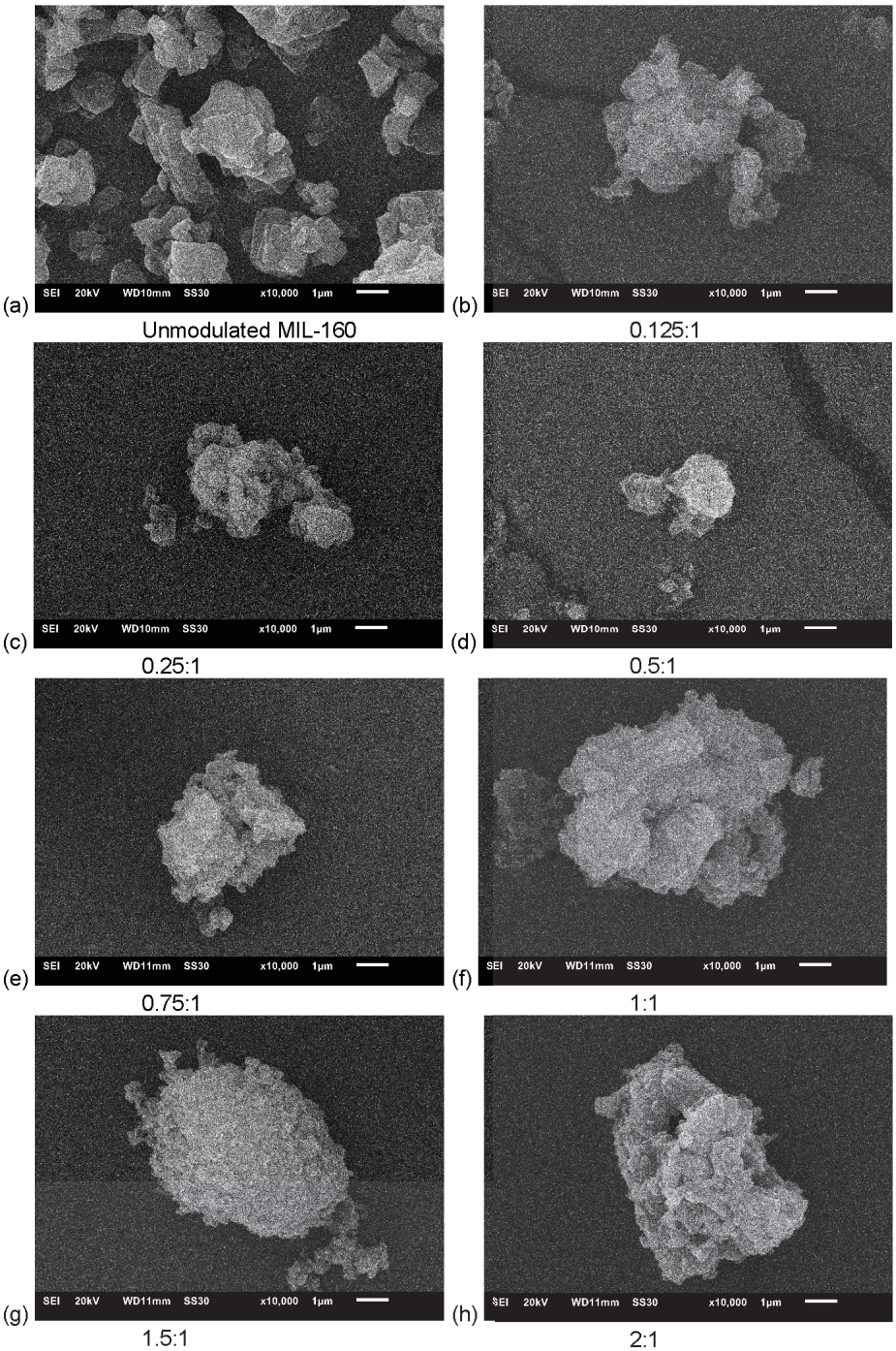

Figure S22. Acetic acid modulated MIL-160 series with modulator to linker ratios of (a) unmodulated MIL-160, (b) 01.25:1, (c) 0.25:1, (d) 0.5:1, (e) 0.75:1, (f) 1:1 and (g) 1.5:1 and (h) 2:1. The ratios are also given under each SEM picture.

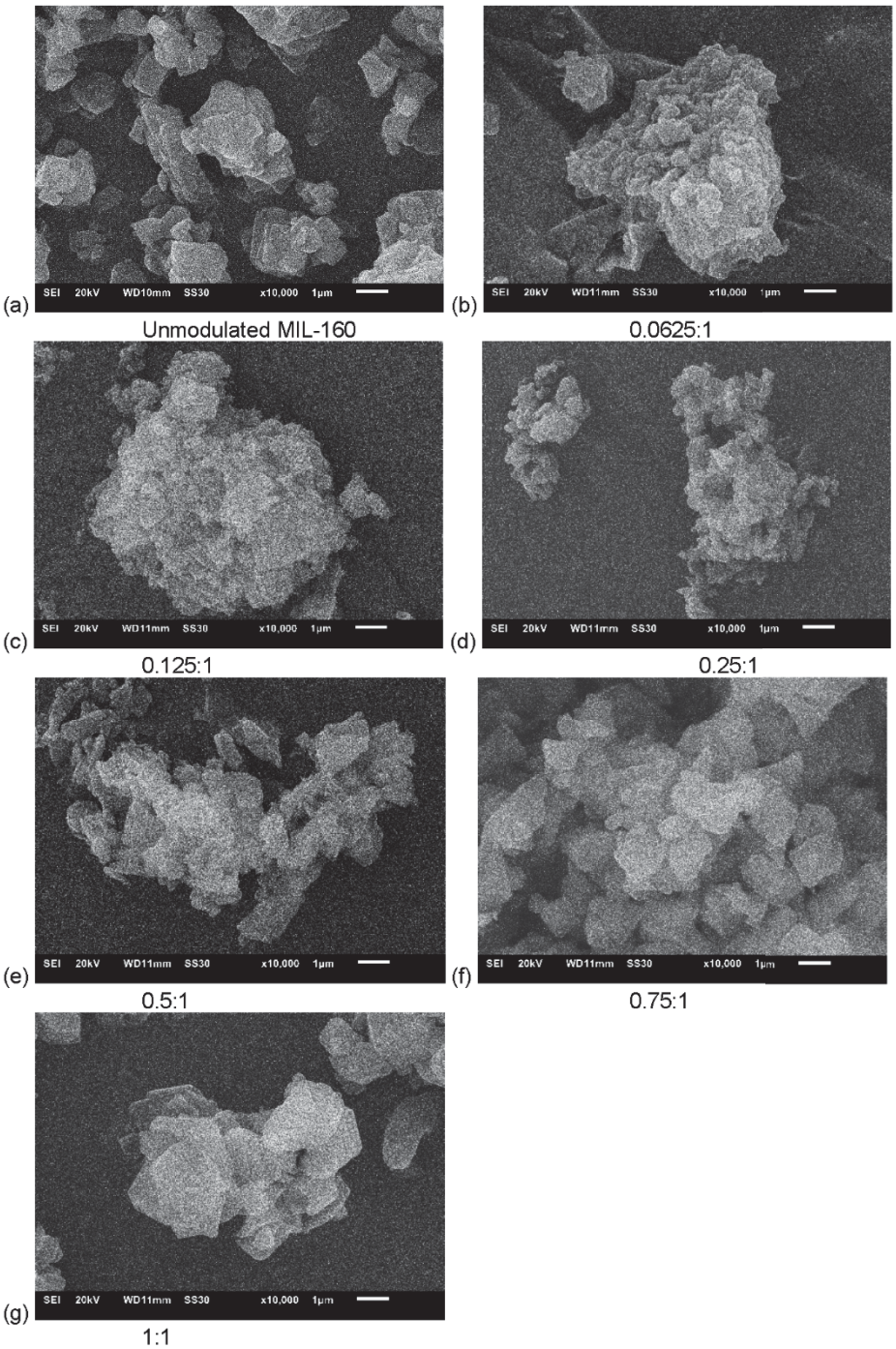

Figure S23. Oxalic acid modulated MIL-160 series with modulator to linker ratios of (a) unmodulated MIL-160, (b) 0.0625:1, (c) 0.125:1, (d) 0.25:1, (e) 0.5:1, (f) 0.75:1 and (g) 1:1. The ratios are also given under each SEM picture.

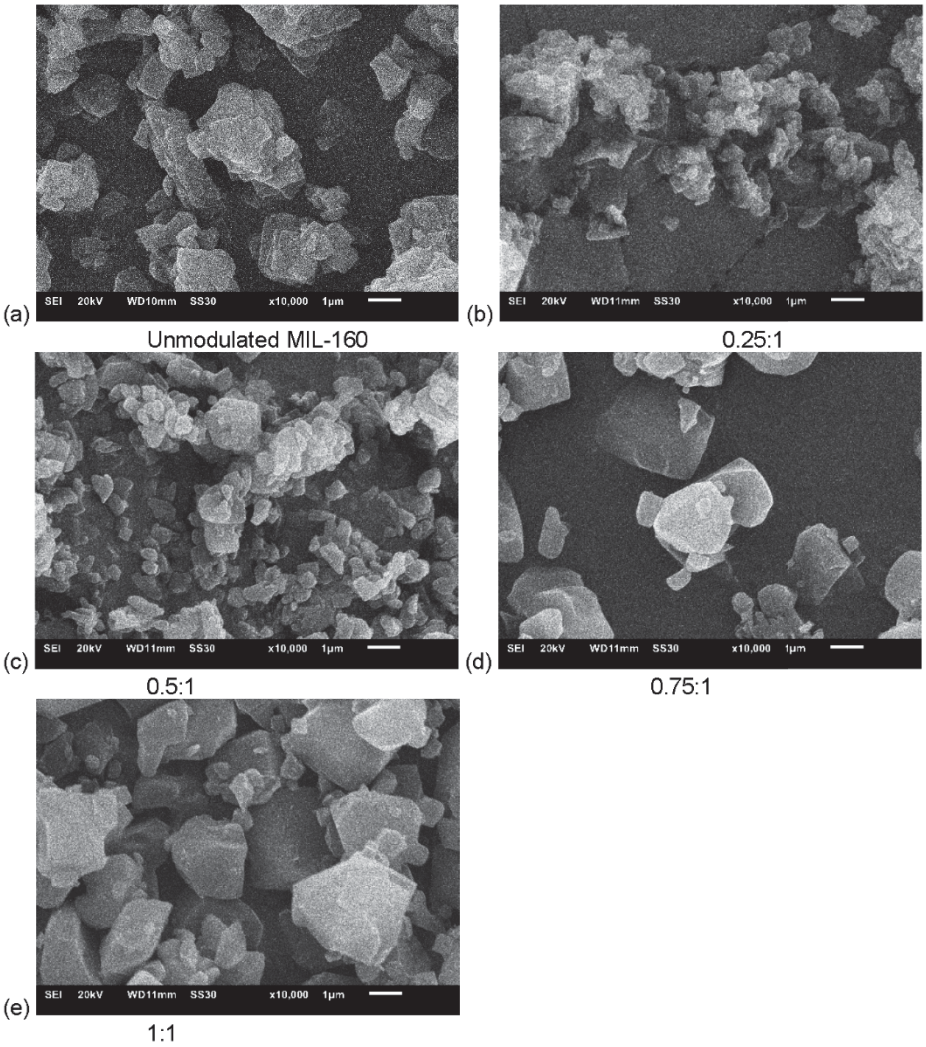

Figure S24. Hydrochloric acid modulated MIL-160 series with modulator to linker ratios of (a) unmodulated MIL-160, (b) 0.25:1, (c) 0.5:1 (d) 0.75:1 and (e) 1:1. The ratios are also given under each SEM picture.

[1] A. Cadiau, J. S. Lee, D. D. Borges, P. Fabry, T. Devic, M. T. Wharmby, C. Martineau, D. Foucher, F. Taulelle, C.-H. Jun, Y. K. Hwang, N. Stock, M. F. De Lange, F. Kapteijn, J. Gascon, G. Maurin, J.-S. Chang, C. Serre, *Adv. Mater.* **2015**, *27*, 4775-4780.

[2] K. Brandenburg, Diamond (version 4.6), Crystal and Molecular Structure Visualization, Crystal Impact - K. Brandenburg & H. Putz Gbr, Bonn (Germany) **2009–2021**.

[3] M. Wahiduzzaman, D. Lenzen, G. Maurin, N. Stock, M. T. Wharmby, *Eur. J. Inorg. Chem.* **2018**, 3626-3632.

[4] A. Permyakova, O. Skrylnyk, E. Courbon, M. Affran, S. Wang, U-H. Lee, A. H. Valekar, F. Nouar, G. Mouchaham, T. Devic, G. De Weireld, J.-S. Chang, N. Steunou, M. Frère, C. Serre, *ChemSusChem*. **2017**, *10*, 1419-1426.

[5] D. D. Borges, G. Maurin, D. S. Galvao, *MRS Adv.* 2017, **2**, 519-524.

[6] M. Wahiduzzaman, D. Lenzen, G. Maurin, N. Stock, M. T. Wharmby, *Eur. J. Inorg. Chem*. **2018**, 3626-3632.

[7] K. Shirasuka, H. Yanagida, G. Yamaguchi; *Yogyo Kyokai Shi,* **1976**, *84*, 610-613.

[8] G. C. Shearer, S. Chavan, J. Ethiraj, J. G. Vitillo, S. Svelle, U. Olsbye, C. Lamberti, S. Bordiga, K. P. Lillerud, *Chem. Mater.* **2014**, *26*, 4068-4071.

[9] S. Canossa, A. Gonzalez-Nelson, L. Shupletsov, M del Carmen Martin, M. A. van der Veen, *Chem. Eur. J.* **2020**, *26*, 3564-3570.

[10] C. Schlüsener, D. N. Jordan, M. Xhinovci, T. J. Matemb Ma Nteb, A. Schmitz, B. Giesen, C. Janiak *Dalton Trans*. **2020**, *49*, 73773-7383.

[11] T. J. Matemb Ma Ntep, H. Reinsch, C. Schlüsener, A. Goldman, H. Breitzke, B. Moll, L. Schmolke, G. Buntkowsky, C. Janiak, *Inorg. Chem*. **2019**, *58*, 10965–10973.

[12] M. J. Cliffe, W. Wan, X. Zou, P. A. Chater, A. K. Kleppe, M. G. Tucker, H. Wilhelm, N. P. Funnell, F.-X. Coudert, A. L. Goodwin, *Nat. Commun*. **2014**, *5,* 4176.

4 Zusammenfassung

Der erste Teil dieser Arbeit fasst den derzeitigen Stand der Forschung zu Metall-organischen Netzwerkverbindungen (MOFs) und ihrer Verwendung als Materialien für Wärmetransformationsprozesse zusammen. Mit ihrer hohen Wasseradsorptionskapazität können MOFs die bestehenden anorganischen Sorptionsmaterialien für Wärmetransformationsanwendungen durch die zyklische Ad- und Desorption von Wasser erweitern. Das Wasseradsorptionsverhalten von MOFs kann durch die hydrophile Natur des Linkers, d.h. des organischen Brückenliganden, gesteuert werden. Auf dem Weg zu ausgereifteren Anwendungen sind weitere Optimierungen der Kinetik der Wasseradsorption, sowie weitere Nachweise der hydrothermalen Stabilität für mehr als 100.000 Adsorptions- und Desorptionszyklen erforderlich. Anstelle von Wasser sind auch Alkohole als Arbeitsflüssigkeiten denkbar, wodurch sich das Spektrum der MOFs, die für Wärmetransformationsprozesse geeignet sind, deutlich erweitert. Einige dieser MOFs werden bereits heute industriell hergestellt (z. B. von BASF und unter dem Namen Basolite™). Eine aktuelle Herausforderung ist noch die Verarbeitung von MOFs zu Formteilen und das Aufbringen von MOFs Werkstücken. Durch das Bewältigen dieser Herausforderungen kann die Wärme- und Stoffübertragung weiter verbessert werden, was MOFs zu begehrten neuen Materialien für zahlreiche Zukunftsaufgaben in der Wärmetransformation und -speicherung, aber auch Katalyse, Gastrennung und -speicherung machen kann. Anhand der vorgestellten Zusammenfassung der unabhängig voneinander erschienenen Forschungsergebnisse konnte ein Überblick des Themenschwerpunktes der Nutzung von MOFs für Wärmetransformationsanwendungen gewonnen werden. Dieser Überblick ermöglicht es zukünftige und weitergehende Untersuchungen in diesem Kontext einzuordnen und das systematische Verständnis auf diesem Gebiert zu erweitern.

Im zweiten Teil dieser Arbeit wurde der Einfluss von verschiedenen Modulatoren auf das Aluminium basierte MOF MIL-160 gezeigt. MIL-160 wird während der Synthese mit Ameisensäure, Essigsäure, Oxalsäure und Salzsäure moduliert. Die eingesetzten Modulator zu Linker Verhältnisse reichen dabei von 0.0625:1 bis 2:1. Die Auswirkungen der Modulatoren wurden mit Pulverdiffraktometrie, Stickstoffsorption, Thermogravimetrie, NMR und Rasterelektronenmikroskopie charakterisiert. Durch die systematische und kleinschrittige Erhöhung der Modulator zu Linker Verhältnis, bis zu der Grenze ab der die die Synthese von MIL-160 effektiv verhindert wird, konnte ein geeigneter Bereich gezeigt werden in dem die Modulation von MIL-160 weiter erforscht werden kann. Dadurch konnte der Kenntnisstand der Modulation von aluminiumbasierten MOFs weiter ausgebaut werden und eine grundlegende Einsicht in das kinetische Verhalten von aluminiumbasierten MOFs in Lösung experimentell gezeigt werden.

5 Literaturverzeichnis

[1] S. R. Batten, N. R. Champness, X.-M. Chen, J. Garcia-Martinez, S. Kitagawa, L. Ohrstrom, M. O'Keeffe, M. Paik Suh, J. Reedijk, *Pure Appl. Chem.* **2013**, *85*, 1715–1724.

[2] C. Janiak, *Dalton Trans.* **2003**, 2781–2804.

[3] C. Janiak, J. K. Vieth, *New J. Chem.* **2010**, *34*, 2366–2388.

[4] A. Schoedel, S. Rajeh, *Top. Curr. Chem.* **2020**, *378*, 19

[5] J. D. Evans, B. Garai, H. Reinsch, W. Li, S. Dissegna, V. Bon, I. Senkovska, R. A. Fischer, S. Kaskel, C. Janiak, N. Stock, D. Volkmer, *Coord. Chem. Rev.* **2019**, *380*, 378–418.

[6] H.-C. Zhou, S. Kitagawa, *Chem. Soc. Rev.* **2014**, *43*, 5415–5418.

[7] J. R. Long, O. M. Yaghi, *Chem. Soc. Rev.* **2009**, *38*, 1213–1214.

[8] R. B. Getman, Y.-S. Bae, C. E. Wilmer, R. Q. Snurr, *Chem. Rev.* **2012**, *112*, 703–723.

[9] K. Adil, Y. Belmabkhout, R. S. Pillai, A. Cadiau, P. M. Bhatt, A. H. Assen, G. Maurin, M. Eddaoudi, *Chem. Soc. Rev.* **2017**, *46*, 3402–3430.

[10] J. Dechnik, C. J. Sumby, C. Janiak, *Cryst. Growth Des.* **2017**, *17*, 4467–4488.

[11] J. Dechnik, J. Gascon, C. J. Doonan, C. Janiak, C. J. Sumby, *Angew. Chem. Int. Ed.* **2017**, *56*, 9292–9310; *Angew. Chem.* **2017**, *129*, 9420.

[12] H. B. Tanh Jeazet, C. Staudt, C. Janiak, *Dalton Trans.* **2012**, *41*, 14003–14027.

[13] A. Nuhnen, D. Dietrich, S. Millan, C. Janiak, *ACS Appl. Mater. Interfaces* **2018**, *10*, 33589–33600.

[14] M. A. Carreon, S. R. Venna "*Metal Organic Framework Membranes for*

Molecular Gas Separations". Vol 6, World Scientific**. 2020**.

[15] S. M. J. Rogge, A. Bavykina, J. Hajek, H. Garcia, A. I. Olivos-Suarez, A. Sepulveda-Escribano, A. Vimont, G. Clet, P. Bazin, F. Kapteijn, M. Daturi, E. V. Ramos-Fernandez, F. X. Llabres i Xamena, V. Van Speybroeck, J. Gascon, *Chem. Soc. Rev.* **2017**, *46*, 3134–3184.

[16] L. Wang, M. Zheng, Z. Xie, *J. Mater. Chem. B* **2018**, *6*, 707–717.

[17] W. Chen, C. Wu, *Dalton Trans.* **2018**, *47*, 2114–2133.

[18] X. Lian, Y. Fang, E. Joseph, Q. Wang, J. Li, S. Banerjee, C. Lollar, X. Wang, H.-C. Zhou, *Chem. Soc. Rev.* **2017**, *46*, 3386–3401.

[19] S. Cohen, *Chem. Sci.* **2010**, *1*, 32–36.

[20] E.-P. Ng, S. Mintova, *Microporous Mesoporous Mater.* **2008**, *114*, 1–26

[21] I. M. Hönicke, I. Senkovska, V. Bon, I. A. Baburin, N. Bönisch, S. Raschke, J. D. Evans, S. Kaskel, *Angew. Chem. Int. Ed.* **2018**, *57*, 13780–13783.

[22] O. K. Farha, A. O. Yazaydin, I. Eryazici, C. D. Malliakas, B. G. Hauser, M. G. Kanatzidis, S. T. Nguyen, R. Q. Snurr, J. T. Hupp, *Nat. Chem.* **2010**, *2*, 944– 948.

[23] S. K. Henninger, F. Jeremias, H. Kummer, C. Janiak, *Eur. J. Inorg. Chem.* **2012**, 2625–2634.

[24] C. Janiak, S. K. Henninger, *Chimia* **2013**, *67*, 419–424.

[25] J. J. Low, A. I. Benin, P. Jakubczak, J. F. Abrahamian, S. A. Faheem and R. R. Willis, J. Am. Chem. Soc., 2009, 131, 15834–15842

[26] O. M. Yaghi, M. J. Kalmutzki, C. S. Diercks, *Introduction to Reticular Chemistry.Metal-organic frameworks and covalent organic frameworks*, Wiley,Weinheim, **2019**.

[27] L. W. Wang, J. Y. Wu, R. Z. Wang, Y. X. Xu, S. G. Wang, X. R. Li, Appl. Therm. Eng., *2003*, *23*, 1605–1617.

[28] R. E. Critoph, Y. Zhong, Proc. Inst. *Mech. Eng., Part E*, **2005**, *219*, 285–300.

[29] S. K. Henninger, M. Schicktanz, P. P. C. Hugenell, H. Sievers, H. M. Henning, Int. J. Refrig., **2012**, *35*, 543–553.

[30] Z. Tamainot-Telto, S. J. Metcalf, R. E. Critoph, Y. Zhong and R. Thorpe, Int. J. Refrig., **2009**, *32*, 1212–1229.

[31] *World Economic Forum, Global Risks **2015***, 10th Edition (World Economic Forum, Geneva, Switzerland, **2015**, accessed Aug, 2020. http://www3.weforum.org/docs/WEF_Global_Risks_2015_Report15.pdf.

[32] M. M. Mekonnen, A. Y. Hoekstra, *Sci. Adv.* **2016**, *2*, 1500323.

[33] S.-I. Kim, T.-U. Yoon, M.-B. Kim, S.-J. Lee, Y. K. Hwang, J.-S. Chang, H.-J. Kim, H.-N. Lee, U.-H. Lee, Y.-S. Bae, *Chem. Eng. J.* **2016**, *286*, 467–475.

[34] F. Trapani, A. Polyzoidis, S. Loebbecke, C. G. Piscopo, *Microporous Mesoporous Mater.* **2016**, *230*, 20–24

[35] H. Kim, S. Yang, S. R. Rao, S. Narayanan, E. A. Kapustin, H. Furukawa, A. S. Umans, O. M. Yaghi, E. N. Wang, *Science* **2017**, *356*, 430-434.

[36] M. S. Hanikel, F. Prevot, E. A. Fathieh, H. Kapustin, H. Lyu, H. Wang, N. J. Diercks, T. G. Glover, O. M. Yaghi, *ACS Cent. Sci.* **2019**, *5*, 1699–1706.

[37] A. J. Rieth, A. M. Wright, S. Rao, H. Kim, A. D. LaPotin, E. N. Wang, M. Dinca, *J. Am. Chem. Soc.* **2018**, *140*, 17591–17596.

[38] E. Elsayed, R. Al-Dadah, S. Mahmoud, A. Elsayed, P. A. Anderson, *Appl. Therm. Eng.* **2016**, *99*, 802–812.

[39] R. Al-Dadah, S. Mahmoud, E. Elsayed, P. Youssef, F. Al-Mousawi, *Energy* **2020**, *190*, 116356.

[40] K. Leus, T. Bogaerts, J. De Decker, H. Depauw, K. Hendrickx, H. Vrielinck, V. Van Speybroeck, P. Van Der Voort, *Microporous Mesoporous Mater.* **2016**, *226*, 110–116.

[41] S. Gokpinar, S.-J. Ernst, E. Hasturk, M. Mollers, I. El Aita, R. Wiedey, N. Tannert, S. Niesing, S. Abdpour, A. Schmitz, J. Quodbach, G. Fuldner, S. K. Henninger, C. Janiak, *Ind. Eng. Chem. Res.* **2019**, *58*, 21493–21503.

[42] S. K. Henninger, F. P. Schmidt, H. M. Henning, *Appl. Therm. Eng.* **2010**, *30*, 1692-1702.

[43] F. Millange, C. Serre and G. Férey, *Chem. Commun.,* **2002**, 822- 823; T. Loiseau, C. Serre, C. Huguenard, G. Fink, F. Taulelle, M. Henry, T. Bataille and G. Férey, *Chem. Eur. J.*, **2004**, *10*, 1373-1382.

[44] C. Kiener, U. Müller and M. Schubert, Germany Pat. WO2007/118841 A2, BASF SE, 2007; C. Kiener, U. Müller and M.

Schubert, US Pat. 12/297,666, BASF SE, 2012; E. Leung, U. Müller, N. Trukhan, H. Mattenheimer and G. Cox, US Pat. 13/249,943, BASF SE, 2012.

[45] E. Alvarez, N. Guillou, C. Martineau, B. Bueken, B. Van de Voorde, C. Le Guillouzer, P. Fabry, F. Nouar, F. Taulelle, D. de Vos, J.-S. Chang, K. H. Cho, N. Ramsahye, T. Devic, M. Daturi, G. Maurin, C. Serre, *Angew. Chem. Int. Ed.*, **2015**, *54*, 3664-3668.

[46] H. Reinsch, M. A. van der Veen, B. Gil, B. Marszalek, T. Verbiest, D. de Vos, N. Stock, *Chem. Mater.*, **2013**, *25*, 17-26.

[47] A. Cadiau, J. S. Lee, D. Damasceno Borges, P. Fabry, T. Devic, M. T. Wharmby, C. Martineau, D. Foucher, F. Taulelle, C.-H. Jun, Y. K. Hwang, N. Stock, M. F. De Lange, F. Kapteijn, J. Gascon, G. Maurin, J.-S. Chang, C. Serre, *Adv. Mater.*, **2015**, *27*, 4775-4780.

[48] N. Tannert, C. Jansen, S. Nießing, C. Janiak, *Dalton Trans*. **2018**, *48*, 2967-2976.

[49] M. Gaab, N. Trukhan, S. Maurer, R. Gummaraju and U. Müller, *Micropor. Mesopor. Mater.*, **2012**, *157*, 131-136.

[50] F. Jeremias, D. Fröhlich, C. Janiak and S. K. Henninger, *RSC Adv.*, **2014**, *4*, 24073-24082.

[51] D. Fröhlich, S. K. Henninger and C. Janiak, *Dalton Trans.,* **2014**, *43*, 15300-15304.

[52] D. Fröhlich, E. Pantatosaki, P. D. Kolokathis, K. Markey, H. Reinsch, M. Baumgartner, M. A. van der Veen, D. E. de Vos, N. Stock, G. K. Papadopoulos, S. K. Henninger and C. Janiak, *J. Mater. Chem. A*, **2016**, *4*, 11859-11869.

[53] W. Liang, L. Li, J. Hou, N. D. Shepherd, T. D. Bennett, D. M. D'Alessandro and V. Chen, *Chem. Sci.*, **2018**, *9*, 3508-3516; L. Feng, S. Yuan, L.-L. Zhang, K. Tan, J.-L. Li, A. Kirchon, L.-M. Liu, P. Zhang, Y. Han, Y. J. Chabal and H.-C. Zhou, *J. Am. Chem. Soc.*, **2018**, *140*, 2363-2372;

[54] U. Betke, M. Klaus, J. G. Eggebrecht, M. Scheffler and A. Lieb, *Micropor. Mesopor. Mater.*, **2018**, *265*, 43-56.

[55] D. Damasceno Borges, P. Normand, A. Permiakova, R. Barbaro, N. Heymans, D. S. Galvao, C. Serre, G. De Weireld and G. Maurin, *J. Phys. Chem. C*, **2017**, *121*, 26822-26832.

[56] S. Couck, Y.-Y. Liu, K. Leus, G. V. Baron, P. Van der Voort and J. F. M. Denayer, *Micropor. Mesopor. Mater.*, **2015**, *206*, 217-225.;

[57] A. Dhakshinamoorthy, N. Heidenreich, D. Lenzen and N. Stock, *CrystEngComm*, **2017**, *19*, 4187-4193.

[58] L. M. Aguirre-Díaz, D. Reinares-Fisac, M. Iglesias, E. Gutiérrez-Puebla, F. Gándara, N. Snejko and M. Á. Monge, *Coord. Chem. Rev.*, **2017**, *335*, 1-27.

[59] P. G. Yot, L. Vanduyfhuys, E. Alvarez, J. Rodriguez, J.-P. Itié, P. Fabry, N. Guillou, T. Devic, I. Beurroies, P. L. Llewellyn V. Van Speybroek, C. Serre. and G. Maurin, *Chem. Sci.*, **2016**, *7*, 446-450.

[60] Y. Belmabkhout, R. S. Pillai, D. Alezi, O. Shekhah, P. M. Bhatt, Z. Chen, K. Adil, S. Vaesen, G. de Weireld, M. Pang, M. Suetin, A. J. Cairns, V. Solovyeva, A. Shkurenko, O. E. Talll, G. Maurin and M. Eddaoudi, *J. Mater. Chem. A*, **2017**, *5*, 3293-3303.

[61] S. Karmakar, J. Dechnik, C. Janiak and S. De, *J. Hazard. Mater.* **2016**, *303*, 10-20.

[62] M. Mon, R. Bruno, J. Ferrando-Soria, D. Armentano and E. Pardo, *J. Mater. Chem. A*, **2018**, *6*, 4912-4947.

[63] M. J. Kalmutzki, C. S. Diercks and O. M. Yaghi, *Adv. Mater.*, **2018**, *30*, 1704304.

[64] H. Kim, S. Yang, S. R. Rao, S. Narayanan, E. A. Kapustin, H. Furukawa, A. S. Umans, O. M. Yaghi and E. N. Wang, *Science*, **2017**, *356*, 430-434.

[65] F. Trapani, A. Polyzoidis, S. Loebbecke and C. G. Piscopo, *Micropor. Mesopor. Mater.*, **2016**, *230*, 20-24.

[66] A. Weiss, N. Reimer, N. Stock, M. Tiemann and T. Wagner, *Phys. Chem. Chem. Phys.*, **2015**, *17*, 21634-21642.

[67] N. Reimer, B. Bueken, S. Leubner, C. Seidler, M. Wark, D. De Vos and N. Stock, *Chem. Eur. J.*, **2015**, *21*, 12517-12524

[68] S. Karmakar, S. Bhattarcharjee and S. De, *J. Environm. Chem. Eng.* **2017**, *5*, 6087-6097.

[69] M. F. de Lange, T. Zeng, T. J. H. Vlugt, J. Gascon and F. Kapteijn, *CrystEngComm*, **2015**, *17*, 5911-5920.

[70] J. Canivet. A. Fateeva, Y. Guo, B. Coasne and D. Farrusseng, *Chem. Soc. Rev.* **2014**, *53*, 5594-5617.

[71] N. C. Burtch, H. Jasuja and K. S. Walton, *Chem. Rev.*, **2014**, *114*, 10575-10612.

[72] M. F. de Lange, B. L. van Velzen, C. P. Ottevanger, K. J. F. M. Verouden, L.-C. Lin, T. J. H. Vlugt, J. Gascon and F. Kapteijn, *Langmuir*, **2015**, *31*, 12783-12796.

[73] D. Lenzen, P. Bendix, H. Reinsch, D. Fröhlich, H. Kummer. M. Möllers, P. P. C. Hügenell, R. Gläser, S. Henninger and N. Stock, *Adv. Mater.*, **2017**, *30*, 1705869.

[74] H. Kummer, F. Jeremias, A. Warlo, G. Füldner, D. Fröhlich, C. Janiak, R. Gläser and S. K. Henninger, *Ind. Eng. Chem. Res.*, **2017**, *56*, 8393-8398.; M. F. de Lange, C. P. Ottevanger, M. Wiegman, T. J. H. Vlugt, J. Gascon and F. Kapteijn, *CrystEngComm*, **2015**, *17*, 281-285.

[75] M. Taddei, *Coord. Chem. Rev*., **2017**, *343*, 1–24.

[76] X. Liu, X. Wang, F. Kapteijn, *Chem. Rev.* **2020**, *120*, 8303-8377.

[77] D. M. Steinert, S.-J. Ernst, S. K. Henninger, C. Janiak, *Eur. J. Inorg. Chem.* **2020**, 4502-4515.

[78] F. Jeremias, D. Fröhlich, C. Janiak, S. Henninger, *New J. Chem.* **2014**, *38*, 1846-1852.

[79] S. M. J. Rogge, A. Bavykina, J. Hajek, H. Garcia, A. I. Olivos-Suarez, A. Sepúlveda-Escribano, A. Vimont, G. Clet, P. Bazin, F. Kapteijn, M. Daturi, E. V. Ramos-Fernandez, F. X. Llabrés i Xamena, V. Van Speybroeck, J. Gascon, *Chem. Soc. Rev*. **2017**, *46*, 3134-3184.

[80] K. Adil, Y. Belmabkhout, R. S. Pillai, A. Cadiau, P. M. Bhatt, A. H. Assen, G. Maurin, M. Eddaoudi, *Chem. Soc. Rev*. **2017**, *46*, 3402-3430

[81] J. Dechnik, J. Gascon, C. J. Doonan, C. Janiak, C. J. Sumby, *Angew. Chem. Int. Ed.* **2017**, *56*, 9292-9310.

[82] J. A. Mason, M. Veenstra, J. R. Long, *Chem. Sci.* **2014**, *5*, 32-51.

[83] Y. He, W. Zhou, G. Qian, B. Chen, *Chem. Soc. Rev.* **2014**, *43*, 5657-5678.

[84] E. Alvarez, N. Guillou, C. Martineau, B. Bueken, B. Van de Voorde, C. Le Guillouzer, P. Fabry, F. Nouar, F. Taulelle, D. de Vos, J.-S. Chang, K. H. Cho, N. Ramsahye, T. Devic, M. Daturi, G. Maurin, C. Serre, *Angew. Chem. Int. Ed*. **2015**, *54*, 3664–3668.

[85] D. S. Sholl, R. P. Lively, *J. Phys. Chem. Lett*. **2015**, *6*, 3437– 3444.

[86] Z. Fang, B. Bueken, D. de Vos, R. A. Fischer, *Angew. Chem. Int. Ed*. **2015**, *54*, 7234–7254.

[87] S. Dissegna, K. Epp, W. R. Heinz, G. Kieslich, R. Fischer, *Adv. Mater*. **2018**, *30*, 1704501.

[88] . Ren, M. Ledwaba, N. M. Musyoka, H. W. Langmi, M. Mathe, S. Liao, W. Pang, *Coord. Chem. Rev.* **2017**, *349*, 169–197.

[89] G. Wißmann, A. Schaate, S. Lilienthal, I. Bremer. A.A. Schneider. P. Behrens, *Microporous Mesoporous Mater.* **2011***, 152,* 64-70.

[90] B. Moll, T. Müller, C. Schlüsener, A. Schmitz, P. Brandt, S. Öztürk, C. janiak, *Mater. Adv.* **2021**, *2*, 804-812.

[91] A. Kirchon, L. Feng, H. F. Drake, E. A. Joseph, H-C. Zhou, *Chem. Soc. Rev.* **2018**, *47*, 8611-8638.

[92] M. Kalaj, K. C. bentz, S. Ayala Jr., J. M. Palomba, K. S. Barcus, Y. Katayama, S. M. Cohen, *Chem. Rev.* **2020**, *120*, 16, 8267–8302.

[93] T. Tsuruoka, S. Furukawa, Y.Takashima, K. Yoshida, S. Isoda, S. Kitagawa, *Angew. Chem. Int. Ed*. **2009**, *48*, 4739–4743

[94] A. Umemura, S. Diring, S. Furukawa, H. Uehara, T. Tsuruoka, S. Kitagawa *J. Am. Chem. Soc.* **2011**, *133*, 15506–15513

[95] S. Diring, S. Furukawa, Y. Takashima. T. Tsuruoka, S. Kitagawa, *Chem. Mater.* **2010**, *22*, 16, 4531–4538.

[96] G. C. Shearer, S. Chavan, S. Bordiga, S. Svelle, U. Olsbye, K. P. Lillerud, *Chem. Mater.* **2016**, *28*, 3749−3761.

[97] S. Gökpinar, T. Diment, C. Janiak, *Dalton Trans.* **2017**, *46*, 9895-9900.

[98] T. Zhao, F. Jeremias, I. Boldog, B. Nguyen, St. K. Henninger, C. Janiak, *Dalton Trans*. **2015,** *44*, 16791.

[99] T. Zhao, L. Yang, P. Feng, I. Gruber, C. Janiak, Y, Liu, *Inorg. Chim. Acta* **2018**, *471*, 440–445.

[100] T. Zhao, S. Li, Y-X. Xiao, C. Janiak, G. Chang, G. Tian, X.-Y. Yang, *Sci China Mater.* **2021**, *64*, 252–258.

[101] L. Yang, T. Zhao, I. Boldog, C. Janiak, X.-Y. Q. Li, Y.-J. Zhou, Y. Xia, D.-W. Lai, Y.-J. Liu, *Dalton Trans.* **2019**, *48*, 989–996.

[102] T. D. Bennett, A. K. Cheetham, A. H. Fuchs, F.-X. Coudert, *Nat. Chem.* **2016**, *9*, 11-16.

[103] H.W. B. Teo, A. Chakraborty, S. Kayal, *Microporous Mesoporous Mater.* **2018**, *272,* 109–116.

[104] T. Loiseau, C. Serre, C. Huguenard, G. Fink, F. Taulelle, M. Henry, T. Bataille, G. Férey, *Chem. Eur. J.* **2004**, *10*, 1373-1382.

[105] C. Kiener, U. Müller and M. Schubert, US Pat. 12/297,666, BASF SE, **2012**.

[106] E. Leung, U. Müller, N. Trukhan, H. Mattenheimer and G. Cox, US Pat. 13/249,943, BASF SE, **2012**.

[107] H. Reinsch, M. A. van der Veen, B. Gil, B. Marszalek, T. Verbiest, D. de Vos, N. Stock, *Chem. Mater.* **2013**, *25*, 17-26.

[108] A. Cadiau, J. S. Lee, D. D. Borges, P. Fabry, T. Devic, M. T. Wharmby, C. Martineau, D. Foucher, F. Taulelle, C.-H. Jun, Y. K. Hwang, N. Stock, M. F. De Lange, F. Kapteijn, J. Gascon, G. Maurin, J.-S. Chang, C. Serre, *Adv. Mater.* **2015**, *27*, 4775-4780.

[109] Gaab, N. Trukhan, S. Maurer, R. Gummaraju, U. Müller, *Microporous. Mesoporous. Mater.* **2012**, *157*, 131-136

[110] F. Jeremias, D. Fröhlich, C. Janiak, S. K. Henninger, *RSC Adv.* **2014**, *4*, 24073-24082.

[111] D. Fröhlich, S. K. Henninger, C. Janiak, *Dalton Trans.* **2014**, *43*, 15300-15304.

[112] D. Fröhlich, E. Pantatosaki, P. D. Kolokathis, K. Markey, H. Reinsch, M. Baumgartner, M. A. van der Veen, D. E. de Vos, N. Stock, G. K. Papadopoulos, S. K. Henninger, C. Janiak, *J. Mater. Chem. A* **2016**, *4*, 11859-11869.

[113] P. Brandt, S.-H. Xing, J. Liang, G. Kurt, A. Nuhnen, O. Weingart, C. Janiak, *ACS Appl. Mater. Interfaces* **2021**, *13*, 29137-29149.

[114] F. Jeremias, A. Khutia, S. K. Henninger, C. Janiak, *J. Mater. Chem*. **2012**, *22*, 10148–10151.

[115] A. Samokhvalov, *Coord. Chem. Rev*. **2018**, *374*, 236–253.

[116] http://avantium.com/yxy/yxy-technology.html, accessed 01.08.**2017**, 01:54 h

[117] Press releases: 'Synvina: Jointventure of BASF and Avantium established', **2016**.

[118] N. Stock, S. Biswas, *Chem. Rev.* **2012**, *112*, 933–969.

[119] S. Yuan, J.-S. Qin, C. T. Lollar, H.-C. Zhou, *ACS Cent. Sci.* **2018**, *4*, 440–450.

[120] S. Yuan, L. Feng, K. Wang, J. Pang, M. Bosch, C. Lollar, Y. Sun, J. Qin, X. Yang, P. Zhang, Q. Wang, L. Zou, Y. Zhang, L. Zhang, Y. Fang, J. Li, H.-C. Zhou, *Adv. Mater.* **2018**, *30*, 1704303.

[121] G. C. Shearer, S. Chavan, S. Bordiga, S. Svelle, U. Olsbye, K. P. Lillerud, *Chem. Mater.* **2016**, *28*, 3749–3761.